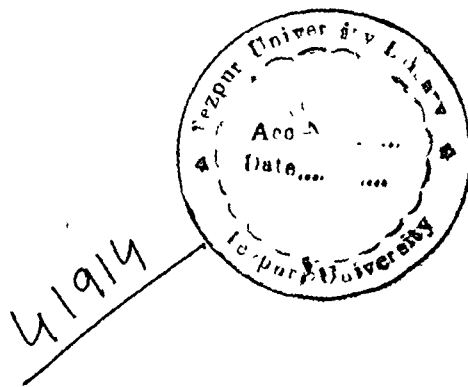


T 07



CENTRAL LIBRARY

EZPUR UNIVERSITY

ession No. 797

26/02/13

**REFERENCE BOOK
NOT TO BE ISSUED
TEZPUR UNIVERSITY '13R. V**

**SYNTHESIS OF QUANTUM DOTS IN POLYMER MATRIX AND
STUDY OF THEIR ELECTRICAL PROPERTIES FOR VARIOUS
DEVICE APPLICATIONS.**

A THESIS SUBMITTED TO

TEZPUR UNIVERSITY

IN PARTIAL FULFILLMENT OF THE REQUIREMENTS
FOR THE DEGREE OF

DOCTOR OF PHILOSOPHY

BY

ARUN KUMAR BORDOLOI

Regd.No: 017 of 2006



DEPARTMENT OF PHYSICS,

SCHOOL OF SCIENCE AND TECHNOLOGY

TEZPUR UNIVERSITY

NAPAAM, TEZPUR-784 028

JANUARY, 2007

Dedicated to

My beloved parents

ABSTRACT

Semiconductor nanostructures (quantum dots) have received much attention from chemists and physicists in the last decade due to the fact that their electrical and optical properties are very different from those of bulk semiconductor crystals. The optical and electrical properties of semiconductor nanostructures can be tailored to a large extent by the dimensions of the crystals. The various effects that occur due to spatial confinement of electrons in such structures are of scientific importance. In addition, semiconductor nanostructures are very promising for a number of applications in the optoelectronic industry. Semiconductor nanostructures will show size-dependent properties different from those of a macroscopic semiconductor if one or more dimensions of the structure are in the same range as the length scale of a physical quantity (e.g. wavelength of light, wavelength of electrons, electrostatic length scales). A crystalline material which is size-restricted in three dimensions such that the electron wave functions are confined within its volume is called a quantum dot (QD). The II-VI nano crystals have a direct band gap which can be tuned in a broad range (up to 4 eV) by their size. This makes them suitable candidates for applications in optoelectronic and electronic devices.

In this work optical characterization of chemically synthesized different II-VI semiconductor quantum dot samples are discussed. The role of interfacial charge transfer is discussed through electrical properties in the form of *I-V* and *C-V* characteristics.

The optical properties of quantum dots are discussed mainly on the basis of two properties of quantum dots eg. size quantization and presence of surface states. For size quantization optical absorption studies have been done. X-Ray diffraction has been employed as first hand approach to

determine the sizes of the quantum dots. However accurate size and shape of the particles (quantum dots) have been estimated with the help of Transmission electron microscopy (TEM). The presence of electronic states called surface states within the band gap of semiconductor nano particles (quantum dots) has been investigated through photoluminescence and thermoluminescence studies.

Three undoped II-VI semiconductor quantum dots samples, namely ZnS, CdS and ZnO and two doped samples viz. Cu doped ZnS quantum dots (ZnS:Cu) and Fe doped ZnS quantum dots (ZnS:Fe) are investigated. The average size of the particles obtained from XRD, Optical absorption and TEM has been found almost similar for a particular sample. The blue shifted absorption edge obtained for the samples is the signature of size quantization.

It is significant that, the size of the particle has been successfully controlled by varying pH value of the solution and the surface temperature and found that the sample having higher pH value and temperature has smaller particle's size.

The photoluminescence studies of Cu doped ZnS and Fe doped ZnS quantum dots systems show enhanced luminescence intensity. Three distinct luminescence peaks are seen in luminescence spectra of ZnS:Cu quantum dots system. The peak at 480 nm is obtained due to transition from conduction band to an intermediate level of excited copper ion in the band gap of ZnS. This luminescence intensity at 480 nm is very sharp in comparison to other two luminescence peaks obtained, one due to donor-acceptor pair emission and other due to presence of surface states. However three observed peaks in luminescence spectra of Fe doped ZnS quantum dots sample are not very sharp in comparison to that in Cu doped ZnS. From the thermoluminescence study it is found that CdS sample contains deep surface states.

The effects of ion-beam irradiation on some doped quantum dot samples are discussed. Two doped samples (ZnS:Cu and ZnS:Fe) and undoped ZnS quantum dots samples have been irradiated with 150 MeV Ti ion selecting four different ion fluences. The sharp and enhanced luminescence peaks are observed in the photoluminescence spectra of the samples irradiated with higher fluence. The magnetic force microscopic (MFM) study has been carried out to find some magnetic properties for possible electrical applications. The aligned and elongated domains obtained in the sample irradiated with higher ion fluence have got application in magnetic tapes and magnetic recording.

By fabricating Schottky junctions of Ag and nano ZnS and Ag and Cu doped nano ZnS the electrical properties are studied in the form of I - V and C - V characteristics at different frequency range. It is observed that the trapped carriers play dominant role in current growth at higher frequencies. Further, current establishment in these devices is dependent either on signal frequency or on doped element.

The photo induced current measured (against applied electric field) in nano ZnS/Polyaniline composite shows higher rate of growth irradiated with laser. This device shows interesting class of field dependent charge generation and photo conductive property. When irradiated with laser, the nano crystals in conducting polymer, isolated from each other are responsible for the charge generation and the polymer is responsible for subsequent charge transport.

The nonlinear nature corresponding to charging and discharging within a given range of forward bias for highly ordered quantum dots has been reported to have application in single electron device, nano junction diode etc. This property is observed in I - V studies for different frequency range. Further fast photo induced current observed in nano ZnS/Polyaniline composite is very important criteria for electro photographic application. On

the other hand the sharp rise in current in high frequency range and in Cu doped nano ZnS/Ag junction is a strong candidate for fast switching. Moreover utilizing the photoluminescence property of the nanoparticles the quantum dots can be used as frequency converter and optical switch.

In comparison with other compound semiconductors, II-VI semiconductors possess high value exciton binding energies (and that is why excitonic absorption can be visible at room temperature) and therefore, further research is essential in the areas of single electron devices, fast optical switching. The research on electrical properties of ion irradiated samples will also open the door in this respect.

DECLARATION

I hereby declare that the thesis entitled '**Synthesis of Quantum dots in polymer matrix and study of their electrical properties for various device application**' being submitted to Tezpur University, Tezpur, Assam in partial fulfillment of the requirements for the award of the Degree of Doctor of Philosophy is a record of research work done by me during the Ph.D. course. This work has not been submitted in part or full for the award of any degree, diploma, associateship, fellowship or any other similar title or recognition from any other institute or organization.

Date: 4.1.07

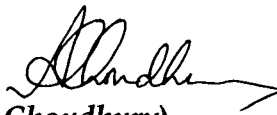
Arun K. Bordoloi
(Arun Kumar Bordoloi)
Department of Physics
Tezpur University
Tezpur-784 028(Assam)

CERTIFICATE

This is to certify that the thesis entitled "**Synthesis of Quantum dots in polymer matrix and study of their electrical properties for various device applications**" submitted to the Tezpur University in the Department of Physics, under the School of Science and Technology, in partial fulfillment for the award of the degree of Doctor of Philosophy (Ph.D.) in Physics is a record of research work carried out by **Mr. Arun Kumar Bordoloi** under my personal supervision and guidance.

All helps received by him from various sources have been duly acknowledged.

No part of this thesis has been reproduced elsewhere for award of any other degree.


(A. Choudhury)

Professor

School of Science and Technology

Department of Physics

Date: 4.1.2007

Place: Napaam, Tezpur

CONTENTS

1 INTRODUCTION	1
1.1 CHARACTERISTIC FEATURES OF QUANTUM DOTS.....	2
1.1.1 <i>Properties of quantum dots</i>	6
1.1.2 <i>Theoretical Support.....</i>	8
1.2 MOTIVATION OF THE WORK.....	13
1.3 OVERVIEW OF THE WORK	14
REFERENCES	16
2 SYNTHESIS OF II-VI SEMI CONDUCTOR QUANTUM DOTS.....	19
2.1 PROPERTIES OF POLYMER MATRICES USED.....	23
2.1.1 <i>Polyvinyl alcohol (PVOH).....</i>	23
2.1.2 <i>Polyaniline.....</i>	25
2.2 CHEMICAL SYNTHESIS.....	26
2.2.1 <i>Synthesis of CdS quantum dots with PVA matrix.....</i>	26
2.2.2 <i>Fabrication of ZnS quantum dots.....</i>	27
2.2.3 <i>Synthesis of Cu doped and Fe doped ZnS quantum dots.....</i>	27
2.3 QUENCHING METHOD.....	28
2.3.1 <i>Preparation of ZnO quantum dots using PVOH matrix (Quenchung method).....</i>	28
REFERENCES	30
3 CHARATERIZATION.....	32
SIZE DETERMINATION	33
3.1.1 <i>X-Ray diffraction</i>	33
3.1.1.a <i>Sample identification :</i>	35
3.1.1.b <i>Size Estimations:</i>	35

3.1.2	<i>Optical absorption</i>	41
3.1.2.a	<i>Information about band gap:</i>	41
3.1.3	<i>Transmission electron microscopy</i>	46
3.2	SURFACE STATES	49
3.2.1	<i>Photoluminescence</i>	49
3.2.1.1	<i>Photoluminescence of ZnS quantum dots</i>	50
3.2.1.2	<i>Photoluminescence of Cu doped ZnS (ZnS:Cu) quantum dot</i>	52
3.2.1.3	<i>Photoluminescence of Fe doped ZnS (ZnS:Fe) quantum dot</i>	54
3.2.2	<i>Thermoluminescence</i>	55
3.2.3	<i>A Schematic Luminescence Model</i>	56
3.3	SUMMARY	59
	REFERENCES	61
4	EFFECT OF SWIFT HEAVY ION IRRADIATION	63
4.1	ENERGY LOSS AND STRUCTURAL MODIFICATION	64
4.2	BRIEF REVIEW OF ION BEAM INTERACTION	65
4.2.1	<i>Ion Matter Interaction:</i>	65
4.2.2	<i>Fluence:</i>	67
4.3	CHARACTERIZATION OF IRRADIATED SAMPLES	71
4.3.1	<i>Sample: Cu Doped Zinc Sulfide (Zns:Cu)</i>	71
4.3.1.1	<i>X-Ray Diffraction:</i>	71
4.3.1.2	<i>Tem Study:</i>	73
4.3.1.3	<i>Optical Absorption Study:</i>	73
4.3.1.4	<i>Photoluminescence:</i>	76
4.3.2	<i>Sample: Fe Doped Zinc Sulfide (Zns:Fe)</i>	79
4.3.2.1	<i>X-Ray diffraction:</i>	79
4.3.2.2	<i>Transmission Electron Microscopy:</i>	81
4.3.2.3	<i>Magnetic Force Microscopy (MFM):</i>	81
4.3.2.4	<i>Photoluminescence:</i>	83
4.4	SUMMARY	87
	REFERENCES	89
5	ELECTRICAL PROPERTIES	91

5.1 FREQUENCY DEPENDENT CURRENT-VOLTAGE (I-V) AND CAPACITANCE-VOLTAGE (C-V) CHARACTERISTICS.....	93
5.1.1 <i>Depletion Region.....</i>	94
5.1.2 <i>Schottky Contact.....</i>	94
5.1.3 <i>I-V characteristics of nano ZnS/Ag.....</i>	96
5.1.4 <i>I-V characteristics of Cu doped ZnS qd/Ag.....</i>	98
5.1.5 <i>C-V characteristics of nano ZnS/Ag.....</i>	99
5.2. CAPACITIVE STRUCTURE.....	104
5.3 PHOTO INDUCED CURRENT.....	110
5.4 SUMMARY.....	112
REFERENCES.....	115
6 APPLICATIONS.....	117
6.1 ELECTRONIC SWITCHING.....	118
6.2 PHOTO DETECTOR.....	120
6.3 APPICATION AS VARIABLE CAPACITOR.....	121
6.4 OPTICAL SWITWING.....	122
6.5 SUMMARY.....	127
REFERENCES.....	129
CONCLUSIONS AND FUTURE PROJECTION.....	131
LIST OF PUBLICATIONS.....	135

LIST OF TABLES

1.1 Energy levels of a spherical quantum dot of radius R	11
2.1 Band gap energy and exciton binding energy of typical II-VI compounds and some other III-V compounds.....	22
2.2 Physical properties of dielectric PVOH.....	24
3.1 Samples with different temperature and pH value.....	37
3.2 Band gap and effective mass of different II-VI semiconductors.....	42
3.3 Comparison of particle sizes.....	49
4.1 Different fluence used along with time of exposure	68
4.2 Energy dependent electronic energy loss (S_e) and nuclear energy loss (S_n) for Ti- ions.....	69
4.3 Ion fluence and corresponding sample code for ZnS:Cu.....	71
4.4 Average particle sizes estimated for virgin and irradiated samples.....	72
4.5 Sizes of the particles calculated from TEM study.....	73
4.6 Optical spectroscopy data of ZnS:Cu samples.....	75
4.7 Ion fluence and corresponding sample code for ZnS:Fe.....	79
4.8 Particles' sizes of virgin and irradiated samples.....	80
6.1 Built-up voltage at different frequencies.....	120
6.2 Ion fluence and corresponding sample code for ZnS:Cu.....	124
6.3 Wave length detection range with output luminescence of different ZnS:Cu samples.....	125
6.4 Ion fluence and corresponding sample code for ZnS:Fe.....	126
6.5 Wave length detection range with output luminescence of different ZnS:Fe samples.....	126

LIST OF FIGURES

1.1 Density of states for ideal crystal structures having different dimensions	3
1.2 The effect of size on the electronic structure of a semiconductor crystal for three different size-ranges.....	5
1.3 Absorption and emission spectra of ZnS quantum dots.....	8
1.4 Exciton formation in a spherical quantum dot having di- electric constant ϵ_r embedded in a matrix of dielectric constant ϵ_d	9
2.1 Cadmium sulphide quantum dots dispersed in PVOH.....	23
2.2 Structure of polyaniline.....	25
3.1 XRD pattern.....	34
3.2 Single XRD peak.....	34
3.3 XRD Images of different ZnS quantum Dot Samples.....	37
3.4 XRD peak for (a) CdS quantum dots (b) bulk CdS.....	38
3.5 XRD peak for ZnO quantum dot.....	39
3.6 XRD peak of ZnS:Cu quantum dot.....	40
3.7 XRD peak of ZnS:Fe quantum dot.....	40
3.8 Absorption spectra of ZnS quantum dot & bulk ZnS (a)for S1,(b) for S2 and (c) for bulk.....	43
3.9 Optical absorption spectra of (a) CdS, (b) ZnO quantum dots.....	45
3.10 Optical absorption spectra of ZnS:Cu quantum dot.....	46
3.11 TEM image of (a) Sample S1 and (b) Sample S2 of ZnS qd.....	47
3.12 TEM image of (a) CdS (b) ZnO quantum dot.....	47
3.13 TEM image of (a) ZnS:Cu (b) ZnS:Fe quantum dots.....	48

3.14 PL spectra of ZnS qd (a) S1 (b) S2.....	51
3.15 PL spectra of ZnS:Cu quantum dot.....	52
3.16 Schematic energy level diagram for (a) bulk ZnS nano, (b) undoped ZnS nano and (c) copper doped ZnS nano.....	53
3.17 PL spectra of ZnS:Fe quantum dot.....	54
3.18 A schematic model for the size dependence of the fluorescence of the surface states in semiconductor nanoparticles.....	57
3.19 Thermoluminescence glow curve of (a) ZnS qd (b) CdS qd.....	57
4.1 Ion irradiation beam hall of Materials Science beam line in Nuclear Science Centre, New-Delhi-110 067, India.....	70
4.2 XRD peaks for (a) S1, (b) S1d ₁ , (c) S1d ₂ and (d) S1d ₃	72
4.3 TEM image (a) for sample S1d ₁ , (b) for S1d ₂ and (c) for S1d ₃	73
4.4 Optical absorption of ZnS:Cu (a) virgin (b) 1 st fluence (2) 2 nd fluence (3) 3 rd fluence & (e) 4 th fluence.....	74
4.5 Photoluminescence spectra Of ZnS:Cu quantum dots (a) S1 (b) S1d ₁ (c) S1d ₂ (d) S1d ₃	76
4.5 (a & b) Photoluminescence spectra ZnS:Cu samples at fluence (a) 0, (b) 5x10 ¹⁰	77
4.5 (c & d) Photoluminescence spectra ZnS:Cu samples at fluence (a) 0, (b) 5x10 ¹⁰	77
4.6 XRD image of ZnS:Fe quantum dots (a) virgin (b) S2d ₁ (1st fluence) (c) S2d ₂ (2 nd fluence).....	80
4.7 TEM images for ZnS:Fe quantum dots (a) S2d ₁ (1st fluence) (b) S2d ₂ (2 nd fluence).....	81
4.8 Phase image of MFM for ZnS:Fe quantum dots (a) for sample S2 (b) for S2d ₁ (c) for S2d ₂ and (d) for S2d ₃	82
4.9 Photoluminescence spectra Of ZnS:Fe quantum dots (a) S2 (b) S2d ₁ (c) S2d ₂ (d) S2d ₃	84
4.9 (a,b and c) Photoluminescence spectra ZnS:Fe samples at fluence 0, 5x10 ¹⁰ and 2x10 ¹¹	85

4.10 Photoluminescence spectra Of ZnS quantum dots (a) virgin (b) 1 st fluence (c) 2 nd fluence (d) 3 rd fluence.....	86
5.1 Schematic energy band diagram of bulk (a) ZnS/Ag and (b) nano ZnS/Ag Schottky barrier.....	95
5.2 I-V characteristics of nano ZnS/Ag junction at frequency range 1 KHz-40 KHz.....	97
5.3 I-V characteristics of nano ZnS/Ag junction at frequency range 1 MHz-4 MHz.....	97
5.4 I -V characteristics of nano ZnS:Cu/Ag junction at freq. Range 1KHz-40 KHz.....	98
5.5 I -V characteristics of nano ZnS:Cu/Ag junction at freq. Range 1MHz-4 MHz.....	99
5. 6 C -V characteristics of nano ZnS/Ag junction.....	101
5.7 Diode Characteristics.....	102
5.8 Ideal Schottky behavior.....	102
5.9 Schematic diagram of capacitive structure of qd samples.....	105
5.10 Voltage-Impedance characteristics for ZnS qd (sample S ₁).....	105
5.11 Voltage-Impedance characteristics if ZnS qd (sample S ₂).....	106
5.12 Voltage-impedance characteristics of ZnS qd (SampleS ₃).....	106
5.13 Comparison of Frequency Vs Impedance curves for different capacitive structures of ZnS qd.....	107
5.14 C-V of nano ZnS (capacitive structure) at diff. Frequencies.....	108
5.15 C-V curves of CdS qd (capacitive structure) at different frequencies.....	108
5.16 Capacitance-frequency curves for ZnS qd (capacitive structure) at different voltage.....	109
5.17 Schematic diagram of the sample for measuring photo induced current.....	111
5.18 Charge generation in nano (a) nano ZnS/polyaniline (with laser) (b) nano ZnS/polyaniline (without laser) (c) polyaniline.....	111

ACKNOWLEDGEMENT

At the very outset, I express my heartiest gratitude to my Supervisor Prof. Amarjyoti Choudhury, Department of Physics Tezpur University, Napaam, Tezpur, Assam, for his role as the philosopher and guide throughout the entire period of my Ph. D. work.

I am also grateful to all the faculty members and research scholars of the department of Physics for T.U. for giving me their timely support and encouragement.

I also acknowledge UGC, NERO, Guwahati for giving me fellowship for this research work.

Last but not the least; I must extend my gratitude to my wife, family members and many others whom I can not mention here for the dearth of space, without whom it would have been difficult to complete this research work.

Date: 4.1.07

Arun Kr. Bordoloi
(Arun Kumar Bordoloi)

Chapter 1

INTRODUCTION

The wizardry of modern semiconductor technology makes it possible to fabricate particles of metals or "pools" of electrons in a semiconductor that are only a few hundred angstroms in size. Electrons in these structures can display astounding behavior. Such structures, coupled to electrical leads through tunnel junctions, have been given various names: single electron transistors, quantum dots, zero-dimensional electron gases and coulomb islands. Like natural atoms, these small electronic systems contain a discrete number of electrons and have a discrete spectrum of energy levels.

Recently semiconductor nanostructures have received much attention from chemists and physicists in the last decade due to the fact that their electrical and optical properties are very different from those of bulk semiconductor crystals. The optical and electrical properties of semiconductor nanostructures can be tailored to a large extent by the dimensions of the crystals. The various effects that occur due to spatial confinement of electrons in such structures are of scientific importance. In addition, semiconductor nanostructures are very promising for a number of applications in the opto-electronic industry. Semiconductor nanostructures will show size-dependent properties different from those of a macroscopic semiconductor if one or more dimensions of the structure are in the same range as the length scale of a physical quantity (e.g. wavelength of light, wavelength of electrons, electrostatic length scales).

1.1 Characteristic features of quantum dots

A crystalline material of which size is restricted in three dimensions such that the electron wave functions are confined within its volume is called a quantum dot (QD). Due to this confinement the electronic properties of quantum dots depend on their size in the nanometer regime.^{1,2} This effect, now called 'size-quantization', was first observed in 1926 with CdS colloids³, but was only properly recognized in the 1980's.^{4,5} Chemists and physicists have studied nanostructures extensively in the past two decades in order to understand the size-quantization effects in semi conducting and metal quantum dots. Due to their extremely small sizes and their interesting electronic properties, quantum dots are promising building blocks for the fabrication of electronic and optoelectronic solid state devices. Integrated circuits (ICs) might be further miniaturized by using nano crystallites.

The main feature of quantum dots (QD)s is real discrete energy spectrum of electrons and holes. In quantum well (QW) carriers are confined only in one direction (Figure 1.1) while in the plane of QW their motion is free and is characterized by continuous energy spectrum. In quantum wire (QWR), carriers freely move along its axis. It means those carrier energy spectra in QWs and QWRs are continuous and there is overlapping of energies of confined states and delocalized states. Such overlapping results in very fast processes of carrier transition between confined and delocalized states as well as between ground and excited states.

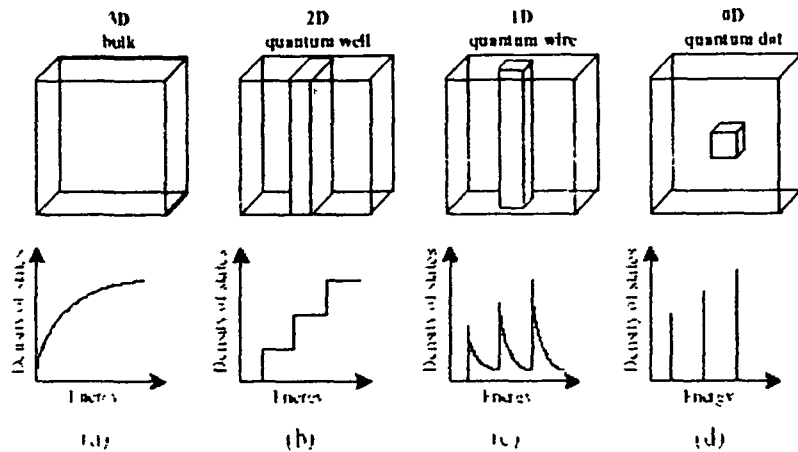


Figure 1.1 Density of states for ideal crystal structures having different dimensions: (a) three-dimensional or bulk, (b) two-dimensional or quantum well, (c) one-dimensional or quantum wire and (d) zero-dimensional or quantum dot.

The II-VI nano crystals have a band gap which can be tuned in a broad range (up to 4 eV) by changing either their size or chemical composition; this makes them suitable candidates for applications as a Light Emitting Diode (LED) ^{6, 7}, a Single Electron Transistor (SET) ⁸⁻¹⁰, chromophores in solar cells¹¹⁻¹⁵, or as a 'building block' for photonic crystals¹⁶. Recently, a LED with an efficiency of 10 %, based on CdSe nanocrystals in a semi conducting polymer matrix, was fabricated^{17,18}. The output colour could be tuned in the entire visible range. A critical parameter for the performance of a SET, the principle of which is based on the Coulomb blockade effect, is the capacitance of the quantum dot, which is determined by its size. Quantum dots can be applied as stable fluorescent indicators in biological research; core-shell quantum structures of CdSe/ZnS have a very high luminescence quantum yield (up to 100%). Since they can

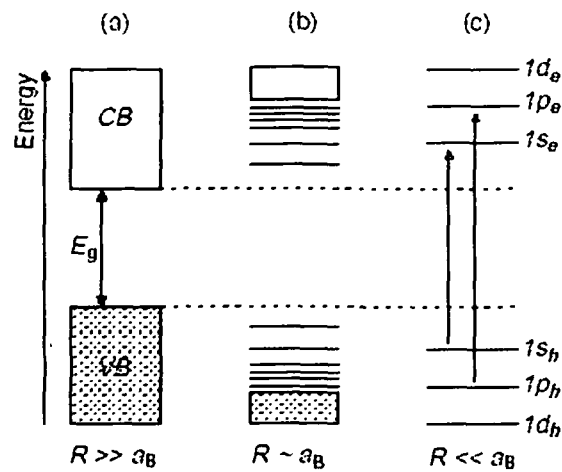
easily be attached to DNA¹⁹ or proteins by a sulphide bond they can act as a luminescent label to monitor biological reactions. Semiconductor colloids can also be employed in photo catalysis; TiO₂ colloids irradiated with UV-light can photo-oxidize organic contaminants²⁰. Methods for the preparation of large quantities of well-defined nanoparticles have been developed in order to study the size-quantization effect. A technique to grow low-dimensional structures, Molecular Beam Epitaxy (MBE), was developed at the end of the 1960's^{21, 22}. Arrays of quantum dots on substrates can be prepared by MBE or lithographic dry-etching²³⁻²⁴. Alternatively, quantum dots can be formed in the gas phase by laser vaporisation²⁴ or as colloids in suspension^{25, 26}. Chemists have succeeded in greatly improving the mono dispersity in size and shape of colloidal semiconductor quantum dots in the past decade²⁷. High-quality suspensions can now be synthesized and the size distribution can be further narrowed by size-selective precipitation or photoetching²⁸⁻³⁰.

In quantum dots the electron and hole, confined in a space with dimensions smaller than the Bohr radius of the exciton, cannot however be considered as independent particles; the Hamiltonian must be expanded by two-particle kinetic terms and the Coulomb and confinement potential. This leads in the Brus model to an expression for the energy of the ground state of the electron-hole pair (1s_e1s_h or first excited state),

$$E(1s_e, 1s_h) = E_g + \frac{\pi^2 \hbar^2}{2m_0 R^2} \left(\frac{1}{m_e^*} + \frac{1}{m_h^*} \right) - A \frac{e^2}{4\pi\epsilon_0 \epsilon_s R} \quad (\text{Eq 1.1})$$

in which the second term describes confinement and the third the Coulomb electron-hole interaction. The coefficient A corresponds to 1.786 for the

$1s_e1s_h$ state and has values between 1.6 and 1.9 for other states.³¹. The equation implies that the gap between the filled valence band levels and the empty conduction band levels increases when the radius of the particle decreases. Due to the electron-hole Coulomb interaction, the measured optical band gap has a slightly lower energy than the 'actual' electronic band gap.



1. Figure 1.2 The effect of size on the electronic structure of a semiconductor crystal for three different size-ranges. (a) a macro crystalline semiconductor ($R \gg a_B$). (b) Semiconductor nanocrystal with a weak size-quantization ($R \sim a_B$) (c) highly quantized dot ($R \ll a_B$) with discrete atomic-like energy levels and optical transitions

The figure 1.2(a) shows a macro crystalline semi conductor ($R \gg a_B$) with continuous energy band with filled valence band (VB) and empty conduction band (CB) and the band gap energy.

Weakly quantized quantum dots with $R \sim a_B$ contain a large number of atoms and unit cells, therefore Bragg reflection at the periodic lattice lead to continuous energy levels. Only the levels at the top of the valence band and bottom of the conduction band, which corresponds to the most delocalised electron wave function, will be discrete (figure 1.2 b).

ultimately influences the luminescence property³⁸. The fast trapping and detrapping process of electrons in the traps is useful for fast optical switching.

(v) Change in optoelectronic and electronic property:

Unlike bulk material, electronic transition between surface states and valance band as well as surface states and conduction band is faster rather than band edge transition. This is due to fast trapping and detrapping of charge carriers by surface states³⁵. This property of quantum dots makes it very efficient for fast optical and photonic

The increase of the band gap and the transition from continuous energy bands to discrete energy levels upon a decrease of particle size has been observed by optical absorption spectroscopy in many semiconductor systems.^{23,39} The absorption and emission spectra of different II-VI semiconductor (ZnS, CdS) quantum dots of different sizes were studied in this work. Upon a decrease of the particle radius, the onset of the absorption and the emission maximum shift towards higher energies. A clear structure in the absorption spectra is observed for the smallest particles, corresponding to discrete optical transitions.

The figure 1.2(c) shows the discrete atomic like energy levels for highly quantised semiconductor quantum dots.

1.1.1 Properties of quantum dots

Due to quantum confinement quantum dots exhibit the following properties

(i) Enhancement in band gap:

As a consequence of quantum confinement, the continuum of states in conduction and valance band are broken down into discrete states with energy spacing relative to the band edge, which is approximately inversely proportional to the square of the particle radius resulting in widening the band gap in comparison to the band gap of the bulk³².

(ii)Blue shift:

As the band gap of quantum dot enhances, the strong absorption of optical signal occurs in UV or shifts towards UV region. That is why quantum dot possess blue shift in UV /VIS absorption spectra³³⁻³⁷

(iii) Large surface to volume (S/V) ratio:

Another important property associated with quantum dot is the existence of large surface to volume ratio (S/V) which results in producing electronic states within the band gap of the semiconductor. These are called surface states, commonly called 'Trap'³⁵.

(iv) Change in photoluminescence property:

Due to the occurrence of surface states unlike in bulk specimen, in quantum dot excited electrons are captured by the surface states, either before or after the direct radiative recombination which

ultimately influences the luminescence property³⁸. The fast trapping and detrapping process of electrons in the traps is useful for fast optical switching.

(v) Change in optoelectronic and electronic property:

Unlike bulk material, electronic transition between surface states and valance band as well as surface states and conduction band is faster rather than band edge transition. This is due to fast trapping and detrapping of charge carriers by surface states³⁵. This property of quantum dots makes it very efficient for fast optical and photonic switch.

The increase of the band gap and the transition from continuous energy bands to discrete energy levels upon a decrease of particle size has been observed by optical absorption spectroscopy in many semiconductor systems.^{28,39} The absorption and emission spectra of different II-VI semiconductor (ZnS, CdS) quantum dots of different sizes were studied in this work. Upon a decrease of the particle radius, the onset of the absorption and the emission maximum shift towards higher energies. A clear structure in the absorption spectra is observed for the smallest particles, corresponding to discrete optical transitions.

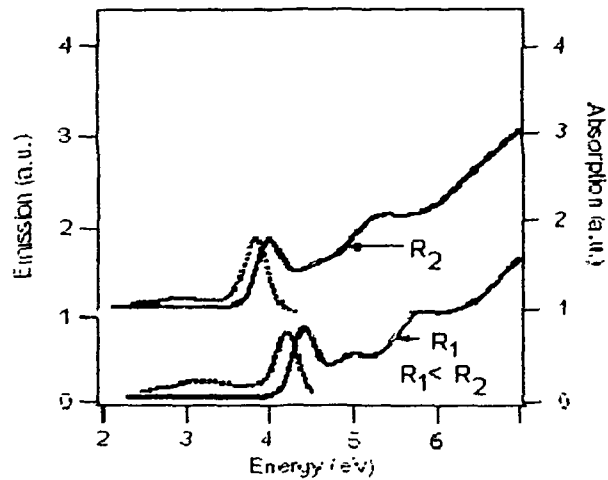


Figure 1.3 Absorption (solid lines) and emission (dotted lines) spectra of ZnS quantum dots, showing that the absorption edge shifts towards higher energies with respect to bulk ZnS (3.54 eV) and that discrete energy bands become more pronounced as the particle size decreases.

The figure 1.3 shows the absorption and emission spectra of ZnS quantum dots. The absorption edge shifts towards higher energy with respect to that of bulk ZnS.

1.1.2 Theoretical Support

The Mott-Wannier exciton is a weakly bound e^-h^+ pair created by photons coupled to a material (figure-1.4). It can be represented in a simple hydrogen like picture, it has energy levels E_n proportional to n^{-2} ($n = 1, 2, 3..$). The corresponding Bohr orbital have the radii $R^{(n)}$ in units of nm given by

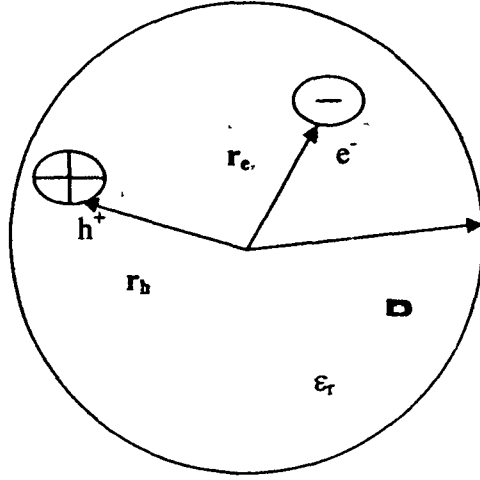


Figure 1.4 Exciton formation in a spherical quantum dot having dielectric constant ϵ_r embedded in a matrix of dielectric constant ϵ_d

$$R^{(n)} = 0.5 \frac{\epsilon_r}{m^*} n^2 \quad (\text{Eq 1.2})$$

where ϵ_r is the relative dielectric constant of the material, m^* is the reduced effective mass of the electron and hole in units of the rest mass (m_0) of the electron and is given by

$$\frac{1}{m^*} = \frac{m_0}{m_e} + \frac{m_0}{m_h} \quad (\text{Eq 1.3})$$

Let us consider a semi conducting material in the form of a sphere of radius R , which is of the order of (or less than) the first Bohr radius of the exciton, $R^{(1)}$. Then the exciton states will surely depend on the magnitude of R . We term such samples as spherical quantum dots. The exciton Hamiltonian is the sum of the kinetic energies of electron and hole, the Coulomb interaction energy (V_c) of the e^-h^+ pair, the potentials $V_e(r_e)$ and $V_h(r_h)$ experienced by the electron and the hole respectively due to the barrier. Thus, we write

$$H = -\frac{\eta^2}{2m_e} \nabla_e^2 - \frac{\eta^2}{2m_h} \nabla_h^2 + V_C + V_e(r_e) + V_h(r_h) \quad (\text{Eq 1.4})$$

subject to the confinement potential for the quantum dot given by

$$V(r_i) = 0, \text{ for } r_i < R, \quad (i = e, h) \quad (\text{Eq 1.5})$$

$$V(r_i) = \infty, \text{ for } r_i > R, \quad (i = e, h) \quad (\text{Eq 1.6})$$

Neglecting the coupling between electron and the hole ($V_c = 0$) one can represent the exciton wave function as a product of the individual particle wave functions expressed by

$$\psi(r_e, r_h) = \varphi_e(r_e) \cdot \varphi_h(r_h) \quad (\text{Eq 1.7})$$

where $\varphi_e(r_e)$ and $\varphi_h(r_h)$ being electron and hole wave functions respectively. The individual wave functions for the electron and the hole are given in terms of Bessel functions and spherical harmonics, which read as ^{38, 39, 40}

$$\varphi_{lmn}(r) = \left(\frac{2}{R^3} \right)^{1/2} \frac{J_l(\alpha_{nl}(r/R))}{J_{l+1}(\alpha_{nl}(r/R))} Y_{lm} \quad (\text{Eq 1.8})$$

The quantum numbers l , m and n are restricted to $-l \leq m \leq l$; $l = 0, 1, 2, \dots$; $n = 1, 2, 3, \dots$. Here J_l are the Bessel functions of order l , and Y_{lm} are spherical harmonics. α_{nl} is the n^{th} zero of the spherical Bessel function of order l .

The spherical Bessel functions, $j_l(x)$, are related to the Bessel functions of the first kind

$$j_l(x) = \left(\frac{\pi}{2x}\right)^{1/2} J_{l+1/2}(x) \quad (\text{Eq 1.9})$$

The values of α_{nl} and corresponding energy levels are given in Table 1.1

Table 1.1 Energy levels of a spherical quantum dot of radius R

n	l	level	$\alpha_{n,l}$	E_h	E_e
1	0	1s	3.1416	$-\frac{9.86965}{m_h} \left(\frac{\eta^2}{2R^2}\right)$	$-\frac{9.86965}{m_e} \left(\frac{\eta^2}{2R^2}\right) + E_g$
1	1	1p	4.4934	$-\frac{20.19064}{m_h} \left(\frac{\eta^2}{2R^2}\right)$	$-\frac{20.19064}{m_e} \left(\frac{\eta^2}{2R^2}\right) + E_g$
1	2	1d	5.7635	$-\frac{33.21793}{m_h} \left(\frac{\eta^2}{2R^2}\right)$	$-\frac{33.21793}{m_e} \left(\frac{\eta^2}{2R^2}\right) + E_g$
2	0	2s	6.2832	$-\frac{39.47860}{m_h} \left(\frac{\eta^2}{2R^2}\right)$	$-\frac{39.47860}{m_e} \left(\frac{\eta^2}{2R^2}\right) + E_g$
2	1	2p	7.7253	$-\frac{59.68026}{m_h} \left(\frac{\eta^2}{2R^2}\right)$	$-\frac{59.68026}{m_e} \left(\frac{\eta^2}{2R^2}\right) + E_g$
2	2	2d	9.0950	$-\frac{82.71902}{m_h} \left(\frac{\eta^2}{2R^2}\right)$	$-\frac{82.71902}{m_e} \left(\frac{\eta^2}{2R^2}\right) + E_g$

As the potential at the surface of the spherical quantum dot suddenly becomes infinite, the chance of finding the electron there must be nil.

Mathematically, this can be represented as a boundary condition on the solution of the wave equation stated as

$$\left. \varphi_i(r) \right|_{r=R} = 0 \quad (\text{Eq 1.10})$$

so that one can obtain energy levels for the electron and hole given by

$$E_{n,l}^{e,h} = \frac{\eta^2}{2m_{e,h}} \left(\frac{\alpha_{n,l}^2}{R^2} \right) \quad (\text{Eq 1.11})$$

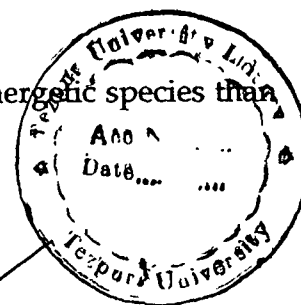
To understand the above facts more precisely, we consider a specific example by assuming a spherical CdS quantum dot of radius R nm having bulk band gap $E_g = 2.42$ eV at room temperature. For CdS system, $m_h = m_0$, $m_e = 0.667 m_0$. Then, the energy values (in eV units) may be usefully expressed for the various states (n, l) in terms of R by³⁷

$$E_{n,l}^h = - \left(\frac{0.0382}{\frac{m_h}{m_0} R^2} \right) \alpha_{n,l}^2 \quad (\text{Eq 1.12})$$

$$E_{n,l}^e = - \left(\frac{0.0382}{\frac{m_e}{m_0} R^2} \right) \alpha_{n,l}^2 + E_g \quad (\text{Eq 1.13})$$

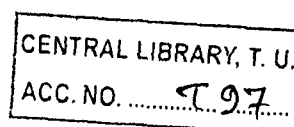
Quantum mechanics selection rules state that the electron jumps only to those levels that obey the conditions $\delta n = 0$ and $\delta l = 0$. In otherwords, $1s(h) \leftrightarrow 1s(e)$, $1p(h) \leftrightarrow 1p(e)$, etc. transitions are supposed to be allowed. That is why the absorption or emission spectra would exhibit a blue-shift as the size (R) of the quantum dot is suppressed³⁸. Therefore, electron inside a

high security jail (here quantum dot) becomes a more energetic species than outside due to band gap enhancement.



1.2 Motivation of the work

The aim of the research in this field is to look for a suitable chemical way for fabrication of quantum dots. Since different II-VI binary semi conducting materials have received much attention due to their various device applications, so these materials have been chosen and tested for fabrication. We have also planned to control the size of the particles by changing different factors like pH value, temperature and reaction time. We have chosen the chemical method for preparing the samples because of its simplicity of fabrication, possibility of large scale productions and possibility of doping of large number of materials (Mn, Ni, Fe, and Cu etc.) even at room temperature. We consider nano particles of semiconductors with sizes typically smaller than 10 nm, which is the range where size effects become observable. The quantum size effect (QSE) predicts the formation of a band gap with decreasing particle size for metals and widening of the intrinsic gap for semiconductors. The band gap for semiconductor quantum dots is usually quite well described by an extended effective mass approximation (EMA). This describes a band gap, which gradually increases for smaller sized particles. Therefore we have planned to characterize the prepared samples by various optical studies like optical absorption, X-ray diffraction, transmission electron microscopy, thermo luminescence and photoluminescence to know the particles' size, shape and formation of discrete energy levels within the band gap. The probing of the particles of nano scale and carrier transport in nano structured films is impossible due



to the presence of weak link boundaries. But things get improved if one has a few number of arrayed quantum particles separated by thin dielectric medium under the influence of high intensity light (basically, hi-power pulsed laser). The interfacial charge transfer could be detectable through photocurrent generation in the external circuit, connected to a biasing source. Previously, the interfacial charge transfer has been reported in coupled, coated and layered systems. In this work we want to study the various electrical properties of semi conductor quantum dots for potential use in electrical devices. For which we want to observe the role of interfacial charge transfer by studying frequency dependent electrical properties of nano ZnS/Ag and nano ZnS:Cu/Ag system in the form I - V and C - V characteristics across different ranges of frequency, since these unusual characteristics known as single electron effects are the prerequisites for single electron transistors (SET).

1.3 Overview of the work

In this work the optoelectronic properties of semiconductor quantum dots, and charge transfer between such structures and a conducting substrate were studied in a novel way. For this purpose, conducting polymer and conducting glass substrates were provided; the opto electrical properties of the systems were investigated by studying photo induced current.

An attempt has been made to synthesize II-VI semiconductor quantum dots. Because of the wide band gap and its efficiency in using with the device in the optical range from uv to visible upon quantum

confinement^{32, 33}. We have chosen these compounds. We have synthesized three undoped quantum dots (ZnS, CdS, ZnO) and two doped quantum dots (ZnS:Cu, ZnS:Fe). Further doped samples have been irradiated with ion beam to see the modification of properties of the particles.

The increase of band gap and the transition from continuous bands to discrete energy levels upon a decrease of particle size has been observed from optical absorption spectroscopy^{30, 34}. The presence of surface states has been confirmed from photoluminescence and thermo luminescence studies. The sizes and shapes of the dots have been obtained from X-ray diffraction (XRD) and Transmission electron microscopy (TEM). To observe any change in properties of quantum dots upon irradiation of ion beam, undoped and doped samples of ZnS quantum dots have been irradiated with 150 MeV Ti ion beam. The Atomic force microscopy (AFM) has been used to see the surface roughness. To exploit the magnetic properties Magnetic force microscopy (MFM) studies have been carried out. The electrical properties have been explored by studying V-Z characteristics for different capacitive structures of dots. From the studies *I-V* and *C-V* characteristics of nano ZnS/Ag and nanoZnS:Cu/Ag across different ranges of frequency, the role of interfacial charge transfer has been observed.

In chapter 2 the basic synthesis processes are summarized. The chapter 3 deals with the characterization of quantum dots. The effects of swift heavy ions on the samples are investigated in chapter 4. The electrical properties of quantum dots are discussed in chapter 5. The chapter 6 contains the applications of quantum dots. Finally the conclusion and perspectives for future investigations are mentioned in chapter 7.

References

1. S.V. Gaponenko, *Optical Properties of Semiconductor Nanocrystals* (1998), Cambridge University Press, United States of America.
2. MRS Bulletin, February (1998)
3. G. Jaeckel, *Z. Tech. Phys.*, **6**, 301 (1926)
4. A. Henglein, *J. Phys. Chem*, **86**, 2291-2293 (1982)
5. L.E. Brus, *J. Chem. Phys.*, **80**, 4403 (1984)
6. H. Mattoussi, L.H. Radzilowski, B.O. Dabbousi, D.E Fogg, R.R. Schrock, E.L. Thomas, M.F. Rubner, and M.G. Bawendi, *J. Appl. Phys.*, **86**, 4390 (1999)
7. Y. Yang, S. Xue, S. Liu, J. Huang, and J. Shen, *Appl. Phys. Lett.*, **69**, 377 (1996)
8. D.L. Klein, P.L. McEuen, J.E. Bowen Katari, R. Roth, and A.P. Alivisatos, *Appl. Phys. Lett.*, **68**, 2574 (1996)
9. M.A. Kastner, *Nature*, **389**, 667 (1997)
10. D.L. Klein, R. Roth, A.K.L. Lim, A.P. Alivisatos, and P.L. McEuen, *Nature*, **389**, 699 (1997)
11. H. Weller, *Advanced Materials*, **5**, 88 (1993)
12. J. Fang, J. Wu, X. Lu, Y. Shen, and Z. Lu, *Chem. Phys. Lett.*, **270**, 145 (1997)
13. S. Kohtani, A. Kudo, and T. Sakata, *Chem. Phys. Lett.*, **206**, 166 (1993)
14. C. Nasr, P.V. Kamat, and S. Hotchandani, *J. Electroanal. Chem.*, **420**, 201 (1997)
15. D. Liu, and P.V. Kamat, *J. Phys. Chem.* **97**, 10769 (1993)
16. Y.A. Vlasov, N. Yao, and D.J. Norris, *Advanced Materials*, **11**, 165 (1999)
17. V.L. Colvin, M.C. Schlamp, and A.P. Alivisatos, *Nature*, **370**, 354 (1994)

18. B.O. Dabbousi, M.G. Bawendi, O. Onitsuka, and M.F. Rubnar, *Appl. Phys. Lett.*, **66**, 1316 (1995)
19. A.P. Alivisatos, K.P. Johnsson, X. Peng, T.E. Wilson, C.J. Loweth, M.P. Bruchez jr, and P.G. Schultz, *Nature*, **382**, 609 (1996)
20. D.F. Ollis, H. Al-Ekabi, *Photocatalytic Purification and Treatment of Water and Air*, Elsevier Science Publishers 1993, Amsterdam, The Netherlands
21. J.R. Arthur, *J. Appl. Phys.*, **39**, 4032 (1968)
22. A.Y. Cho, *J. Vac. Sci. Technol.*, **8**, S31 (1971)
23. D. Heitmann, and J P. Kotthaus, *Physics Today*, **June**, 56 (1993)
24. M.A. Kastner, *Physics Today*, **January**, 24 (1993)
25. L. Spanhel, M. Haase, H. Weller, and A. Henglein, *J. Am. Chem. Soc.*, **109**, 5649 (1987)
26. M.L. Steigerwald, A.P Alivisatos, J.M. Gibson, T.D. Harris, R. Kortan, A.J. Muller, A.M. Thayer, T.M. Duncan, D.C. Douglas, L.E. Brus, *J. Am. Chem. Soc.*, **110**, 30460 (1988)
27. X. Peng, L. Manna, W. Yang, J. Wickham, E. Scher, A. Kadavanich, and A.P. Alivisatos, *Nature*, **404**, 59-61 (2000)
28. C.B. Murray, D.J. Norris, and M.G. Bawendi, *J. Am. Chem. Soc.*, **115**, 8706 (1993)
29. H. Matsumoto, T. Sakata, H. Mori, H. Yoneyama, *J. Phys. Chem. B*, **100**, 13781 (1996)
30. A. van Dijken, A. Meijerink, D. Vanmaekelbergh, *Chem. Phys. Lett.*, **269**, 494 (1997)
31. H.M. Schmidt, and H. Weller, *Chem. Phys. Lett.*, **129**, 615-618 (1986)
32. Al L Efrons and A L Efros *Sov. Phys Semicon.* **16**, 722 (1992)
33. R N Bhargava, D, Gallagher, X Hong, A Nurmikko. *Phys. Rev. Lett.* **72**, 3, 416 (1994)

34. L E Brus IEEE, *Quantum electron*, **72**, 416 (1994)
35. Wei Chen, Zhamguo Wang, Jhaojum Lin and laying; *Journal Of Applied Physics*, **82**, 2 (1997)
36. S Mahamuni, A S Brenrdre, J Lepert, C A Smith, D cook, S H Risfud and H W H Lee; *Nanostructured Material*, **7**, 6, (1996).
37. Y V G S Murti , P Nandakumar, C Vijayan, *Phys Edn* **99**.
38. S N Behra, S N Sahu, K K Nanda; *Indian J. Phys*, **74A(2)** (2000)
39. Stolz,G preprint (in Germany) *Mathematics Institute*, University Frakfurt,Germany (1989)
40. Efros,AI L and Efros AL *Sov. Semicond* **16**,772 (1982)

Chapter 2

SYNTHESIS OF II-VI SEMI CONDUCTOR QUANTUM DOTS

The prehistory of quantum dots began in the early 1970s with nanometer-thick foils called quantum well where charge carriers (electron and holes) become trapped in a few nanometer-thick layer of wells. By the end of 1970, nanostructures could be fabricated in such a way that the mesoscopic variation of the material composition gave rise to the desired electronic potentials, eigen energies, tunneling probabilities and optical absorption. The quantum engineering of microelectronics materials was promoted by the Nobel prizes awarded in 1973 to L. Esaki for the discovery of the tunneling in semiconductors and in 1985 to K. von Klitzing et al for the discovery of quantum Hall effect. Rapid progress was made in the development of epitaxial growth techniques: Molecular beam epitaxy (MBE) and chemical vapour deposition (CVD) made it possible to grow semiconductor crystals at one mono layer accuracy.

The other common methods to synthesize semiconductor quantum dots are

1. Vapor phase epitaxy
2. Magnetron sputtering
3. Radio frequency sputtering
4. Optical ablation and
5. Chemical method

Due to several advantages, chemical route is now-a-days followed for growing semiconductor nanoparticles. Before discussing the synthesis of our quantum dots, let us have an over view of the quantum dot preparation technique, adopted by other workers:

Y.C Zhang et al synthesized InAs quantum dots on GaAs substrate using RIBBER 32 MBE technique¹. S. Benerjee et al prepared ZnSe nanoparticles with d.c magnetron sputtering². Nayoki Veda et al used rf sputtering to obtain CdO nanostructure³. L patrone et al. fabricated Si nanoclusters by laser ablation⁴. Similarly, Y Marfaing used optical source to control the growth of ZnSe crystal⁵. Among these methods Chemical method for quantum dot preparation has been popular and adopted by many workers⁶. Here is an over view of that:

P Nandakumar et al and Y.V.G.S Murty et al. synthesized CdS quantum dot using polymer perfluoroethylene sulfonic acid⁷. Wei Chen et al prepared ZnS quantum dots where the particle size was varied by changing the reaction temperature⁸. S.B. Qadri et al synthesized ZnS quantum dots by using some lipids and surfactants that act like Matrix⁹. Similarly J. Nanda prepared ZnS nanocrystal with 1-thyglycolas capping agent¹⁰. Using poly vinyl pyrrolidane as capping. S. Mahamuni et al obtained ZnO quantum dot¹¹.

Both large scale synthesis and preservation of nanoparticles is important from application point of view. In order to improve rigidity and to protect nanoparticles from environmental attack, embedding them in glass, zeolites or in polymer is desired.

It is clear that the organic ligand environment used to encapsulate and passivate semiconductor nanoparticles is for future developments in the field, as the ligands establish the solution properties of the nanoparticles, aid in their luminescence by quenching surface defects and maintain their nanoscopic integrity by preventing aggregation¹²⁻¹⁵. One of the most promising topics in organic-inorganic hybrid materials is found in attempts to integrate semiconductor nano crystals and polymers. The unique properties of polymers, including their thermal behavior and ability to assemble into ordered structures, offer the potential for compatibilizing nanocrystals, directing their assembly and hence provide a mechanism for charge transport. Confirmation of theoretical predictions of the spatial distribution of nanoparticles within polymer hosts¹⁶ will to some extent depend on the interactions between the ligand periphery and the polymer environment. Indeed, polymer-nanocrystal composite materials are already finding applications ranging from electronically active materials to the biological sciences.¹⁷⁻²⁰

Since different II-VI binary semi conducting materials have received much attention due to their various device applications, so these materials have been chosen and tested for fabrication. Wide gap II-VI compounds are characterized by the direct band gap with either zinc blend or wurtzite structures and large exciton binding energy. The table 2.1 summarizes band gap energy and exciton binding energy of typical II-VI compounds and some other III-V compounds which have similar band gap energies. As a general tendency, the exciton binding energy of II-VI compounds is larger than that of III-V compounds with similar band gap energy. These properties make the materials very attractive both from scientific point of views and optical device application.

Table 2.1 band gap energy and exciton binding energy of typical II-VI compounds and some other III-V compounds

Compounds	Energy band gap at room temp. (eV)	Exciton binding energy (meV)
ZnO	3.37	60
ZnS	3.54	39
ZnSe	2.70	20
CdSe	1.74	16
GaAs	1.43	4.2
GaN	3.39	21

The synthesis of II-VI semiconductor quantum dots in Nafion® and Syrlin® membranes ²¹⁻²³ was satisfactorily done to obtain stable nanoparticles. We have selected wide and direct band gap II-VI group semiconducting systems, as such systems in reduced dimensionality case are capable of showing excitonic absorption even at room temperature due to enhancement in excitonic binding energies.

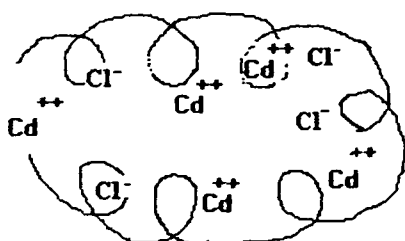
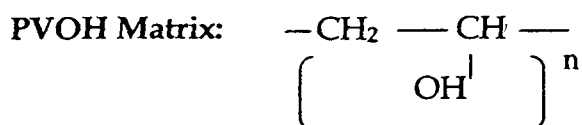
The chemical routes for the preparation of the samples have been opted because of its simplicity of fabrication, relatively shorter synthesis time, large scale production and possibility of doping. We have used polyvinyl alcohol (PVOH) as polymer matrix for sample preparation

2.1 Properties of polymer matrices used

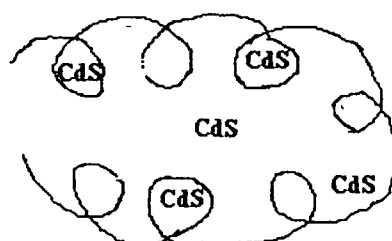
Structurally, the polymers possess arbitrary coil shaped shapes (figure-2.1). The free end groups, the number and size of the coils can be controlled as they depend on the molecular weight as well as synthesis parameters (concentration, density and nature of the solvent etc). Thus, they provide unique scope for atomic layer dispersion to form nanoparticles when a proper stoichiometry is maintained in choosing respective salts and solvents.

2.1.1 Polyvinyl alcohol (PVOH)

Unlike many polymers, it is a water soluble solid. It dissolves slowly in cold water but at higher temperature it goes fairly fast into the solution.



CdCl₂ mixed with PVOH solution



CdS dispersed in PVOH

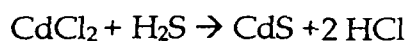


Figure 2.1 Cadmium sulphide quantum dots dispersed in PVOH

PVOH solution like starch solution, gives an intense blue colour reacted with iodine. PVOH is a good protective colloid for aqueous emulsions and is

employed for this purpose in a large variety of emulsion and suspension systems. It also finds use in wet strength adhesives. Further, it is used in the manufacture of textile fibres, where one major aspect to be taken care of is that the fibre as the final product should be made insoluble in water. PVOH fibres have excellent dimensional stability. They can be easily washed and dried. The fibres are also found to possess excellent resistance to abrasion and remarkable tenacity.

The physical properties of the polymer (PVOH) used in the fabrication process are given below in table-2.2.

Table 2.2 physical properties of dielectric PVOH

Physical properties	
Glass transition temperature (K)	343
Melting temperature (K)	413
Refractive index	1.55
Specific gravity	1.30
Specific heat (J/gm-K)	1.66
Thermal conductivity ($W m^{-1}K^{-1}$)	2.0
Molar mass a single structure unit (g)	58.2
Dielectric constant	2.0

2.1.2 Polyaniline

Polyaniline is composed of aniline repeat units connected to form a backbone of alternating nitrogen atoms and benzene rings. In the last few years, polyaniline has emerged as the class of conducting polymers with the highest potential for technological applications as this material combines ease of process ability, is of synthesis, satisfactory environmental stability and chemical versatility. Polyaniline is found to be suitable for a number of applications in computer manufacturing processes. Polyaniline can play significant roles in the lithographic processes used to fabricate integrated circuits. Thin films of conducting polyaniline are found to be effective discharge layers for electron- beam lithography. Polyaniline provides attractive chemical flexibility and processing options, including secondary doping. It also provides an opportunity for use in welding of thermoplastics and thermosets. The structure of polyaniline is shown in figure 2.2.

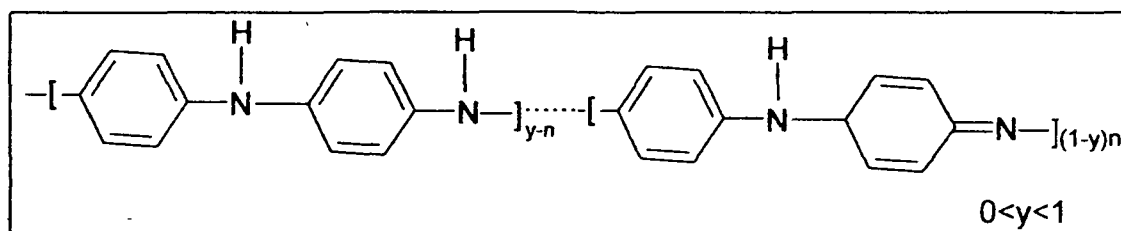


Figure 2.2 Structure of polyaniline

We have grown the following quantum dots in the dielectric host matrices by chemical processes. The sizes of the nano particles have been controlled by varying pH value and surface temperature.

Sample prepared

1. ZnS
2. CdS
3. ZnO
4. ZnS:Cu (Copper doped ZnS)
5. ZnS:Fe (Iron doped ZnS)

Substrate used: Simple glass and ITO glass

Matrix used: Polyvinyl alcohol (PVA), Poly aniline

2.2 Chemical synthesis

2.2.1 *Synthesis of CdS quantum dots with PVA matrix*

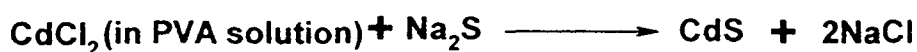
5 grams of PVA were measured by using digital balance [Mettler Toledo SNR-11170663322] and then put into 100 ml double distilled (D/D) water. Then the whole solution was stirred in a magnetic stirrer with stirring rate of 200 rpm at constant temperature of 70 ° C for three hours. Thus a transparent D/D water solution of PVA was prepared. Next the solution has been put in dark chamber at room temperature for 12 hours. This solution is called 5 wt% solution of PVA.

In parallel 2 gms of CdCl₂ powder was mixed with 100 ml D/D water by means of stirring for half an hour at the rate of 50 rpm, at 40°C. Like PVA solution, this solution was put in the same condition.

Also 2wt % solution of Na₂S was prepared just by mixing 2 gms Na₂S with 100 ml D/D water.

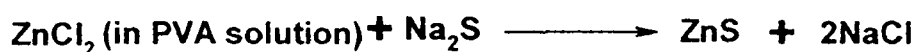
Next, PVA solution and CdCl₂ solution were mixed in the volume ratio of 2:1 and stirred at the speed of 250 rpm at a constant temperature of 55°C, then Na₂S solution was put into it, by means of a dropper up to its maximum absorbance i.e. unless the whole solution turns yellow. This solution was again put in a dark chamber at room temperature for 12 hours for its stabilization.

After that, it was cast over the glass substrate and then dried in oven at 50°C. This film contains CdS quantum dot embedded in the PVA matrix.



2.2.2 Fabrication of ZnS quantum dots

The aqueous solution of 6 wt % of poly vinyl alcohol (PVA), 2 wt % of Zinc chloride (ZnCl₂) and 2wt % of Sodium sulfide (Na₂S) were prepared and then PVA solution and ZnCl₂ solutions were mixed in the ratio of 2:1. The solution was then stirred at a constant stirring rate for 4 hours and Na₂S solution was dropped up to maximum absorbency and kept in a dark chamber for 12 hours. The film was deposited over glass substrate and dried in oven. The particle sizes were controlled by varying the surface temperature and pH value.



2.2.3 Synthesis of Cu doped and Fe doped ZnS quantum dots

ZnCl₂ and CuCl₂ aqueous solutions were prepared and mixed in a ratio 99.5:0.5. This solution was then mixed with aqueous solution of 7.5 wt %

PVOH in ratio 1:2 and stirred for 4 hours at constant temperature. After adding Na₂S solution drop wise up to maximum absorbency it was kept for 24 hours for casting on glass substrate. For doping iron the same procedure was adopted, but 0.01% (by volume) of FeCl₃ was added to 50 % (by volume) of ZnCl₂

2.3 Quenching Method

In quenching method bulk semi conductor is heated at a very high temperature (below its melting point) for a long period of time and then immediately put into a very cold host (matrix.). Sudden cooling will cause the fragmentation of the material into smaller parts in 'nm' range and then enter into the gap of matrix, to produce nano structure (quantum dots). In this method the particle size can be varied by changing -

- i) The temperature at which bulk material is heated
- ii) The heating duration
- iii) The temperature of the host matrix.

2.3.1 Preparation of ZnO quantum dots using PVOH matrix (Quenching method)

0.05 g-mol ZnO powder (99.99% pure, Merck) was taken in a quartz crucible and heated in a furnace slowly up to a maximum temperature of 800 °C for 6 hours in N₂ atmosphere. 8 wt% aqueous PVOH was made and kept in a specially designed ice-cold environment. The sintered powder was quenched into the aqueous PVOH followed by moderate stirring for about 2 hours. The whole process was carried out in a dark room to avoid the effect of light exposure on the growth mechanism of quantum crystals of ZnO in the polymer host matrix.

The sample is heated gradually until the temperature reaches to 800^o C. Initially the temperature is increasing with heating period and once it reaches the desired temperature (800^o C) then maintained at that temperature , after that it is constantly heated for 6 hours keeping the temperature fixed.

References

1. Y C Zhang, C J Huag, F A Liu, Z G Wang; *Journal Of Applied Physics*, **90**, 4 (2001).
2. S Benergee, R Pal, A B Mity, S Choudhury and A K Pal; *Nanostructured material*, **18**, 3 (1997)
3. Nayuki Veda, Hirro and Hiroshi Kawazoe; *Journal Of Applied Physics*, Vol **84**, 11 (1998)
4. L Patrone, D Nelson and marine; *Journal Of Applied Physics*; **87** (2000)
5. Y Marfaing, Senicound. Sci, Semicond sciency; *Semicond. Sci Techno* **6** (1999)
6. D. Mohanta, S K Dolui and A Choudhury; *Indian J Phys*, **75** (A), (2001)
7. Y V G S Murti, P Nandakumar, C Vijayan, *Phys Edn* **99**.
8. Wei Chen, Zhamguo Wang, Jhaojum Lin and laying; *Journal Of Applied Physics*. **82**, 2 (1997)
9. S B Qadri and E F Skeltion; *Journal Of Applied Physics*, **89**, 1 (2001)
10. J Nanda, D D Sarma, *Journal applied Physics*, **90**, 5 (2001)
11. S Mahamuni, A S Brenrdre, J Lepert, C A Smith, D cook, S H Risfud and H W H Lee; *Nanostructured Material*, **7**, 6 (1996)
12. M A Marcus W., Flood. M, Stiegerwald., L Brus. M, Bawendi. *J Phys. Chem.* **95**, 1572-1576 . (1991)
13. A A Guzelian. J.E.B, Katari, A.V Kadavanich, U Banin, K Hamad, E Juba, A.P Alivisatos, R.H Wolters, C C Arnold., J R Heath. *J. Phys. Chem.* **100**, 7212-7219 (1996)
14. L R Becerra, C.B Murray, R G Griffin, M G Bawendi. *J Phys. Chem.* **100** 3297-3300 (1994)

15. Y A Wang, J J Li, H Chen, X G Peng. *J. Am. Chem. Soc.*, **124** 2293-2298. (2002)
16. A Balazs., V V Ginzburg., F Qui., G Peng., D Jasnow *J Phys. Chem B*, **104**, 3411-3422 (2000)
17. D Gerion., F Pinaud., S.C Williams., W.J Parak., D Zachet., S Weiss., A.P Alivisatos., *J Phys. Chem. B*, **105**, 8861-8871 (2001)
18. S Pathak, S K Choi, N Arnheim., M E Thompson. *J. Am. Chem. Soc.*, **123**, 4103-4104 (2001)
19. V L Colvin., M C Schlamp., A.P Alivisatos. *Nature*, **370** 354-357 (1994)
20. X Michalet., F Pinaud., T D Lacoste., M Dahan., M.P Bruchez., A.P Alivisatos., S Weiss. *Single Mol*, **2**, 261-276 (2001)
21. E Helsinki, P Lucas and Y Wang, *J. Chem. Phys.* **89**, 3435 (1988)
22. Y Wang, A Suna, W Mahler and R Kasowski, *J. Chem. Phys.* **87**, 7315 (1987)
23. W Mahler. *Inorg. Chem.* **27**, 435 (1988)

Chapter 3

CHARACTERIZATION

The quantum dots are well characterized by their optical and electrical properties. In this chapter we have tried to summarize the optical properties of the quantum dots.

The study of optical properties of nano crystals (qd) have become a topic of both theoretical and experimental interest. It is known that the semiconductor quantum dots exhibit the "quantum confinement effect"¹⁻³ which results widening of band gap compared to that of the bulk. We have described three different methods to confirm the formation of nano particles.

Another important factor associated with quantum dots is large surface to volume ratio which results in electronic states within the band gap of semiconductor nano crystals¹. These states are called surface states and influence photoluminescence and thermoluminescence. The excited electrons are captured by surface states either before or after the occurrence of direct radiative recombination which ultimately influences the photoluminescence intensities. This property of the quantum dots has been explored through thermo luminescence and photoluminescence studies.⁴⁻⁶

3.1 Size Determination

Three different methods used for size determination of the quantum dots are X-Ray diffraction (XRD), Optical absorption and Transmission electron microscopy (TEM).

3.1.1 X-Ray diffraction

X-ray diffraction (XRD) is the first-hand approach for crystal size investigations. We have used this method for estimating average size of ultra small crystallites (quantum dots). In a bulk system, one observes a set of narrowed peaks corresponding to a definite crystal structure. However, the diffraction lines at subsequent peaks are found to be broadened with size reduction.

X-ray can be diffracted by crystals in the same way as that of the visible light diffracted by diffraction grating. Our goal with the diffraction of X-ray by crystals is only in connection with direct exploration of the interior of crystals. i.e., in connection with finding out the different crystal parameters like crystal size, crystal structure, face, and lattice parameters. Such study is possible because of the fact that the intensities of the diffracted beams and their direction angles are related to atomic arrangement in crystals. Thus, measurement of their intensities and directions would provide the desired information about crystals. The diffraction occurs according to Bragg's law

$$2d \sin\theta = n \lambda \quad (\text{Eq 3.1})$$

Where, $n = 1, 2, 3, \dots$, the order of diffracted beam.

$d =$ inter planner spacing

X-ray diffractometer detects the diffracted ray from the crystal and gives a plot between intensity and diffraction angle. Intensity is given in terms of counts and the angle in degrees. This plot is called X-ray diffractogram. Figure 3.1 shows a schematic diagram for diffraction pattern of X-ray.

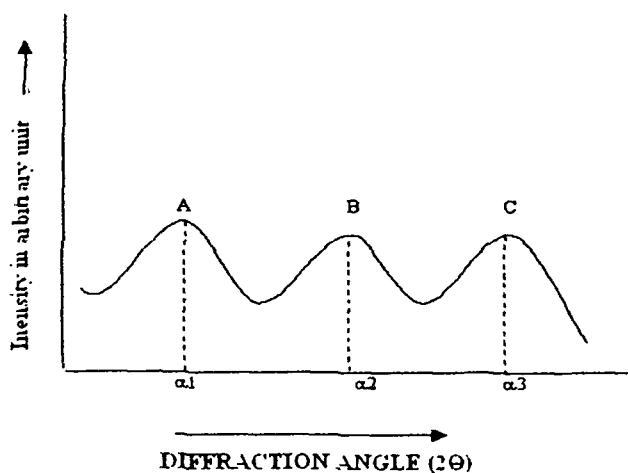


Figure 3.1 XRD pattern

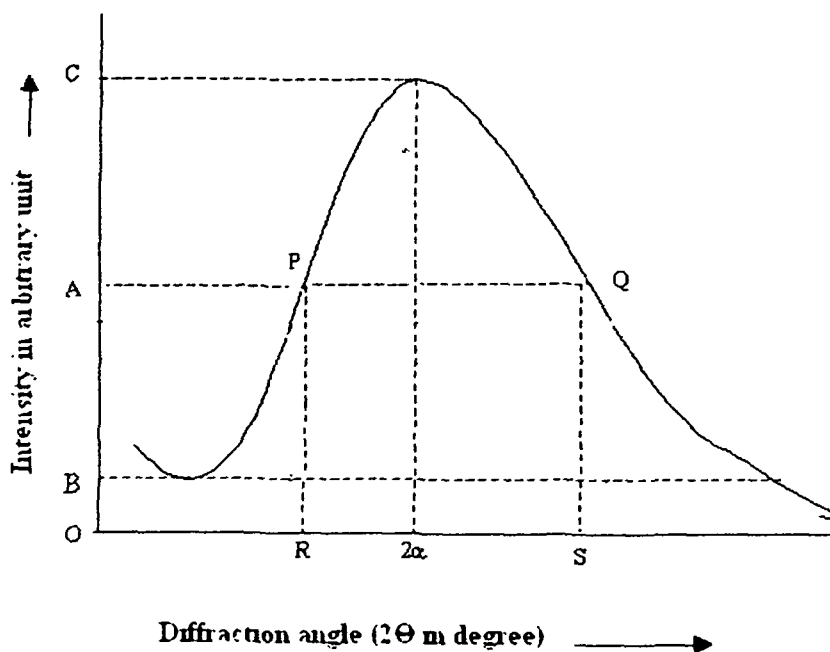


Figure 3.2 Single XRD peak

This diffractogram is used to analyze the various properties of crystals

3.1.1.a Sample identification :

The standard values of diffraction angles for any particular sample are compared with the standard diffraction angles. A matching between practical and theoretical values of diffraction angles is needed to identify any specimen.

3.1.1. b Size Estimations:

X-ray diffractogram is extensively used to calculate particle size using Debye-Scherrer equation⁷ which gives reasonably accurate particle diameter 'd'. The equation can be written as

$$d = \frac{0.9\lambda}{W\cos\theta} \quad (\text{Eq 3.2})$$

Where d is the particle diameter in nm.

λ is the wavelength of X-ray used.

W is the Full Width at Half Maximum (FWHM)

θ is the diffraction angle in radians.

The above parameters can be obtained from X-ray diffractogram, in the following way.

(i) Full Width at Half Maximum (FWHM):

As shown in figure 2, the maximum height of an XRD peak is BC, OB is the noise. Half of the maximum height is either AB or AC. i.e., the middle point of the peak is A. Two more points P and Q are taken on the

plot collinear to point A. Lines from P and Q are drawn which cut the angle axis perpendicularly at the points R and S respectively. The segment RS represents the required Full Width at Half Maximum in degrees. Finally, this value is converted into radian which gives the actual required FWHM (W).

(ii) The value of diffraction angle θ :

In the diffractogram, the angle axis is calibrated in terms of ' 2θ ' in degrees. The obtained θ is converted in to radian. The wavelength of X-ray used is noted as 1.541\AA . Finding the above-mentioned parameters, the particle size can be assessed. Various data obtained from XRD study for any specific specimen may slightly differ from the actual values due to the following reasons.

- i. Instrument calibration error
- ii. Instrumental error
- iii. Sudden power fluctuation during experiment
- iv. Due to external noise

The XRD pattern obtained for different samples are explained below. By using Scherrer formula (equation 2) particles' sizes are obtained. The wavelength (λ) of the x-ray source is 1.541\AA .

3.1.1.1. Sample (a) Zinc Sulphide (ZnS) in PVOH

We have synthesized two ZnS samples by varying surface temperature and pH value as shown in the table 3.1

Table 3.1 Samples with different temperature and pH value

pH value	Surface Temperature	Samples' name	Particle size
7	273°K	S1	6.2 nm
6.5	283°K	S2	7.1 nm

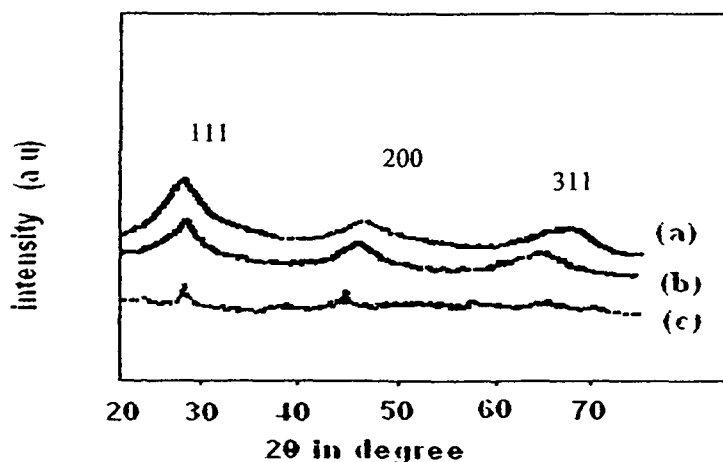


Figure 3.3 XRD Images of different ZnS quantum Dot Sample

The figure 3.3 shows the XRD pattern of two samples of ZnS quantum dots .It is found that the peaks are broadening and their width become larger as the particle's size become smaller The particles' sizes have been estimated as 6.2 nm and 7.1nm for two ZnS samples of different pH values. It is also revealed that the particles exhibit a zinc-blende crystal structure. The three different peaks correspond to (111), (200) and (311)

planes of cubic crystalline ZnS respectively. The sample S1 having higher pH value has smaller particle size. Semiconductor nano crystals embedded in polymer matrix shows quantum size effect. We have observed the change in particle size when pH value is changed. It has also been observed that the particle size at pH value 7.00 has smaller size than at 6.5. It is believed that when the pH approaching neutral value the critical binding is triggered by polymer matrix and therefore there is more surface aggregation of the nano particles in the polymer.³⁶ It suggest smaller size of the particle at neutral pH value.

3.1.1.2. Sample (b): Cadmium Salphide (CdS) in PVOH

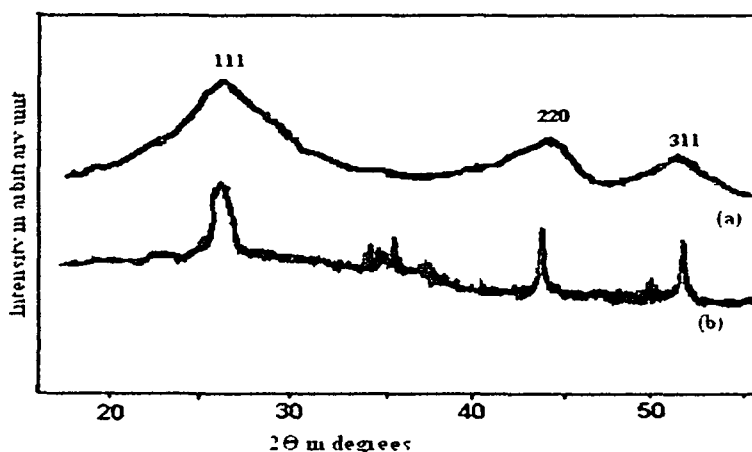


Figure 3.4 XRD peak for (a) CdS quantum dots (b) bulk CdS

X-ray diffraction peaks (111), (220) and (311) of CdS quantum dots in polymer corresponding to $2\theta = 26.8^\circ$, 44.5° and 53° suggest the possibility of cubic - β phase. The average size of CdS has been found to be 5.8 nm (figure - 3.4).

3.1.1.3 Sample (c): Zinc oxide (ZnO) in PVOH

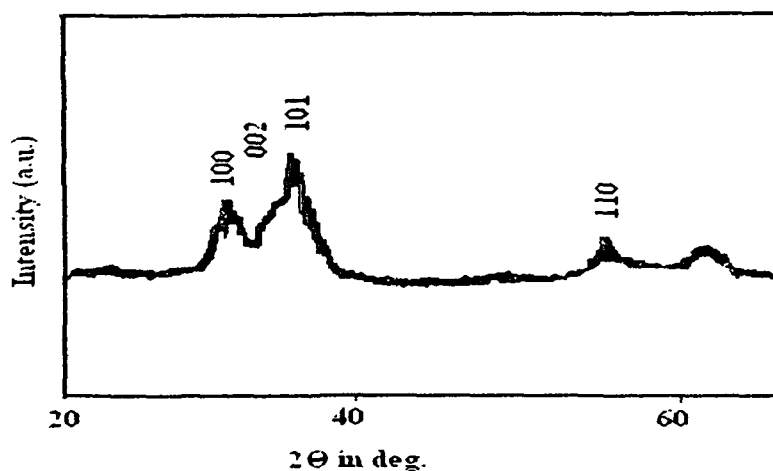


Figure 3.5 XRD peak for ZnO quantum dot

XRD peaks of ZnO quantum dots (figure 3.5) exhibit the formation of wurtzite phase. Our result is very similar to the report by Spanhel et al. ⁹. The diffraction peaks are relatively wider and reflection corresponding to (002) plane appears to be a shoulder. The size has been calculated as 9.6 nm.

3.1.1.4 Sample (d): Cu doped Zinc Sulphide (ZnS:Cu) in PVOH

The XRD peak of ZnS:Cu quantum dot exhibits zinc blende structure like that of ZnS. Because the doping percentage of Cu is very small, so there is no any change in the structure. The particles' average size has been found as 7.4 nm (Figure 3.6).

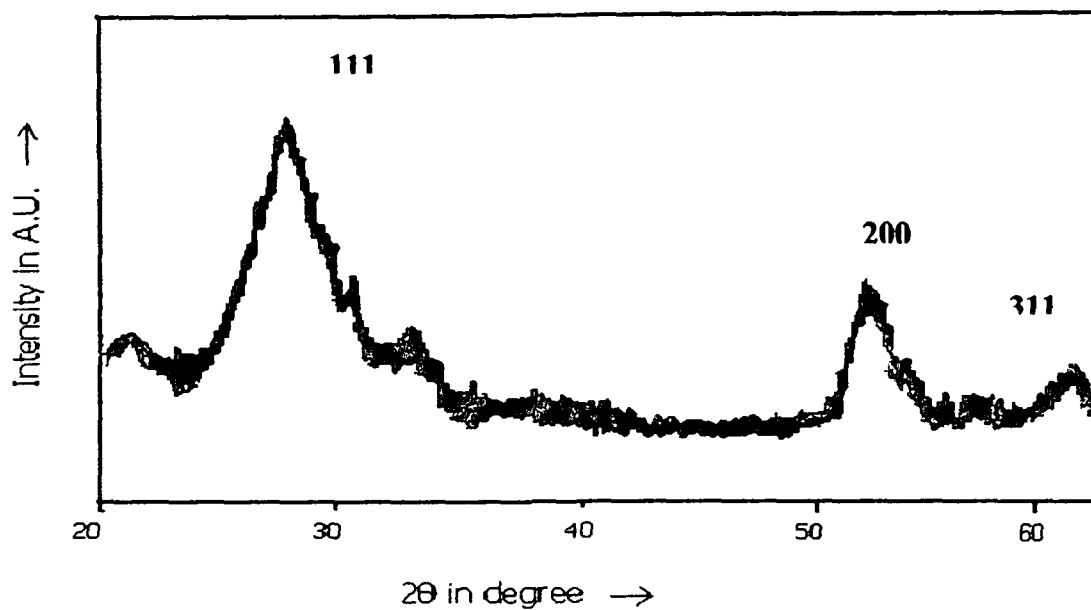


Figure 3.6 XRD peak of ZnS:Cu quantum dot

3.1.1.5. Sample (e): Iron doped Zinc Sulphide (ZnS:Fe) in PVOH

The XRD study of ZnS:Fe quantum dot also reveals the Zinc blende structure. The particles' size has been calculated as 7.6 nm. (Figure 3.7)

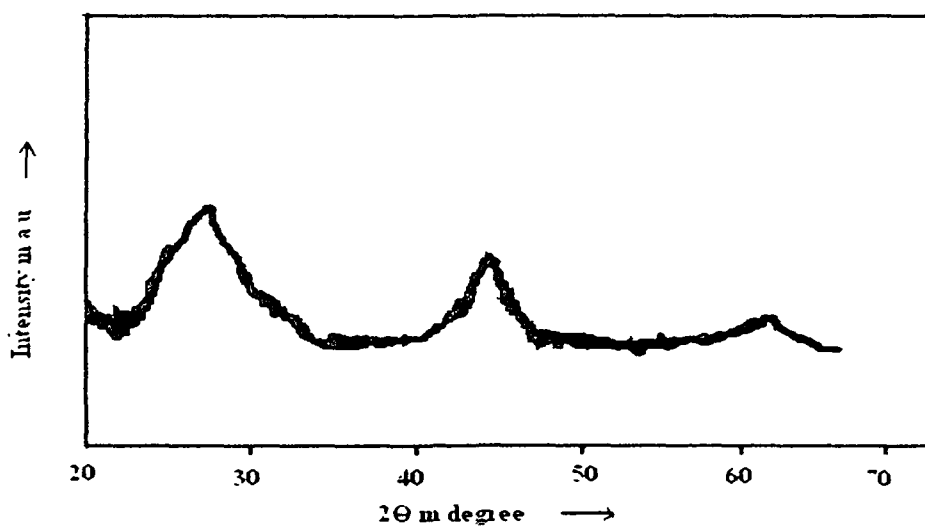


Figure 3.7 XRD peak of ZnS:Fe quantum dot

3.1.2 Optical absorption

3.1.2.a Information about band gap:

It is reported earlier that the reduction in particle size i.e., size quantization results in increase of band gap. The energy band gap of semiconductor quantum dots (E_g') is greater than that of the bulk (E_g). The electrons in conduction band and holes in valence band experience an overall confining potential due to the finite size of the quantum dots. As a result there will be size dependant discrete states in the conduction and valence band resulting in the effective enhancement of the band gap. That is why E_g' is greater than E_g .

If E_g be the band gap of a bulk specimen, and E_g' be that of quantum dot, then

$$E_g' > E_g$$

If $h\nu$ and $h\nu'$ be the required energy to excite the electrons from valence band to conduction band in bulk and quantum dot samples, then obviously

$$h\nu' > h\nu$$

$$\nu' > \nu$$

$$\lambda_a' < \lambda_a$$

Where, λ_a' and λ_a are the absorption edges of quantum dot and bulk sample. This infers that optical absorption edge in quantum dot is blue shifted. From this blue shift, the band gap and particles' size can be estimated.

For estimating particle size from blue shift, a theoretical model has been proposed. This model is known as high parabolic band model¹⁰ and the radius of the particle can be written as.

$$R = \sqrt{\frac{2\pi^2 h^2 E_{gb}}{m^* (E_{gn}^2 - E_{gb}^2)}} \quad (\text{Eq 3.3})$$

where R is the particle radius

E_{gb} is the bulk band gap

E_{gn} is the quantum dot band gap

h is planck's constant

m^* is the effective mass of the specimen

The standard value of m^* is expressed in terms of electronic mass m_e . Bulk band gaps and effective masses of three semiconductors CdS, ZnS, ZnO are listed in the table 3.2

Table 3.2 Band gap and effective mass of different II-VI semiconductors

Name of the samples	Bulk Band gap (eV)	Effective mass (m^*)	Values of effective mass
CdS	2.42	0.2 m_e	1.82×10^{-31} Kg
ZnS	3.54	0.4 m_e	3.64×10^{-31} Kg
ZnO	3.2	0.27 m_e	2.45×10^{-31} Kg

m_e - mass of electron (9.1×10^{-31} Kg)

The proposed model gives the approximate size of particles, sometimes with a deviation from the accurate size by 2 to 3 nm. This is due to lack of uniform particle distribution in the polymer matrix and its non-spherical geometry. But, as the particle size increases, the results from the model tend to accuracy in spite of the said factors.

ZnS quantum dot

Optical absorption was studied at room temperature using UV/VIS spectrophotometer in the wavelength range 200-700 nm. Fig 3.8 shows the room temperature absorption of the different ZnS quantum dots samples. The plot (c) for bulk ZnS gives the usual inter band absorption spectrum. The plots (a) and (b) stand for the sample S1 (ZnS / PVA) at higher pH value and S2 (ZnS / PVA) at lower pH value respectively. Both the plots infer the strong blue shift of the particles (qd) with an absorption edge of 270 nm and 300nm corresponding to an energy gap of 4.60 eV and 4.14 eV respectively.

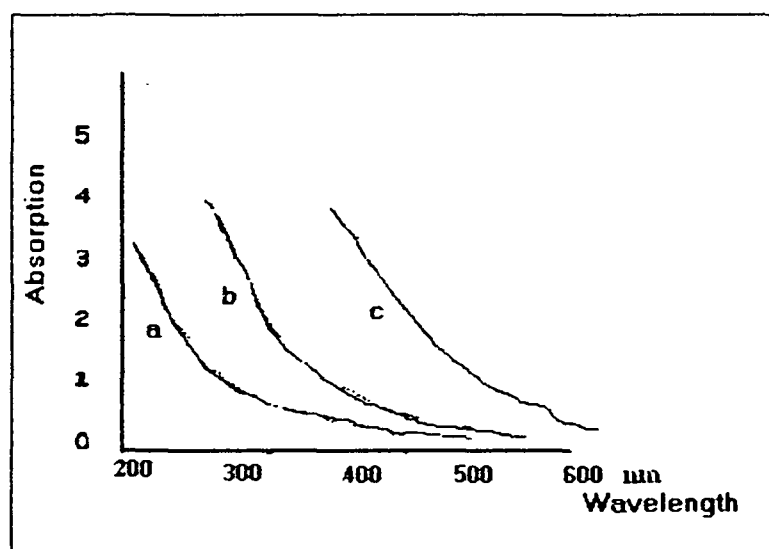


Figure 3.8. Absorption spectra of ZnS quantum dot & bulk ZnS (a)for S1,(b) for S2 and (c) for bulk

The absorption edge for bulk ZnS occurs at 346 nm corresponding to a band gap of 3.54 eV. The increase in band gap of quantum dots by 1.06 eV and 0.6 eV for the samples with different sizes is significant. The strong blue shift obtained due to decrease in particle size establishes size quantization effect¹¹

CdS and ZnO quantum dots

The optical absorption of CdS and ZnO quantum dots show absorption edge at 418 nm and 350 nm respectively in figure 3.9 resulting increase in band gap compared to their bulk counter part.

The ZnS, CdS films are expected to consist of a large number of quantum crystallites with varying shape and sizes and so the absorption peaks corresponding to level to level inter band transitions are less sharp due to the enhanced phonon broadening and inhomogeneous broadening effects^{12, 13}.

Synthesizing hydroxyl free ZnO always needs many precautions. It has been reported that ~ 4 nm sized ZnO quantum dots exhibit excitonic absorption features at about 330 nm with and without capping agents¹⁴. We have found that ZnO quantum crystals supposed to be hydroxyl free (prepared by sintering followed by quenching on polymer matrix) show absorption edge at ~ 350 nm (figure-3.9). The delayed stronger blue shift in ZnO is attributed to discrete excitonic states and less concentration of surface states with respect to CdS and ZnS samples.

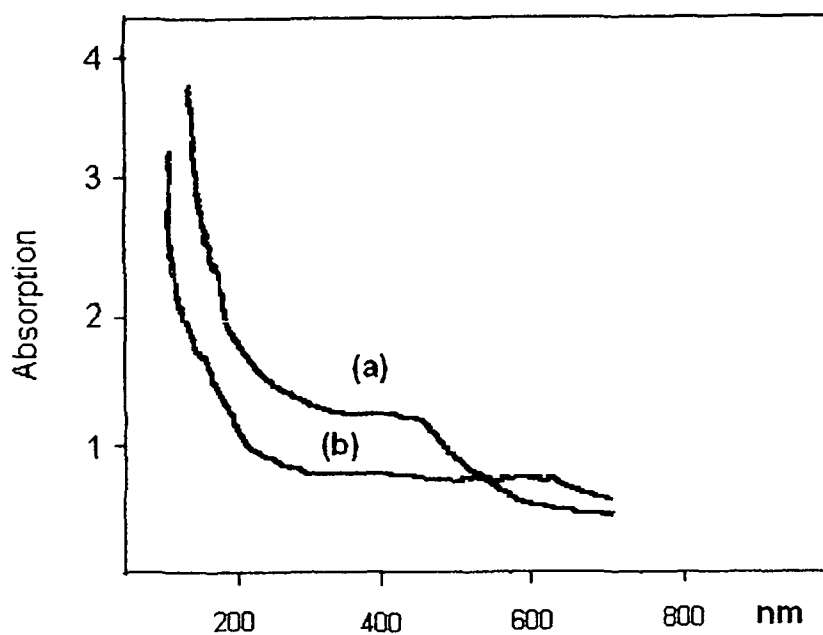


Figure 3.9 Optical absorption spectra of (a) CdS, (b) ZnO quantum dots

ZnS:Cu quantum dot

The absorption spectrum of ZnS:Cu quantum dot doped with copper is shown in figure 3.10. The single absorption peak observed at 280 nm is an indication of the existence of a narrow size distribution of quantum particles. The absorption is essentially similar to that of the undoped ZnS quantum dot. This is due to the fact that the doping concentration is very small and is effective only in altering the luminescence properties of the material and not the quantum particle size under similar synthesis condition.

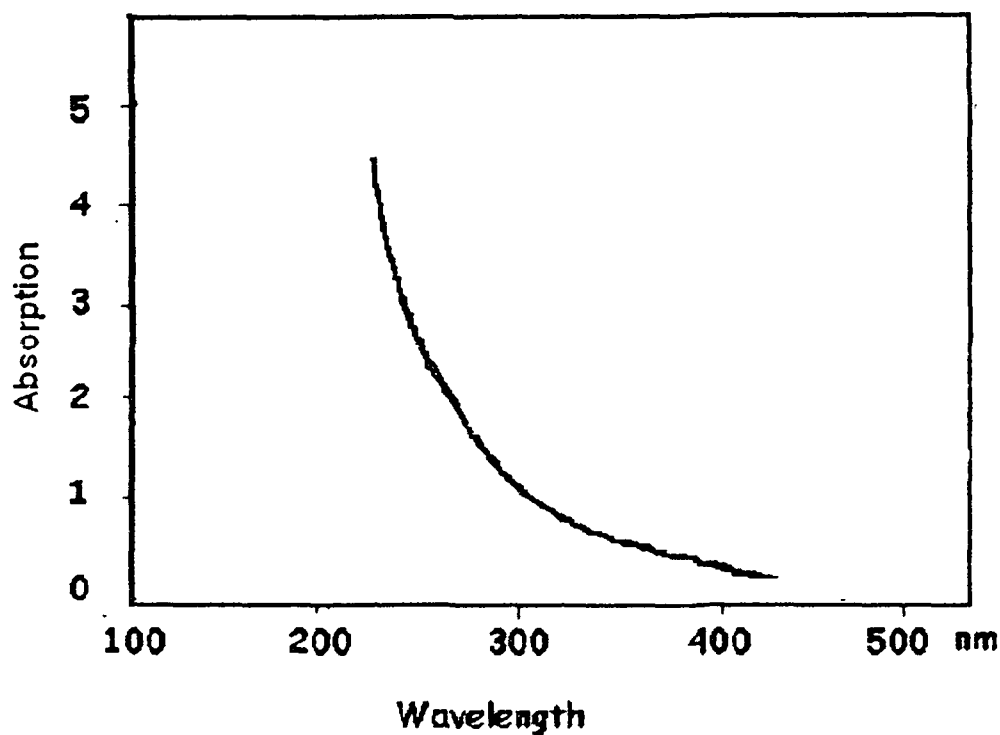


Figure 3.10 optical absorption spectra of ZnS:Cu quantum dot

3.1.3. *Transmission electron microscopy*

Neither UV-visible absorption spectroscopy nor XRD is a direct probing method for accurate size determination, but it is important to know the accurate size of the nanoparticle to study their properties. Since optical microscopy has several limitations with respect to magnification and resolution; it cannot give accurate result in the nm range. However, electron microscopy is the appropriate tool for accurate size determination.

Transmission electron microscopy allows imaging of individual crystallites and the development of a statistical distribution of the shape of

the particles in a sample. High magnification imaging with lattice contrast allows the determination of individual crystallite morphology¹⁵.

The shapes of the particles are found generally as spherical although a few are irregular in shape. The careful size measurements have been done by taking 20 to 40 individual nanocrystals in a single image.

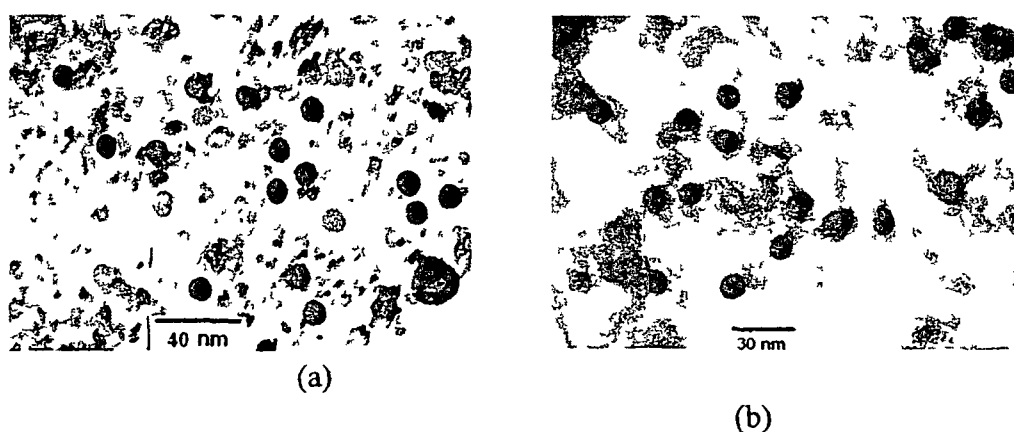


Figure 3.11 TEM image of (a) Sample S1 and (b) Sample S2 of ZnS qd

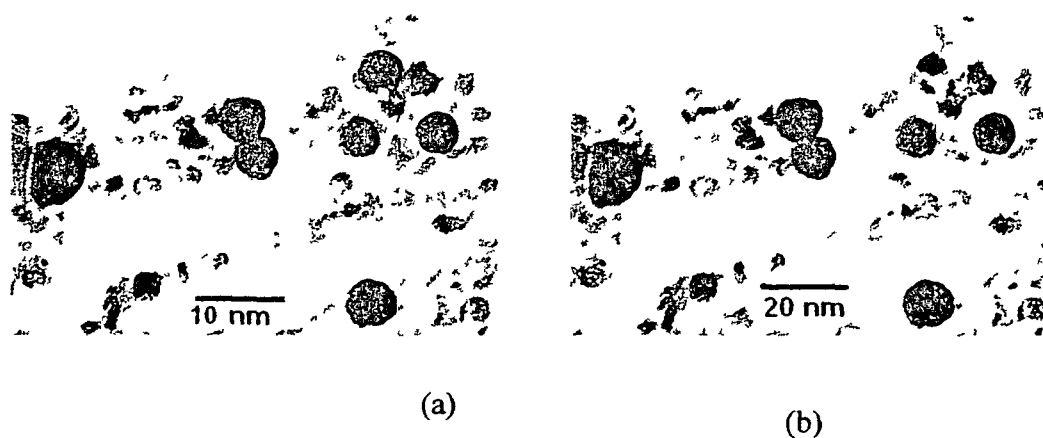


Figure 3.12 TEM image of (a) CdS (b) ZnO quantum dot

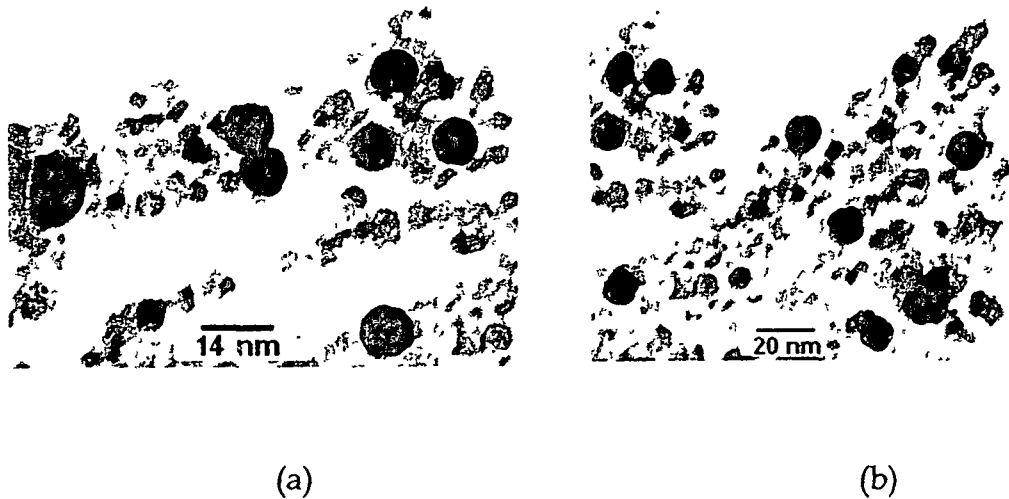


Figure 3.13 TEM image of (a) ZnS:Cu (b) ZnS:Fe quantum dots

The figure 3.11(a) and 3.11(b) depict TEM images of two ZnS samples. The sizes of the nanoparticles have been estimated as 6 nm and 7.4 nm respectively. The sizes of the particle for CdS and ZnO quantum dots have been calculated as 5.8 nm and 9.6 nm respectively (Figure 3.12 (a) and 3.12 (b)). The particle size for ZnS:Cu (Figure 3.13 (a)) and ZnS:Fe (Figure 3.13 (b)) have been found as 7.8 nm and 9.2nm.

The particle sizes estimated from XRD, Optical absorption and TEM for different samples are shown in the table 3.3. It is seen that XRD and TEM show almost same size of the particles, but a small variation of size is noticed in case of optical absorption study.

Table 3.3 Comparison of particle sizes

Sample	Size from XRD	Size from optical absorption (HBM)	Size from TEM
ZnS (S1)	6.2 nm	7.1 nm	6 nm
ZnS (S2)	7.1 nm	8.2 nm	7.4 nm
CdS	5.8 nm	7.9 nm	5.4 nm
ZnO	9.6 nm	10.2 nm	9.2 nm

3.2. Surface States

The electronic states within the band gap of semiconductor nanocrystals are created during sample preparation. The existence of these electronic states called surface states have been confirmed through photoluminescence and thermo luminescence studies.

3.2.1. Photoluminescence

Luminescence in solid is the phenomenon in which electronic states of solids are excited by some energy from an external source and the excitation energy is released as light. the energy comes from short-wavelength light, usually ultraviolet light, the phenomenon is called photoluminescence.

Luminescence is one the most important methods to reveal the energy structure and surface states of these particles. The fluorescence of semiconductor nanoparticles has been studied extensively^{15, 16}. It is reported

that the fluorescence process in semiconductor nanoparticles is very complex and most nanoparticles exhibit broad and Stokes-shifted luminescence arising from the deep traps of the surface states^{15,17}. Only clusters with good surface passivation may show high band-edge emission¹⁸. The absence of band edge emission has been previously attributed to a large nonradiative decay rate of the free electrons to the deep-trapped states. As the particles become smaller, the surface to volume ratio and the surface states increase rapidly, thus reducing the excitonic emission via non radiative surface recombination¹⁹. The above phenomenon indicates that the surface states play a dominant role in determining the physical properties, especially the optical properties, of the nanoparticles. The size dependence of the excitonic fluorescence has been studied extensively and is now well understood. However, little is known about the physical properties of the surface states. Some reports^{4,20}, stated that the trapped fluorescence of the surface states does not vary as much upon decreasing size, while others²¹, showed that the surface luminescence shifts to the blue as the size is decreased.

3.2.1.1. Photoluminescence of ZnS quantum dots

Photoluminescence spectra of ZnS quantum dots are shown in figure 3.14. Among many semiconductors; ZnS plays an important role as phosphors for luminescence. The photoluminescence of ZnS quantum dots were recorded at room temperature excited with 220 nm wavelength. The broad luminescence peaks called trapped luminescence arise from surface states. The luminescence peak is shifted towards higher energy for the particles of smaller size.

The transition appearance of photoluminescence peaks figure(3.14) at energies lower than the band gap demonstrate that the luminescence is from surface states²². The density of surface states of nano particles would increase with decrease in particle size due to large surface to volume ratio. The presence of these surface states reduces the chance of excitonic emission via non radiative surface recombination ^{23, 24}. The band edge or excitonic emission thus overlaps with the absorption of the surface states which results photoluminescence at energies less than the band gap. The peak is shifted towards greater energy for the sample S1 having smaller size. The shift of the surface emission due to size variation has been reported earlier ²³

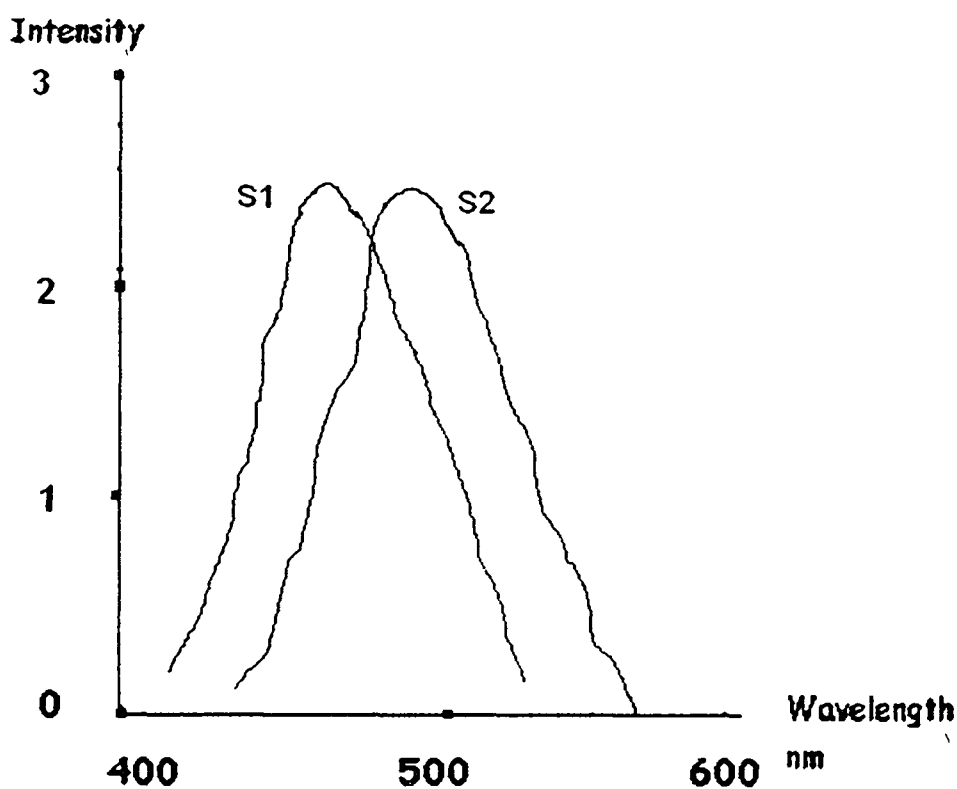


Figure 3.14 PL. spectra of ZnS qd (a) S1 (b) S2

3.2.1.2. Photoluminescence of Cu doped ZnS (ZnS:Cu) quantum dot

In the beginning of 1970s, the optical properties and luminescence mechanism of ZnS phosphors doped with transition metal impurities were investigated in detail by Shionoya's group^{25, 26}. It was shown¹⁹ that the quantum efficiency for luminescence increases with decreasing particle size accompanied by luminescence decay time at least five orders of magnitude faster than the corresponding transition in bulk crystal of Mn doped ZnS.

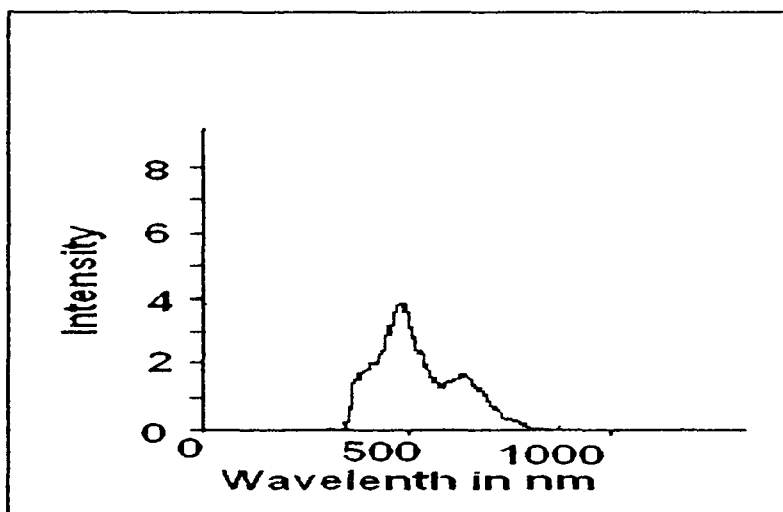


Figure 3.15 PL spectra of ZnS:Cu quantum dot

The band to band excitation in ZnS has been used to excite the Cu^+ emission. The subsequent transfer of electrons and holes into the electronic level of Cu^+ ion leads to the characteristic emission of Cu^{+2} in ZnS system. Luminescence at 480 nm is due to copper induced levels. According to Peka and Schutz²⁷ luminescence is due to transition from conduction band of ZnS to the t_2 level of excited $\text{Cu}^{2+}(\text{d}^9)$ within the band gap of nano ZnS.

The energy levels of (a) bulk ZnS nano, (b) undoped ZnS nano and (c) copper doped ZnS nano are shown in figure 3.16

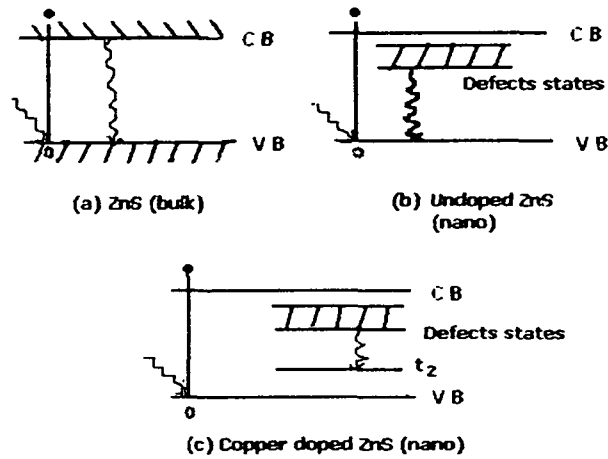


Figure 3.16 Schematic energy level diagram for (a) bulk ZnS nano, (b) undoped ZnS nano and (c) copper doped ZnS nano

The photoluminescence study has been carried out for Cu doped ZnS quantum dots (ZnS:Cu) and three distinct peaks are obtained at 480 nm, 430 nm and at 640 nm (figure 3.15). Among these three, the peak at 480 nm is very sharp. Luminescence at 480 nm is due to copper induced levels, the peak at 640 nm is due to surface states, the emission peak at 430 nm is due to donor acceptor pair transition.

3.2.1.3 Photoluminescence of Fe doped ZnS (ZnS:Fe) quantum dot

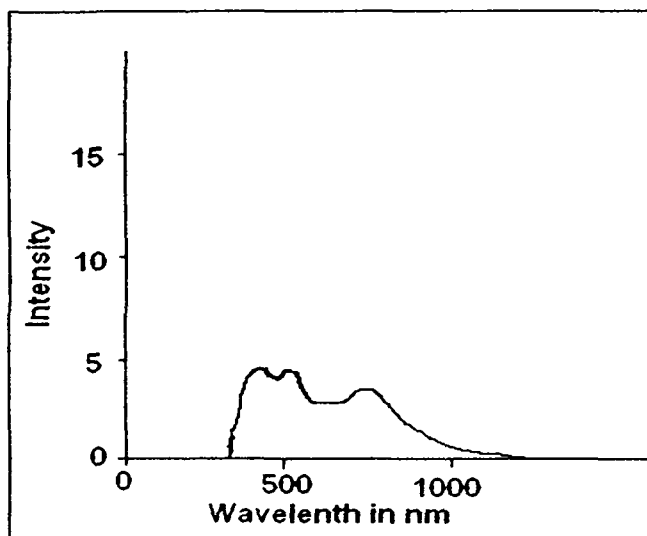


Figure 3.17 PL spectra of ZnS:Fe quantum dot

Photoluminescence spectra of ZnS:Fe are shown in figure 3.17. Three distinct peaks at around 483 nm, 546 nm and 749 nm are seen for iron doped sample. The emission peak at 483 nm is due to donor acceptor pair transition, the peak at 749 nm is the result of surface states present in the sample. the blue green emission peak at 546 nm might be due to transfer of Fe ion in substitutional site of Zn^{2+} . It is reported (Borse PH et al) that removal of even .001 wt% of Fe may turn out to be advantageous to further increase the blue luminescence at ZnS.

Earlier shifting of luminescence peak of ZnS nano due to addition of Cd^{2+} ion was studied by Weller et al²⁸. They observed the shifting of luminescence peak to 580 nm.

3.2.2 Thermoluminescence

When suitable energy is supplied to semiconductor, electrons and holes are created. If electron-hole pairs recombine immediately and emit a photon than it is known as fluorescence and if the electrons and holes created do not recombine rapidly, but are trapped in some metastable states separately, they need energy to be released from the traps and recombine to give luminescence. If the detrapping process is caused by heating or thermostimulation, the luminescence is called thermoluminescence. Thermo luminescence is a good way to detect the recombination emission caused by detrapping of carriers thermally. The energy corresponding to the glow peak is equal to the trap depth. The traps and carriers (electrons and holes) are produced during sample processing and also may be produced by irradiation. Since, as the particles become smaller, ions at the surface increase rapidly, and most ions at the surface are not saturated in coordination, electrons or holes may be excited easily and escaped from the ions, and then are trapped at surface states located in the forbidden gap.²⁹ Carriers trapped at the surface states or defect sites may be released by heating to recombine and to give the so called thermoluminescence. Obviously, the thermoluminescence process is different from the photoluminescence process, since the energy of thermostimulation is not sufficiently high to excite the electrons from their ground states to their excited states. Only the carriers ionized from the surface states or defect sites are involved in the TL process, i.e., the thermoluminescence has arisen from the surface states. The increase of the TL intensity upon decreasing sites reveals the increase of the surface states as the size is decreased. This result

is in agreement with that from the fluorescence and absorption measurements. According to the theories of TL,^{30, 31} the TL intensity of nanoparticles may be given by

$$I = -dm/dt = mnA, \quad (\text{Eq 3.4})$$

where m and n represent the density of holes and electrons respectively for recombination, and A is the carrier recombination probability or rate. Obviously, m and n are proportional to the surface states. As the size of the particles decreases, surface states increase rapidly, thus providing more accessible carriers for TL and enhance the TL efficiency. Furthermore, in nanoparticles, the wave functions of electrons and holes are overlapped effectively, which may result in the increase of their recombination probability or rate (A). These two effects may make the TL of small particles much stronger than that of the bulk and increase as the size is decreased.

3.2.3 A Schematic Luminescence Model

As has been pointed out, the surface states or defect sites in nanoparticles are so abundant that the trapping of carriers is a very fast process^{32,33}. Fluorescence has been considered to have occurred via the detrapping of carriers from the surface states or traps. The detrapping of carriers is an important process in determining the fluorescence efficiency and to reveal the luminescence mechanism. The detrapping rate is correlated to the trap depth, which is measured with respect to the bottom of the conduction band for electron traps and to the top of the valence band for hole traps in bulk

materials. In nanoparticles (or clusters, nanocrystals, and quantum dots), we define the trap depth to the lowest excited state or exciton state for electron traps. The trap depth determining the activation energy of the detrapping may be estimated from the glow curves. As in conventional TL theories,^{31, 34} only the electron traps were considered.

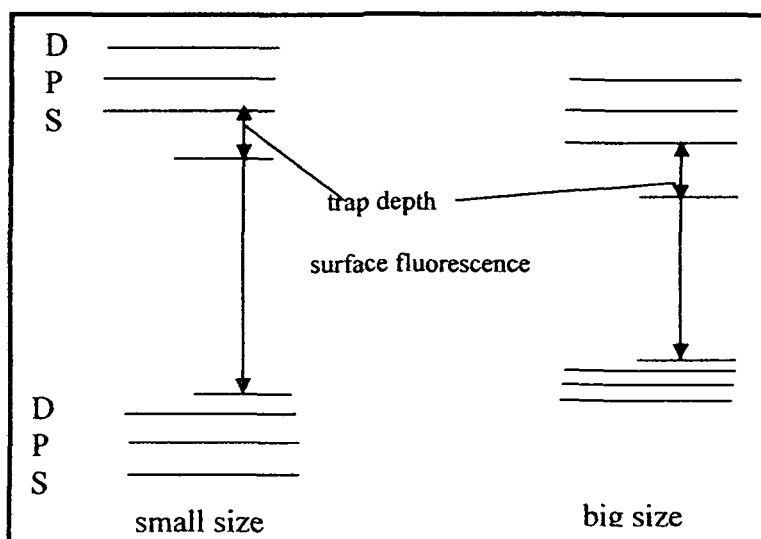


Figure 3.18 A schematic model for the size dependence of the fluorescence of the surface states in semiconductor nanoparticles

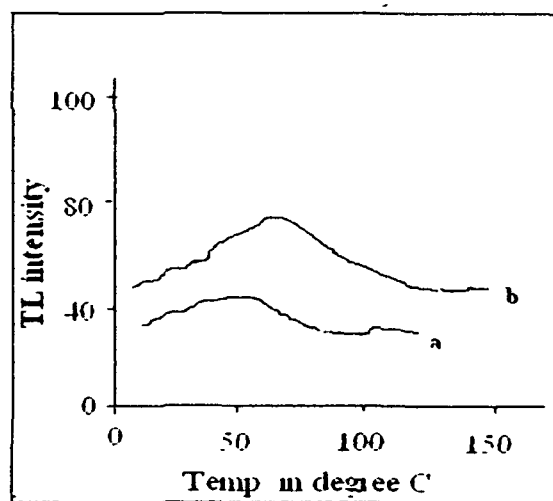


Figure 3.19 Thermoluminescence glow curve of (a) ZnS qd (b) CdS qd

The thermoluminescence glow curves of ZnS and CdS quantum dots are shown in figure 3.19. The peak for ZnS qd is observed at a temperature of 50^o C and the same for CdS qd is found at 70^o C. In nanoparticles number of defects sites is very high. Defect sites can act as trapping centers for '-ve' carriers (i.e., electrons). Therefore e^-h^+ recombination takes place at slow rate. The CdS sample may have more number of deep traps of defect states for which comparatively higher energy (temperature) is required ³⁵ for emission than that of ZnS. The higher intensity of glow curve of CdS qd also suggests the existence of higher number of defect sites which indicates formation of quantum dots of smaller size. The physical properties of these defects sites (traps) may be reflected from the temperature, shape or symmetry of the glow peak.

The nature of temperature dependent luminescence intensity is due to uniform emission of photons measured in terms of photo current which assess the e^-h^+ recombination take place at slow rate. We shall try to interpret our result with regard to two possibilities (1) whether the released electrons retrap in some other surface states or (2) recombine with free charge of opposite kind. Here recombination plays a dominant role over the retrapping and there are plenty of surface states due to small particle size. The electrons are released after thermal excitation. At recombination centers the detrapping of electrons takes place after recombination with opposite charges. As such glow peaks are obtained.

One of the characteristics of fast retrapping is that TL peak is symmetric and spreading over wide range of temperature and that obtained in our result (figure 3.19). This can be understood from a consideration of the fact that in a fast retrapping significant concentration of released electrons are retrapped before they recombine, which gives rise to a delay in

the emission over a wide range of temperature. We therefore concludes that the glow curve obtained is due to fast retrapping. The spreading of glow curve for (CdS) quantum dots for wider range of temperature also suggests that CdS quantum dots has higher concentration of defects sites than that of ZnS quantum dots.

3.3. Summary

The optical properties of quantum dots are discussed in this chapter. Mainly two basic properties, size quantization and presence of surface states have been confirmed with the characterization. For size quantization optical absorption studies have been done. X-Ray diffraction has been employed as first hand approach to determine the sizes of the quantum dots. However accurate size and shape of the particles (quantum dots) have been estimated with the help of Transmission electron microscopy (TEM). The presence of electronic states called surface states within the band gap of semiconductor nano particles (quantum dots) has been investigated through photoluminescence and thermoluminescence studies.

We have investigated three undoped II-VI semiconductor quantum dot samples, namely ZnS, CdS and ZnO and two doped samples. The doped samples are Cu doped ZnS quantum dots (ZnS:Cu) and Fe doped ZnS quantum dots (ZnS:Fe). Comparing the sizes of the particles obtained from XRD, Optical absorption and TEM almost same size of the particles has been found. The blue shifted absorption edge obtained for all the samples is clear indication of size quantization. A delayed stronger blue shift obtained in ZnO is due to discrete energy states.

It is significant that, we are successful in controlling the size of the particles by varying pH value of the solution and the surface temperature and found that the sample having higher pH value and temperature has smaller particle's size. Further a considerable increase in band gap (1.06 eV) is observed in the ZnS quantum dots sample having higher pH value.

We have carried out photoluminescence study of ZnS, Cu doped ZnS and Fe doped ZnS quantum dots systems. An enhanced luminescence intensity is observed in both the doped samples. However, three distinct luminescence peaks are seen in luminescence spectra of ZnS:Cu quantum dots system. The peak at 480 nm is obtained due to transition from conduction band to an intermediate level of excited copper ion in the band gap of ZnS. On the other hand, this luminescence intensity at 480 nm is very sharp in comparison to other two luminescence peaks obtained, one due to donor- acceptor pair emission and other due to presence of surface states.

We have also observed three peaks in luminescence spectra of Fe doped ZnS quantum dots sample. But peaks are not very sharp as found in Cu doped ZnS. The emission peak at 546 nm is due to transfer of Fe ion in substitutional site of Zn^{2+} .

The thermoluminescence study of ZnS and CdS quantum dots show glow peak at 50^o C and 70^o C respectively. The higher temperature required for glow peak in CdS quantum dots sample advocates the presence of deep surface states. All the works stated above are our original contribution and we are successful in fabricating quantum size particles through chemical route. The characterizations stated above clearly establish the size quantization.

References

1. AI L Efrons and AL Efros *Sov.Phys.Semicon.* **16**, 722 (1982)
2. M O'Neil, J Marohn, G Mclendon. *J.Phys.Chem.*, **90**, 4356 (1990)
3. M G Bawendi, P.J Carrol., W.L Wilson., L.E Brus. *J.Phys.Chem.*, **96**, 946 (1992)
4. M Agata, H Kurase, S Hayashi, K Yamamoto. *Solid State Commun* **76**, 1061 (1990)
5. K K Nanda, S N Sarangi, S Mohanty, S N Sahu. *Thin Solid Films.* **322**, 21 (1998)
6. S N Behera, S N Sahu, K K Nanda. *Indian J.Phys.* **74A**, (2) 81-87 (2000)
7. X K Zhao and J H Fendler. *Chem. Matter.* **3**, 168 (1991)
8. M. O Neil, J Morohm and A Meclendon,; *J.Phys, Chem.* **94**, (1990)
9. L Spanhel and M A Anderson, *J. Am. Chem. Soc.* **113** 2826 (1991)
10. Y Wang, A Suna, W Mahler and R Kasowski; *J Chem. Phys.* **87**, (1997)
11. LE Brus, *J Phys.Chem.* **90**, 2555 (1986)
12. S Schmitt-Rink , D A B Miller and D S Chemla, *Phys. Rev. B* **35**, 8113 (1987)
13. R Pal, D Bhattacharyya, A B Maity, S Chaudhuri and A K Pal, *Nanaostruct. Mater.* **4**, 329 4 (1994)
14. K Borgohain and S Mahamuni, *Semicond. Sci. Technol.* **13**, 1154 (1998)
15. A D Yoffe. *Adv.Phys.* **42**, 173 (1993)
16. K Msawa, H Yao, T Hayashi and T Kbayashi. *J.Lumin* **48/49**, 269 (1991)
17. Y Wang and N Herron. *J.Phys.Chem.* **92**, 4988 (1988)
18. C B Murray, D Norris and J Biwandi *J.Am.Chem.Soc.* **115**, 8706 (1993)
19. R N Bhargava, D Gallagher, X Heng and A Nurmikko. *Phys.Rev.Lett.* **72**, 416 (1994)

20. T Arai, H Fujumura, I Umeza, T Ogawa and A Fujii. *J.Appl.Phys.* **28**, 484 (1989)
21. A Hasselbarth, E Echymullar and H Well. *Chem Phys. Lett.* **203**, 271 (1993)
22. A Eychmuller, A L Hasselberth, L Katiskas, H Waller and Ber. Bunsen Ges, *J.Phys.Chem.* **95**, 79 (1991)
23. W Cheng, Z Wang, Z Lin and L Lin, *J Appl. Phys.* **82**, 3111 (1997)
24. T Sekikawa, H Yao, T Hayashi and T Kobayashi, *Solid State Commun*, **83**, 969 (1992)
25. S Shionoya, in: Goldberg P (Ed) *Luminescence of Inorganic Solids*, Academic Press, New york, 205 (1966)
26. A Suzuki and S Shionoya. *J.Phys.Soc. Japan* **31**, 1455 (1971)
27. P. Peka and H. J. Schulz, *Physica B* **193**, 57. (1994)
28. H. Weller, L Ler, U. Koch, M. Gutierrez and A. Henglien, Ber. Bunsenges. *J.Phys. Chem.* **88** (1984)
29. N Chestnoy, T D Harris, R Hull and L E Brus. *J Phys.Chem.* **90**, 3393 (1986)
30. L E Brus. *IEEE J. Quantum Electron* **22** 1909(1986); *Appl. Phys.* **53**, 45 (1991)
31. R Chen and Y Kirsh *Analysis of Thermally Stimulated Processes* (Pergamon, Oxford)
32. M Kaschke, N P Ernsting, H Weller and U Muller. *Chem.Phys. Lett.* **168**, 543 (1990)
33. N P Ernsting, M Kaschke, H Weller and L Katikas. *J.Opt.Soc.Am.* **B 7**, 1630 (1990)
34. J T Randal and H F Wilkins. *Proc. R.Soc. London Ser. A* **184**, 366 (1945)
35. S S Nath, D Mohanta, A K Bordoloi, S Choudhury, S K Dolui and A Choudhury . *Proc. of Conf. On Laser and Its Application* Dibrugarh University (2001)

Chapter 4

EFFECT OF SWIFT HEAVY ION IRRADIATION

Energetic ion beams play a vital role in the field of research in materials science¹⁻³. Swift Heavy ions (SHI) lose energy in materials mainly through inelastic collisions with the atomic electrons. Along the trajectory a trail of defects (point defects, defect clusters, structural phase transformation) known as latent track may be formed depending on the type of ion and its energy as well as the physical properties of the materials. This damage is always created in the close vicinity of the trajectory of projectile.

SHI is very useful for modification of the properties of films, foils and surface of bulk solids. It penetrates deep into the materials and produces a long and narrow disordered zone along the trajectory. The passage of SHI induces very rapidly developing processes which are difficult to observe during or immediately after their occurrence.

The information about these processes is stored in the resulting damage, such as size, shape and structure of defects.

The modification of properties of materials due to electronic excitation during SHI irradiation and formation of latent tracks in materials using suitable combination of projectile and target has emerged as an exciting field of research and development.

SHI is capable of depositing electronic excitation energy about 1 to 10 KeV/A⁰ in the material.

Heavy ions of high energy (1MeV/nucleon) often referred as Swift Heavy Ion (SHI) are capable of producing modification in materials due to their large electronic excitation. Online monitoring of ion-induced modification is one of the most interesting aspects of the ERDA technique^{4,5} with a large area position sensitive detector. SHI are capable of producing modification at the surface, bulk, and the interface of thin films deposited on the substrate.

ERDA (Elastic Recoil Detection Analysis) is a technique especially suited for depth profiling of light elements, which overcomes the limitations of Rutherford back scattering (RBS). The developments in the technique enabled depth profiling of elements from hydrogen up to very heavy elements with single electron resolution in the light mass region.

4.1 Energy loss and structural modification

The collision of an individual energetic ion in solid cause the motion of atoms and the excitation of electronic states. At the outset the ions primarily induce gentle electronic transitions that cause relatively little structural damage. Nevertheless the electronic structure is excited by coulomb interaction with moving ions. A relatively narrow lightning like trail surrounds the ion track and defines a region of intense electronic excitation, e.g. ionization, secondary and auger electron production, e-h pair production, luminescence etc.

Low dose $\ll 10^{13}$ ions/cm² \ll high dose

The dose of ions required to amorphise a crystalline matrix can be roughly estimated by assuming that the energy density is essentially the same as that needed for melting.

For ions of energy E_0

$$\text{Dose } \phi = 10^{24} R_p / E_0 \text{ ions/cm}^2$$

Where R_p is the ion range

Dose is related to the measured time integrated current or charge Q deposited per unit surface area A .

$\phi = Q/nqA$, where n is the number of electronic charge, q is charge/ion. The projected range R_p is the depth, most ions are likely to come to rest at yielding a peak concentration of $\phi / \sqrt{2\pi} \Delta R_p$.

Experimental spread in the ion range is accounted by the term ΔR_p , the standard deviation or longitudinal straggle of the distribution. Similarly ΔR_l , the lateral straggle is a measure of the spread in the transverse direction.

4.2 Brief Review of ion beam interaction

4.2.1 Ion Matter Interaction:

When SHI passed through a material, the free electrons available in its path get excited within a time scale $\sim 10^{-15}$ sec. This electronic excitation leads to rise in temperature of the ions track known as electronic temperature which

is of the order of 10^5 °K. Next the energy is relaxed into lattice and so photons get excited within a time frame of 10^{-12} second giving rise to lattice temperature of the order of 10^3 °K. Then the energy of the ion is quickly transferred into other parts of the specimen. Due to fast quenching the ion path melts and one gets amorphized zone (very often, termed as ion track in the literature). The example of amorphization can be understood as the effect when a red hot piece of iron is suddenly dropped into a cold water reservoir. In fact, an energetic ion passes through the material it suffers two kinds of energy loss. First nuclear energy loss [$S_n = (dE/dx)_n$] which is due to the interaction between the ion and the nuclei and is predominant for the ions carrying low energy value (keV). Second, when energy increases it is the electronic energy loss $S_e = (dE/dx)_e$ that comes into picture which significantly dominates over S_n for the beams in MeV range. S_{eth} is the threshold energy of ions below which only point defects are expected^{6,7}. Ion tracks are formed only for the case when electronic energy loss (S_e) exceeds the threshold energy (S_{eth}) value.

In our samples quantum dots are embedded in polymer matrix, therefore the problem of grain boundary is absent. This grain boundary is source of weak link resistivity. Because, the quantum dots or nanoparticles are separated each other by finite distances (inter particle separation is more than the size of the quantum dots) and thus, ion bombardment study in these novel systems promise to be exciting area of study to understand better the ion-matter interaction in terms of well known models e.g. (a) thermal spike model and (b) coulomb explosion model⁸⁻¹⁰.

For $S_e < S_{eth}$ point defects are created which segregates into grain boundaries⁷. A fast ion produces ~ 5 nm track for $S_e > S_{eth}$ in polymers¹¹.

So, now if the ion finds a few embedded nano particles, either or combination of the following possibilities would be guaranteed.

- Fragmentation into still smaller nanoparticles
- Amorphization of the nanocrystallites
- Simple evaporation
- Melting into bigger crystallites
- No effect

4.2.2 Fluence:

It is defined as total number of ions, exposing the sample per square centimeter (Ions/ cm²). It is not fixed, but varies from sample to sample depending upon the sizes of the specimen. This is also known as dose. Generally denoted by ϕ .

Calculation of ion dose:

For example, if the particle size (radius) is 10 nm. Then the required fluence, can be calculated as follows:

The total area of the particle -

$$\begin{aligned} A &= \pi R^2 = (3.14) \times (10 \times 10^{-9})^2 \text{ m}^2 \\ &= (3.14) \times (10 \times 10^{-7})^2 \text{ cm}^2 \\ &= 3.14 \times 10^{-14} \text{ cm}^2. \end{aligned}$$

$$\begin{aligned} \text{Fluence } \phi &= \frac{1}{A} = \frac{1}{3.14 \times 10^{-14}} \text{ ions / cm}^2 \\ &= 0.00318 \times 10^{14} \text{ ions / cm}^2 \\ &= 3.18 \times 10^{11} \text{ ions / cm}^2 \end{aligned}$$

We prepared three samples of quantum dots for ion irradiation.

- (i) ZnS
- (ii) Cu doped ZnS
- (iii) Fe doped ZnS

The samples were irradiated at high vacuum (2.5×10^{-6} torr) by 150 MeV Ti ion beam with approximated beam current 1.0 pA (particle nano ampere). The fluence was varied in the range 10^{10} to 10^{12} ion/cm². In order to expose the whole target area the beam was scanned vertically over the sample plane. The table 4.1 shows the different ion fluences used along with time of exposure. The motive behind ion irradiation was also to see any change in electrical properties of the irradiated samples

Table 4.1 Different fluence used along with time of exposure

Fluence	Time (second)	Notation
5×10^{10} ion/cm ²	8	ϕ_1
2×10^{11} ion/cm ²	32	ϕ_2
8×10^{11} ion/cm ²	128	ϕ_3
3.2×10^{12} ion/cm ²	512	ϕ_4

The energy of the ion beam was chosen in such a way that the projectile range of the incident ion (21.3 μm , as computed by SRIM program) exceeds thickness of the sample films ($\sim 2.5 \mu\text{m}$). Again the ion beam energy and thickness of the target was selected so that modification due to electronic energy loss (S_e) affects the sample. Energy dependent electronic energy loss (S_e) and nuclear energy loss (S_n) for Ti-ions has been shown in table 4.2.

Table 4.2 Energy dependent electronic energy loss (S_e) and nuclear energy loss (S_n) for Ti-ions

Energy MeV	Electronic Energy Loss $S_e=(dE/dx)_e$ eV/Å	Nuclear energy loss $S_n=(dE/dx)_n$ eV/Å	Projectile range R (μm)
10^{-2}	1.53	18.99	0.0419
10^{-1}	5.03	20.59	0.2913
1	25.47	8.59	0.2820
10	109.75	1.76	1.446
100	512.37	0.23	15.26
150	587.29	0.17	21.32

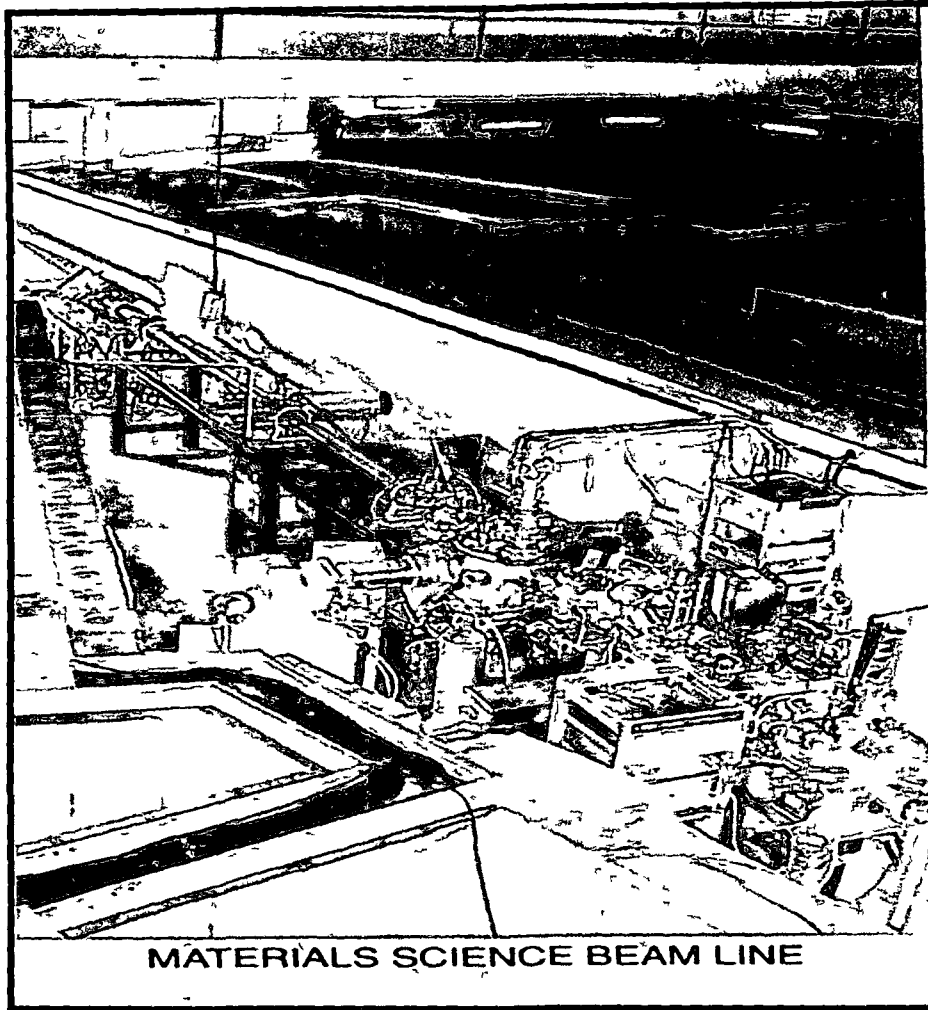


Figure 4.1 Ion irradiation beam hall of Materials Science beam line in Nuclear Science Centre, New-Delhi-110 067, India

The irradiated and un irradiated samples were characterized with

- (i) X Ray diffraction (XRD)
- (ii) Transmission Electron microscopy (TEM)
- (iii) Photoluminescence
- (iv) Optical absorption study
- (v) Magnetic Force microscopy (MFM)

4.3 Characterization of irradiated samples

To probe either optical or electrical properties it is very essential to know the accurate size of the nanoparticles. Therefore, for size determination XRD and TEM studies were carried out with irradiated samples. Further surface morphology and distribution of nano particles (quantum dots) in the sample is also very important for probing electrical properties. Through atomic force microscopy (AFM) these information were revealed.

4.3.1 Sample: Cu doped Zinc Sulfide (ZnS:Cu)

The ion fluence and corresponding sample code ZnS:Cu sample is shown in table 4.3

Table 4.3: Ion fluence and corresponding sample code for ZnS:Cu

Fluence notations	Irradiated sample notation
ϕ_1	S1d ₁
ϕ_2	S1d ₂
ϕ_3	S1d ₃
ϕ_4	S1d ₄
Un irradiated	S1

4.3.1.1 X-Ray diffraction:

XRD study has been carried out to estimate the sizes of the particles in virgin and irradiated samples. The figure 4.2 shows that the diffraction peak

becomes narrower and narrower as the ion fluence increases. This is the signature of formation of bigger particles upon ion irradiation. The average particle sizes estimated for virgin and irradiated samples are shown in table 4.4.

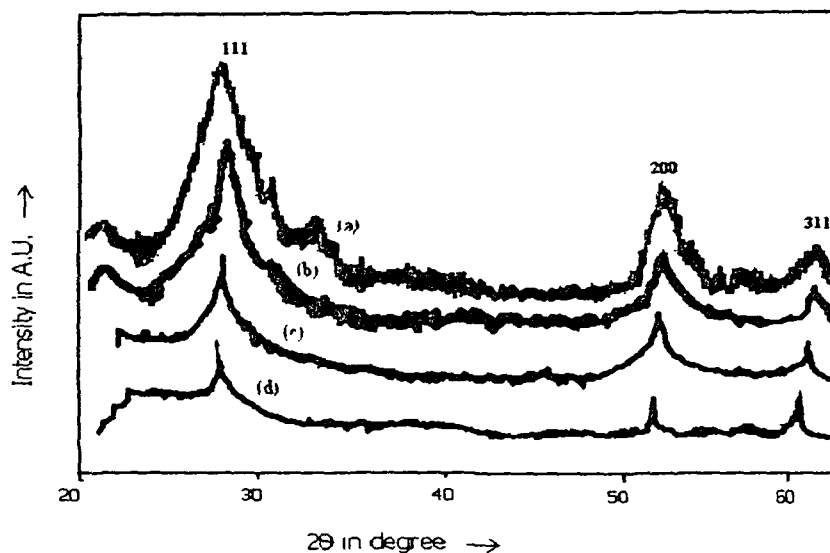


Figure 4.2 XRD peaks for (a) S1, (b) S1d₁, (c) S1d₂ and (d) S1d₃

Table 4.4: Average particle sizes estimated for virgin and irradiated samples

Average sizes(nm)of S1 corresponding to three diffraction angle	Average sizes(nm)of S1d ₁ corresponding to three diffraction angle	Average sizes(nm)of S1d ₂ corresponding to three diffraction angle	Average sizes(nm)of S1d ₃ corresponding to three diffraction angle
7.4	8.2	15.5	22

4.3.1.2 TEM Study:

The TEM study has been carried out for accurate measurement of particle sizes of irradiated samples. The images are depicted in figure (4.3) and sizes of the particles are mentioned in table 4.5.

Table 4.5: Sizes of the particles calculated from TEM study

Sample	S1d ₁	S1d ₂	S1d ₃
Size in nm	8	15	22

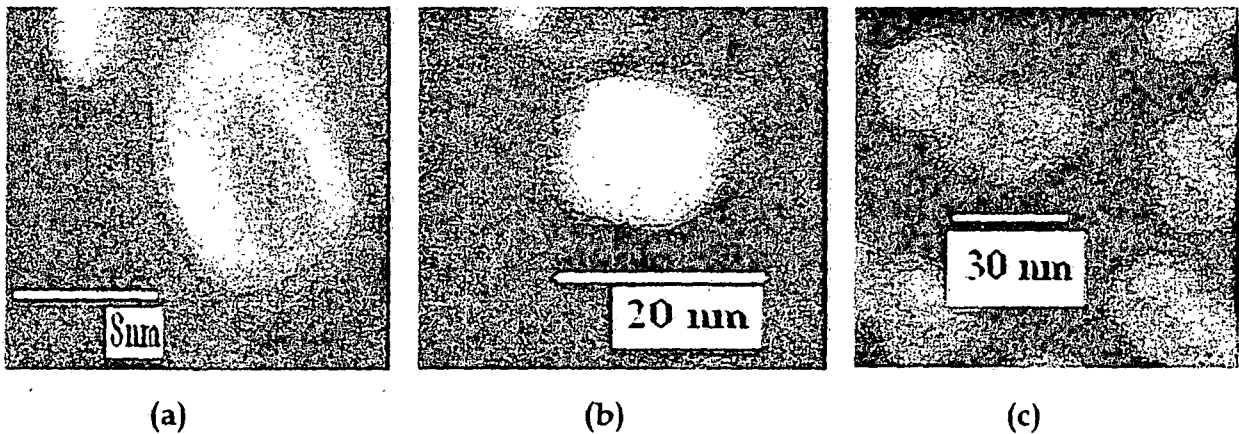


Figure 4.3 TEM image (a) for sample S1d₁, (b) for S1d₂ and (c) for S1d₃

We have not considered the sample S1d₄ since it was almost damaged due to exposure of very high fluence (3.2×10^{12} ion/cm²), and no appreciable result was found.

4.3.1.3 Optical absorption Study:

It is known that the band gap of nano particles increases the size decreases. Therefore blue shifted absorption peak is observed in optical absorption study. As the band gap increases, many electronic states are created within

it. The electrons are trapped in these states plays vital role in influencing photoluminescence. Further these trapped electrons are very instrumental in current generation at metal nanoparticle Schottky junction. The virgin and ion irradiated ZnS:Cu quantum dots samples have been characterized with optical absorption study . It has been observed that as ion fluence increases the band edge is found shifting towards red. This suggests that due to ion bombardment quantum particle behaviour is modified. Fast ion beam melts the quantum particles and rapid quenching leads to formation into bigger clusters within a time scale of about 10^{-12} sec. Beyond threshold fluence, polymer is supposed to be amorphized completely. The quantum particles thus loose their support in the polymeric matrix and they coalesce into bigger clusters. At the highest fluence, the larger sized quantum dots behave as free-standing particles. It is thus observed growth of nanoparticles under energetic ion irradiation. The particle fragmentation has already been reported ¹³.

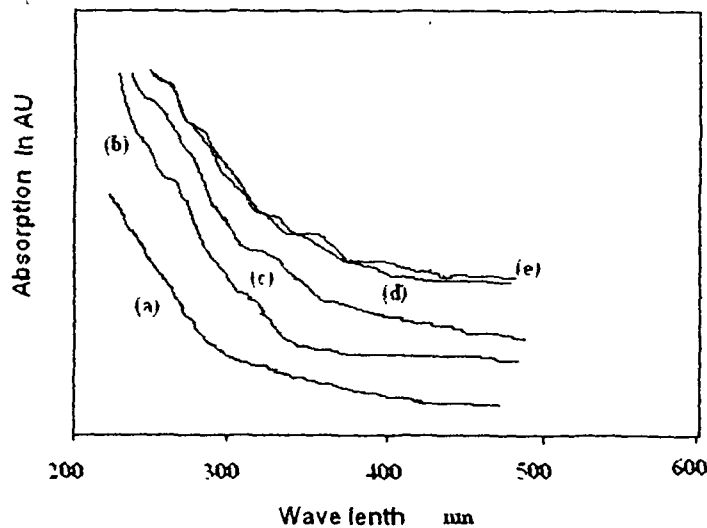


Figure 4.4 Optical absorption of ZnS:Cu (a) virgin (b) 1st fluence (2) 2nd fluence (3) 3rd fluence & (e) 4th fluence

Figure 4.4 shows the optical spectra of the samples. However this spectra show two parts

- (i) Strong absorption and
- (ii) Tail absorption

(i) Strong absorption edge:

This edge is due to band gap of any specimen. table 4.6 shows the optical spectroscopy data.

Table 4.6: Optical spectroscopy data of ZnS:Cu samples

Sample	Strong absorption edge	Size (nm)
S1	275	8
S1d ₁	280	9
S1d ₂	300	14.5
S1d ₃	330	20
S1d ₄	345	24.5

(ii) Tail absorption edge:

Tail absorption is due to the defects present in the sample. In unexposed samples, due to surface states, negligible tail absorption in the spectra was present. But, in irradiated samples, due to increase in particle size, surface states reduce, but Zn vacancies enhance due to SHI exposure and replace

surface state absorption. It is found that higher the dose more is the Zn vacancies and hence more is the tail absorption.

4.3.1.4 Photoluminescence:

The emission spectra of an irradiated Cu doped ZnS (ZnS:Cu) quantum dots samples have been discussed in Chapter 3.

In this chapter, we have studied luminescence properties of ion irradiated samples. The luminescence spectra of ion irradiated ZnS:Cu samples at different fluence have been included in the chapter.

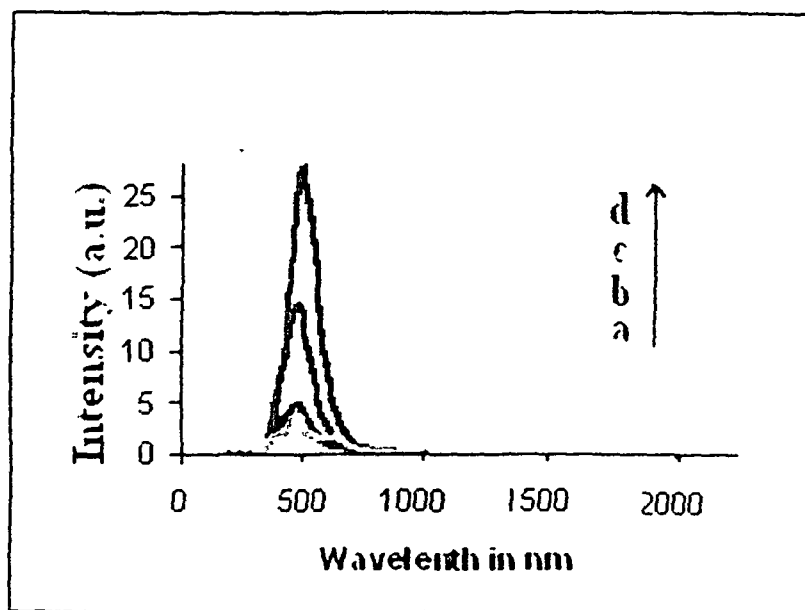


Fig. 4.5 Photoluminescence spectra Of ZnS:Cu quantum dots (a) S1 (b) S1d₁ (c) S1d₂ (d) S1d₃

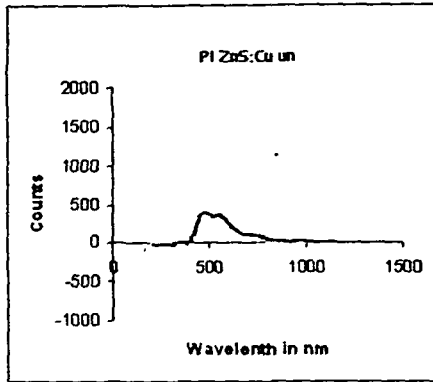


Fig. 4.5 (a)

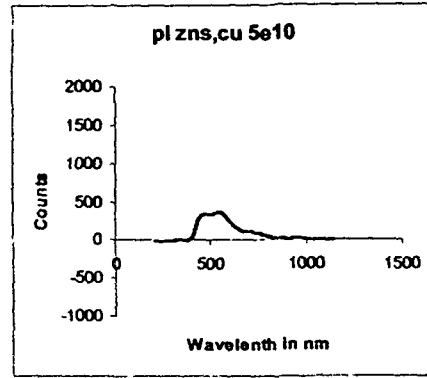
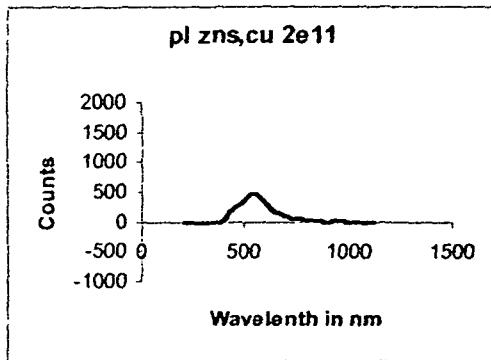
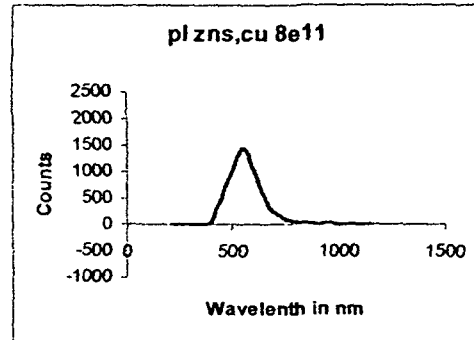


Fig. 4.5 (b)

Fig. 4.5 (a) and Fig. 4.5 (b) Photoluminescence spectra ZnS:Cu samples at fluence (a) 0, (b) 5×10^{10}



4.5 (c)



4.5 (d)

Fig. 4.5 (c) and Fig. 4.5 (d) Photoluminescence spectra ZnS:Cu samples at fluence (a) 2×10^{11} ion/cm², (b) 8×10^{11} ion/cm²

Figure 4.5 shows the comparative emission spectra of un irradiated and ion irradiated ZnS:Cu quantum dots samples. The same for the samples at fluence 0, 5×10^{10} ion/cm², 2×10^{11} ion/cm² and 8×10^{11} ion/cm² respectively are shown in the figure 4.5 (a), 4.5 (b), 4.5 (c) and 4.5 (d)

Luminescence is one of the most important methods to reveal the energy structure and surface states of quantum dots. In the emission spectra

of virgin and irradiated samples of ZnS:Cu quantum dots system (figure 5), three distinct peaks have been observed for virgin and irradiated sample with 1st fluence (5×10^{10} ion/cm²) but only single peak has been observed for other irradiated samples. However intensity of luminescence becomes more and more as ion fluence increases. The band to band excitation in ZnS has been used to excite the Cu⁺ emission. As discussed in chapter 3 'the subsequent transfer of electrons and holes into the electronic level of Cu⁺ ion leads to the characteristics emission of Cu²⁺ in ZnS system. Luminescence at 480 nm is due to copper induced levels. According to Peka and Schutz¹⁴ green luminescence is due to transition from conduction band of ZnS to the t₂ level of excited Cu²⁺(d⁹) in ZnS band gap'. The peak at 640 nm is due to surface states. The emission peak at 430 nm is due to donor acceptor pair transition. At higher fluence the quantum particles embedded in polymer matrix loose their support and coalesce into bigger particles. Therefore, the larger sized quantum dots behave as free-standing particles. It has been found from XRD and TEM reports the virgin and the sample of 1st fluence have almost same particle sizes. So the impact of ion beam with 1st fluence on the sample does not have much effect in changing the size of the particles. So we expect similar nature of band structure and surface states in both samples. That is the reason that we have got similar nature of emission spectrum for virgin sample as well as for the sample irradiated with 1st fluence .

The resulting intense emission for the samples at higher fluence may be regarded as the total luminescence contributed by all the fully free standing particles. Because for heavily exposed samples, the nano particles are completely free from matrix encapsulation when irradiated with higher fluence, Cu induced luminescence dominates.

4.3.2 Sample: Fe doped Zinc Sulfide (ZnS:Fe)

The ion fluence and corresponding sample code ZnS:Fe sample is shown in table 4.7

Table 4.7: Ion fluence and corresponding sample code for ZnS:Fe

Fluence notations	Irradiated sample notation
ϕ_1	S2d ₁
ϕ_2	S2d ₂
ϕ_3	S3d ₃
ϕ_4	S4d ₄
Un irradiated	S2

4.3.2.1 X-Ray diffraction:

The X-ray diffraction pattern of un irradiated and irradiated ZnS:Fe samples are depicted in figure 4.6. The narrow peaks for the sample S2d₂ (fluence 2×10^{11} ion/cm²) suggests formation of bigger particles. The particles' sizes of virgin and irradiated samples are placed in table 4.8.

Table 4.8: Particles' sizes of virgin and irradiated samples

Average sizes(nm)of S2 corresponding to three diffraction angle	Average sizes(nm)of S2d ₁ corresponding to three diffraction angle	Average sizes(nm)of S2d ₂ corresponding to three diffraction angle
7.6	9	16.5

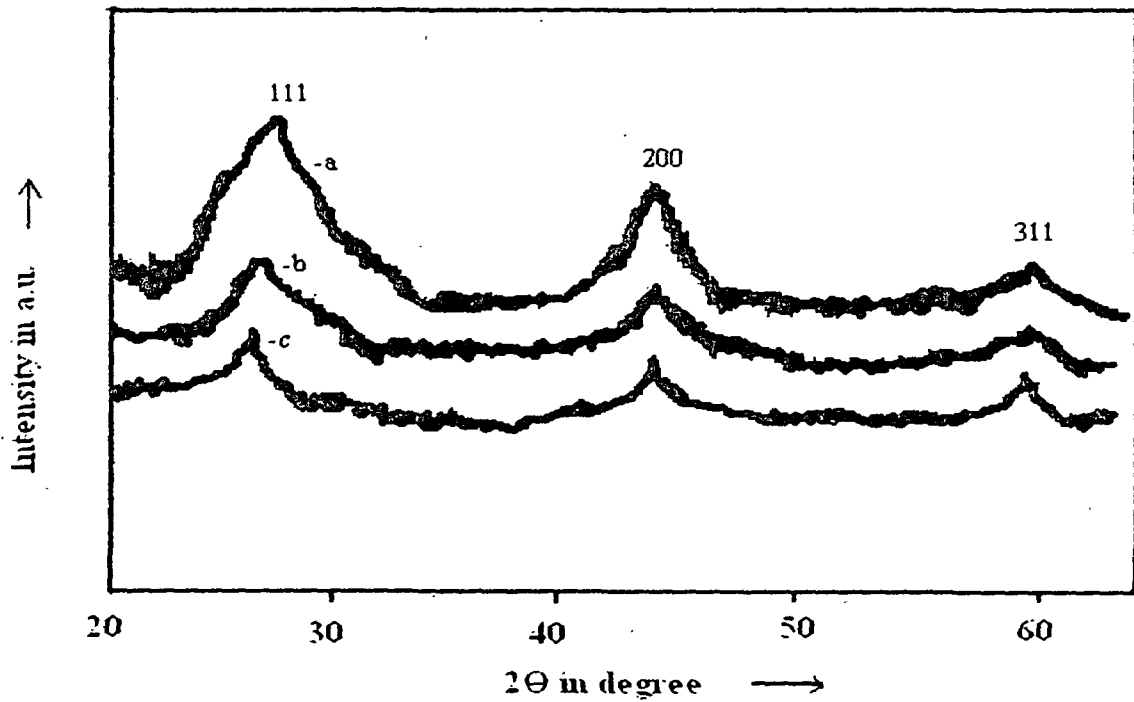
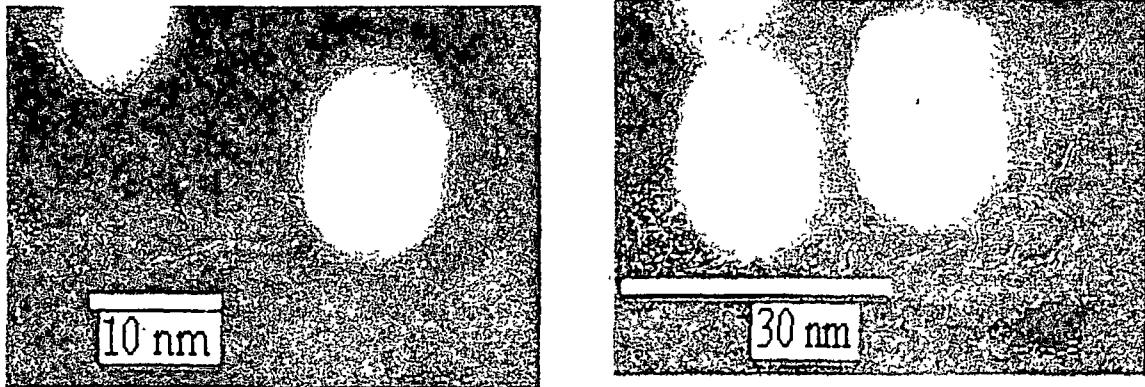


Fig. 4.6 XRD image of ZnS:Fe quantum dots (a) virgin(b) S2d₁ (1st fluence) (c) S2d₂ (2nd fluence)

4.3.2.2 *Transmission Electron Microscopy:*



(a)

(b)

Fig: 4.7 TEM images for ZnS:Fe quantum dots (a) S2d₁ (1st fluence) (b) S2d₂ (2nd fluence)

The TEM images of two irradiated samples of ZnS:Fe quantum dots are shown in figure 4.7. The sizes of the particles are estimated as 10 nm and 16 nm.

4.3.2.3 *Magnetic Force Microscopy (MFM):*

Generally MFM based techniques have been exploited to characterize properties and performance of magneto resistive devices such as the effect of shield on magneto resistive read-head performance¹⁵ and the magneto resistive response of patterned giant magneto resistance sensors with different edge stabilization schemes¹⁶.

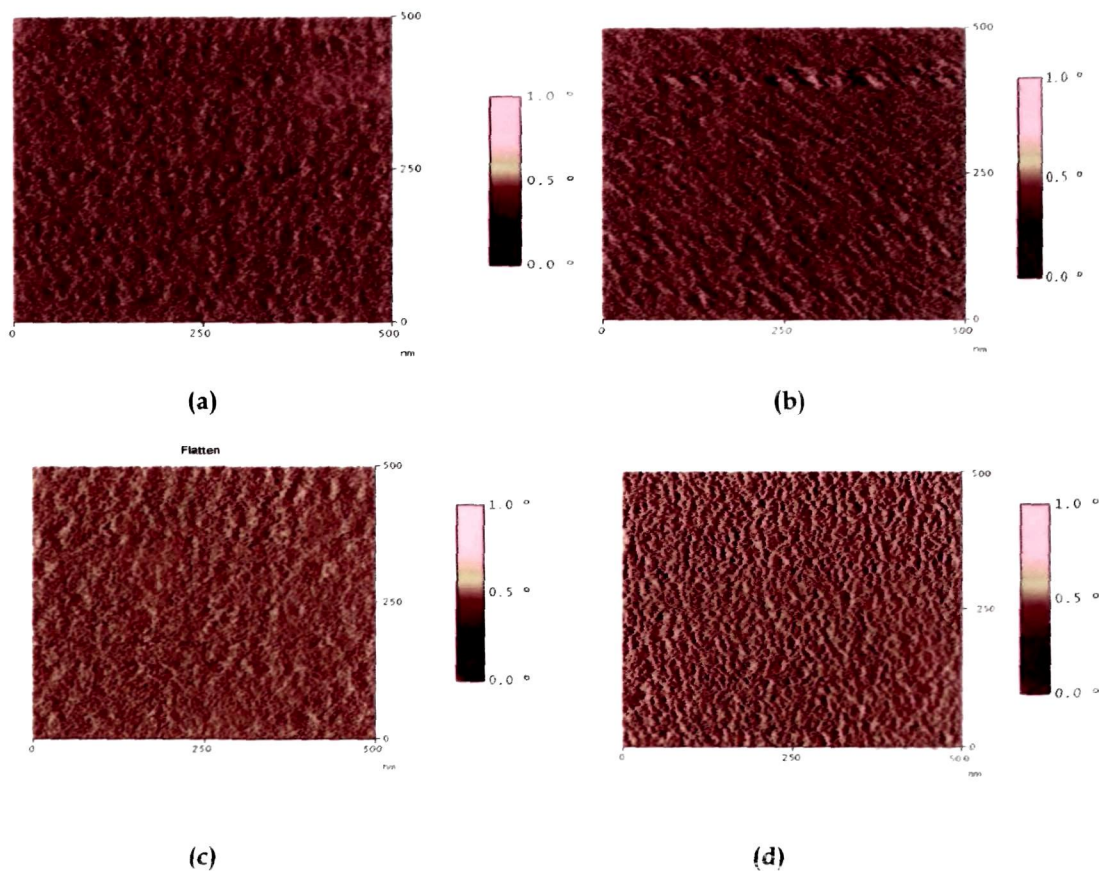


Fig: 4..8 Phase image of MFM for ZnS:Fe quantum dots (a) for sample S2 (b) for S2d₁ (c) for S2d₂ and (d) for S2d₃

We have carried out magnetic force microscopic studies on Fe doped ZnS quantum dots system using Digital instrument Nano Scope. It has been reported that when doped with some magnetic impurities, the nanostructures develop a unique class of material called diluted magnetic semiconductors (DMS) which are promising candidates for magnetic memories, sensors and other spin-based devices^{17, 18}. Such semi magnetic and semi conducting structures, where carrier and spin confinement is possible provides a matchless system for spin manipulation and spin transportation¹⁹. Especially MFM studies on Fe doped ZnS quantum dots

samples have been done to see magnetic properties of the samples to find electrical applications.

The figure 4.8 (a, b, c and d) represent phase image of magnetic force microscopy of pristine (S2), irradiated with 1st fluence (S2d₁), 2nd fluence (S2d₂) and 3rd fluence (S2d₃) ZnS:Fe quantum dots samples respectively. The phase image of un irradiated and irradiated (1st fluence) ZnS:Fe do not show any appreciable results on the magnetic domains due to matrix encapsulation. But almost elliptical shaped single domains are visible in case of the sample irradiated at fluence 2×10^{11} ion/cm². At fluence 8×10^{11} ion/cm² the domains are in elongated nature. These aligned domains are extended up to 80-100 nm and would find application in magnetic tapes, magnetic recording devices and other spin based devices.

It is obvious that some atoms when doped quantum dots can not have observable magnetic effect embedded in polymer matrix. In our result we therefore have not obtained any appreciable result for the un irradiated sample as well as the sample at 1st fluence. But at higher fluence the particles become free from matrix encapsulation and magnetic domains are observed.

4.3.2.4 *Photoluminescence:*

Photoluminescence spectra of Fe doped ZnS (ZnS:Fe) quantum dots samples have been discussed in Chapter 3.

we have studied luminescence properties of ion irradiated ZnS:Fe samples. The luminescence spectra of ion irradiated ZnS:Fe samples at fluence 0, 5×10^{10} ion/cm² and 2×10^{11} ion/cm² are depicted in figure 4.9(a), 4.9(b) and 4.9(c). The comparative emission spectra of un radiated and ion radiated ZnS:Fe quantum dots is depicted in figure 4.9 Like ZnS:Cu sample,

we have got similar luminescence spectra for samples at fluence 0 and 5×10^{10} ion/cm² [Figure 4.9 (a) and 4.9 (b)]. Again at higher fluence [Figure 4.9 (c)] single luminescence peak with efficient intensity has been obtained due to free standing of the particle. As discussed in chapter 3 three distinct peaks at around 483 nm, 546 nm and 749 nm are seen for iron doped sample. The emission peak at 483 nm is due to donor acceptor pair transition, the peak at 749 nm is the result of surface states present in the sample. The blue green emission peak at 546 nm might be due to transfer of Fe ion in substitutional site of Zn²⁺. Also the luminescence intensity becomes intense at higher fluences. We also observe that two other peaks found in virgin sample, disappear at higher fluence. At higher fluence Fe induced luminescence dominates surface luminescence and luminescence due to donor acceptor pair transition.

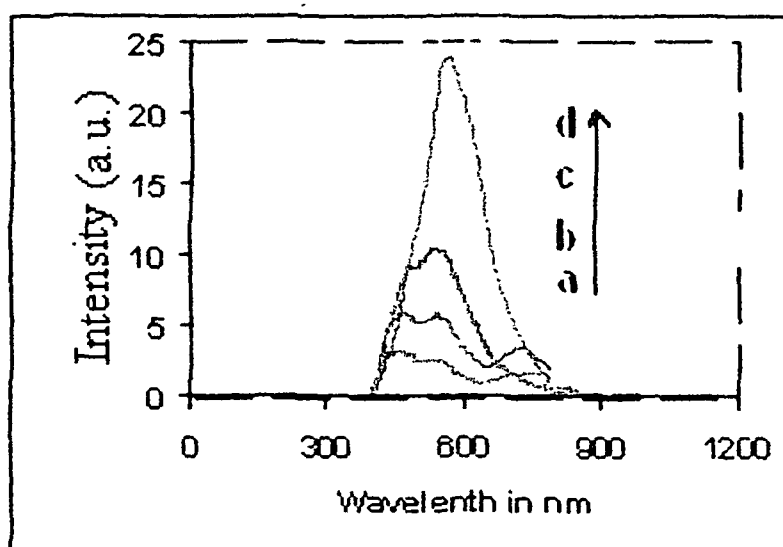


Fig: 4.9 Photoluminescence spectra Of ZnS:Fe quantum dots (a) S2 (b) S2d₁ (c) S2d₂ (d) S2d₃

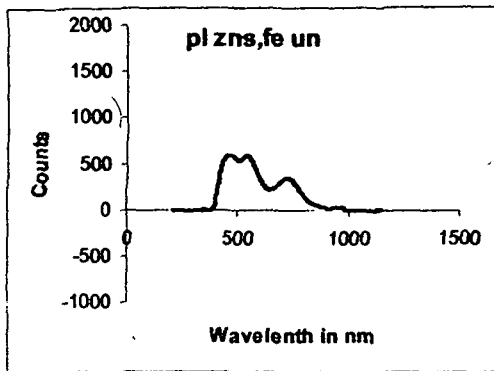


Fig. 4.9 (a)

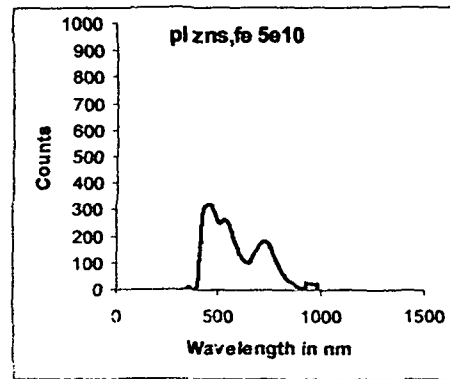


Fig 4.9 (b)

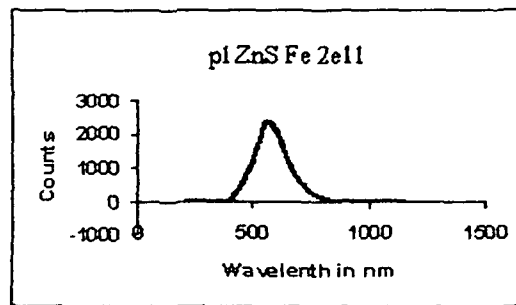


Fig 4.9 (c)

Fig. 4.9 (a), (b) and (c) Photoluminescence spectra ZnS:Fe samples at fluence 0, 5×10^{10} and 2×10^{11}

Photoluminescence spectra of undoped ZnS quantum dots also show intense luminescence intensity for irradiated samples (Fig.4.10). However intensity is lower in comparison with corresponding intensities of Cu doped and Fe doped ZnS quantum dots.

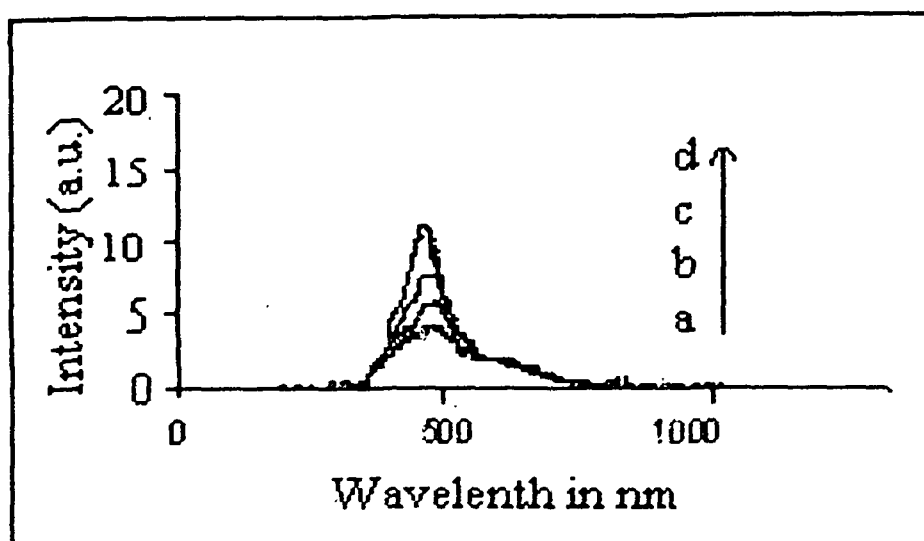


Fig: 4.10 Photoluminescence spectra Of ZnS quantum dots (a) virgin (b) 1st fluence (c) 2nd fluence (d) 3rd fluence

It is concluded that the regular grain growth process is observed in embedded polymer system under ion irradiation. The size of the grains can be tuned by selecting proper ion fluence. The samples irradiated with the higher fluence become free from polymer encapsulation which results strong surface emissions in PL spectra which arise basically from the surface states. The surface emission energies for ZnS:Cu quantum dots assembly are calculated and found as 1.94 eV, 1.94 eV and 2.19 eV for fluences 0, 5×10^{11} and 2×10^{12} ions/cm², respectively, the same for ZnS:Fe samples have been calculated as 1.65 eV, 1.65 eV and 2.1 eV for fluences 0, 5×10^{11} and 3×10^{12} ions/cm² respectively. The sharp enhancement of luminescence intensity observed on highly exposed samples is due to breaking of barrier. The shifting of emission peaks towards blue was not due to size effect. Here, main contribution comes through existence of the surfaces states (even in the presence of significant grain growth). Therefore, sensitivity of the optical sensors and other optoelectronic devices can be improved using ion irradiated and doped semiconductor quantum dots.

4.4 Summary

The ion-beam irradiation has many effects on matter and especially on nano particles. Upon irradiation the effect like fragmentation into smaller particle, amorphization, evaporation and formation of bigger particle may occur depending on energy of ion beam, fluence etc. Since nano particles (quantum dots) are separated each other by a finite distance, the ion irradiation on such system assures an exciting area of research.

Two doped samples (ZnS:Cu and ZnS:Fe) and undoped ZnS quantum dots samples were irradiated with 150 MeV Ti^{+11} ion selecting four different ion fluences. The virgin and irradiated doped samples were characterized with optical absorption, XRD and TEM for size determination. Photoluminescence study was performed to collect the information about surface states within the band gap of nano particles of the samples. The information of surface morphology and distribution of particles was collected from atomic force microscopy (AFM). Through magnetic force microscopy (MFM) study, some magnetic properties are investigated for possible electrical applications.

The MFM study was done on virgin and irradiated Fe doped ZnS samples. The phase images of this study for virgin sample and the sample with lowest fluence do not demonstrate any appreciable result. When ion fluence increases elliptical shaped domains are formed and these domains become elongated at further increase in fluence. These aligned domains have got application in magnetic tapes, magnetic recording devices and other spin based devices.

The optical absorption study reveals that at higher fluence the absorption edge is red shifted. XRD and TEM studies also confirm formation of bigger particles ion fluence increases.

Emission spectra of Cu doped ZnS (ZnS:Cu) quantum dots and Fe doped ZnS (ZnS:Fe) quantum dots show enhanced luminescence intensity for the samples irradiated with higher ion fluence. However it is significant that three distinct emission peaks observed in virgin samples of ZnS:Cu and ZnS:Fe become absent in the emission spectra of the samples with higher ion fluence. At higher fluences Cu induced luminescence in ZnS:Cu and Fe induced luminescence in ZnS:Fe dominate other two emission peaks noticed in virgin samples. When ion fluence become higher, bigger particles are formed due to agglomeration, hence enhanced and efficient luminescence intensity is obtained.

References

1. Proceedings of 11th International Conference on Ion Beam Modification of Materials Amsterdam (eds A M Vredenberg,, A Polman,, P A Stolk, , E Snolesand, and L. M Brongersma,,), North Holland, Amsterdam, (1998)
2. Proceedings of the International Conference on Swift Heavy Ions in Matter (eds S Klaumuenzer and N Stolterfoht), North Holland, Berlin, May (1998)
3. Proceedings of the International Conference on Swift Heavy Ions in Materials Engineering and Characterization (eds D K Avasthi,.. and D Kanjilal.), New Delhi, North Holland, Amsterdam, October (1998)
4. J. L Ecuyer, C Brassard, C Cardinal, and B Terrault, *Nucl. Instrum. Methods, , 149*, 271. (1978).
5. D K Avasthi, *Nucl. Istrum. Methods B, , 136*, 729. (1998)
6. C H Kiang, W A Goddard, R Beyers and D S Bethune, *J. Phys. Chem.* **100** 3749 (1996)
7. P M Ajayan, V Ravikumar and J C Charlier, *Phys. Rev. Lett.* **81** 1437 (1998)
8. M Toulemonde, C Dufour and E Paumier , *Phys. Rev. B* **46** 14362 (1992)
9. Z G Wang, C Dufour, E Paumier and M Toulemonde, *J. Phys.: Cond. Mat.* **6** 6733 (1994)
10. D Lesueur and A Dunlop, *Radiat. Eff. Def. Solids* **126** 163 (1993)
11. R L Fleischer, P B Price and R M Walker, (eds.) *Nuclear Tracks in Solids*, University of California Press, Berkely, CA (1975)
12. A Berthelot, S Hemon, F Gourbilleau, E Dufour, Paumier E, *Nucl. Instru. and Meth. B* **146** 437 (1998)

13. P Peka and H J Schulz. *Physica B* **193** 57 (1994)
14. D Han, M E Hansen, J Ding and J J Fernandez-de Castro. *J. Appl. Phys.* (2000)
15. S Foss-Schroeder, J van Ek, D Song, G Louder, Al Jumaily, P Ryan, C Prater, E Hachfeld, M Wilson and R Tench *J. Appl. Phys.* **89** 6769 (2001)
16. G A Prinz, *Science* **282** 1660 (1998)
17. D P Divincenzo, *J. Appl. Phys.* **85** 4785 (1999)
18. T Dietl, *Braz. J. Phys.* **34** 2B (2004)

Chapter 5

ELECTRICAL PROPERTIES

Quantum dots are well characterized by their optical properties. During the past few years, much progress has been made in understanding these particles through their non linear optical properties. But on the other hand transport properties are of great interest and are important for technological applications like imaging and electro luminescence display.

For all kinds of applications however, detailed understanding of the electronic properties of the quantum dots and the processes of carrier capture and exchange with the matrix material is also important. Up to now, mainly optical techniques have been applied to study the properties of self organized quantumdots¹⁻⁴. Such experiments are limited to the detection of light emission due to excitonic recombination and can not hence reveal direct information on the energy levels of electrons and holes in quantum dots. From the observation of luminescence only indirect conclusions on the carrier dynamics of carriers can be drawn. The determination of emission rates of both types of carriers individually is therefore almost impossible. Finally, the presence of charge, which is the fundamental ingredient of all electronic applications, can not be detected at all by optical techniques. Hence a method capable of accounting for these effects is consequently called for.

In order to explore transport related applications of semiconductor nano particles, a matrix that is capable of both transporting carriers and interacting with the semiconductor is useful.

For tunneling from dot to dot embedded in PVA a minimum voltage (knee voltage) is needed, but in case of dot embedded in conducting polymer this minimum voltage is not needed. A large number of semiconductor nanocrystals can be doped into conducting polymers to form good photoconductive composites⁵⁻⁹. The availability of these semiconductor nanocrystal/polymer composites opens the doorway for exploiting transport related applications such as photoconductivity, electroluminescence¹⁰.

The probing of the particles of nano scale and carrier transport in nano structured films is impossible due to presence of weak link boundaries. But things get improved if one has a few number of arrayed quantum particles separated by thin dielectric medium under the influence of high intensity light (basically, hi-power pulsed laser). The interfacial charge transfer is detectable through photocurrent generation in the external circuit, connected to a biasing source. Previously, the interfacial charge transfer has been reported in coupled, coated and layered systems. But charge transfer in an embedded system due to resonant excitation of *e-h* pairs in a weakly confined quantum dot system provides deep insight to carrier tunneling at room temperature. This can be observed in the form of steps in I - V characteristics. These unusual characteristics known as single electron effects are the prerequisites for single electron transistors (SET). Electron transport in metal-semiconductor contacts is of great technological importance and has been a long-standing topic of research¹¹⁻¹³. A principal

part of this work is devoted to understanding the origin of the Schottky barrier height in order to increase the uniformity of the electrical characteristics from device to device. Traditionally, measurements have used only current versus voltage ($I-V$), capacitance versus voltage ($C-V$).

In this chapter we try to explain frequency dependent current-voltage ($I-V$) and capacitance-voltage ($C-V$) characteristics of chemically grown nanoZnS / Ag junction and nano ZnS:Cu/ Ag junction.

Photo induced current generation in ZnS/Polyaniline is also discussed.

By fabricating capacitive structure of CdS and ZnS quantum dots the studies of voltage-impedance ($V-Z$) and voltage-capacitance ($V-C$) characteristics are discussed.

5.1 Frequency dependent current-voltage ($I-V$) and capacitance-voltage ($C-V$) characteristics

The metal semiconductor interfaces could produce Schottky barrier or ohmic contacts based on the work functions and other electronic properties, such as Fermi level pinning, barrier height and barrier width. When size of the semiconductor nanocrystal is a few nanometers, SET effects such as Coulomb blockade is observed. But when the size of a metallic cluster on a semiconductor is not small enough for SET effect, the structure can exhibit Schottky barrier behavior.

5.1.1 Depletion Region

The energy of electrons in a metal and in a semiconductor (or two differently doped semiconductors) with respect to the vacuum level will not generally be the same. If a metal and a semiconductor (or two differently doped semiconductors) are brought in electrical contact, charge in the form of free carriers will flow until both parts are in thermodynamic equilibrium and the Fermi energy E_F is equal throughout the whole structure. As a consequence, ionized donors or acceptors are left behind in the semiconductor leading to a local violation of charge neutrality in the vicinity of the interface. The layer depleted of free carriers is usually referred to as the 'depletion region'¹⁴⁻¹⁶. The width of the depletion region depends on the doping concentration and the potential difference, of which the later can easily be modified by an externally applied bias. Due to the absence of free carriers, the depletion region is electrically isolating and the origin of the rectifying properties of such semiconductor diode devices. A metal-semiconductor contact can be described by the Schottky model and is therefore commonly referred to as 'Schottky contact'.

5.1.2 Schottky Contact

Actual metal-semiconductor contacts are usually described in the framework of the Schottky model, as they can be characterized by a barrier height ϕ_b which is essentially dependent of an applied external bias.

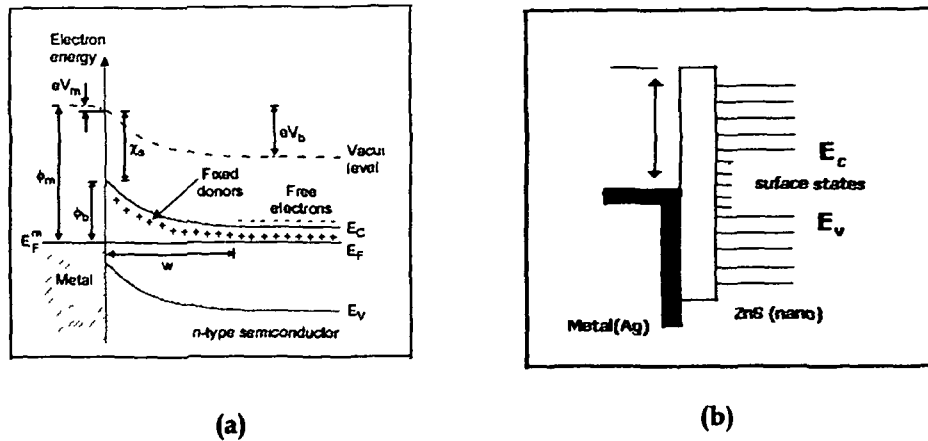


Fig: 5.1 Schematic energy band diagram of bulk (a) ZnS/Ag and (b) nano ZnS/Ag Schottky barrier

According to the Schottky model the energy band diagram is constructed with reference to the vacuum level. The work function of the metal ϕ_m and the electron affinity of the semiconductor χ_s are defined as the energies required removing an electron from the Fermi level or semiconductor conduction band edge, respectively, to the vacuum level. These values are supposed to be material properties, and it is further assumed that the vacuum level is continuous across the interface. Since at the interface the vacuum level is the same for the two materials, there must be a step between the Fermi level of the metal and the conduction band of the semiconductor due to the difference between ϕ_m and χ_s as depicted in Figure 5.1(a). The figure 5.1(b) depicts energy band diagram of nano ZnS/Ag schottky-junction showing surface states within the band gap of ZnS quantum dots.

We have fabricated Schottky junction depositing Ag (2 mm in diameter) on thick film (1.6 μm) of ZnS quantum dots and deposited on conducting ITO glass. The forward Current-Voltage (I - V) characteristics

were studied for nano ZnS/Ag junction and nano ZnS: Cu/Ag junction using LCR meter.

5.1.3 I-V characteristics of nano ZnS/Ag

Current-voltage ($I-V$) characteristics of ZnS/Ag junction for frequency range 1 KHz-40 KHz are shown in figure 5.2. It is seen that current does not grow up to a certain applied voltage and this built up voltage is reducing as applied frequency is increasing. It is reported that Nano ZnS/Ag junction draws current at lower voltage than that bulk ZnS/Ag junction does due to presence of high density of surface states¹⁷. Further rate of current growth is higher at higher frequency. In metal nano semiconductor contact the surface states are not in direct touch with the metal and permanently belong to nano semiconductor. The electrons are trapped within these surface states and become available when bias voltage increases. It is expected that the trapped carriers of ZnS quantum dot follow the signal and provide conducting passage through the sample and hence there is current establishment. As the signal frequency increases, more number of carriers participate for current establishment by dislodging themselves from the trapped centers (surface states). The current growth in such system is ascribed to the built in potential across the ZnS/Ag nano junction¹⁸ and trap related ($I \propto V^m$) current model^{19,20} would be relevant to our case as linear current growth response indicates faster charge decay of the nanoparticles as signal frequency rises considerably. Here 'm' stands for ideality factor.

The figure 5.3 shows the $I-V$ characteristics of nano ZnS/Ag junction for frequency range 1 MHz-4 MHz. It is observed that in this regime current

starts at lower potential and comparatively higher current is drawn than that in case of 1 KHz-40 KHz range. It suggests that very large number of carrier injection from surface states plays dominant role for current establishment at higher and higher frequency.

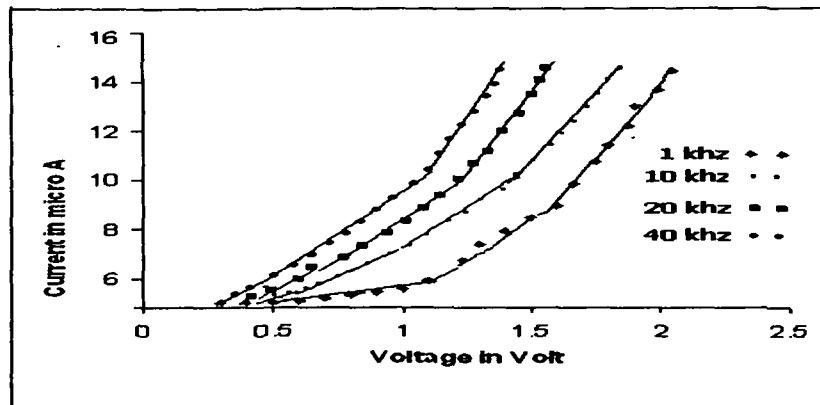


Fig: 5.2 *I-V* characteristics of nano ZnS/Ag junction at frequency range 1 KHz-40 KHz

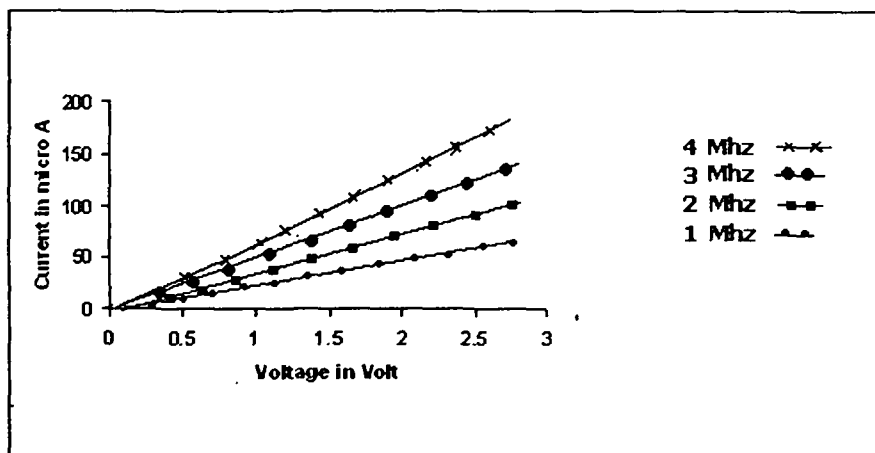


Fig: 5.3 *I-V* characteristics of nano ZnS/Ag junction at frequency range 1 MHz-4 MHz

5.1.4 I-V characteristics of Cu doped ZnS qd/Ag

The I-V characteristics of Cu doped ZnS qd/Ag junction for frequency range 1KHz-40KHz and 1MHz-4MHz are shown in figure 5.4 and 5.5 respectively. We observe that the nature of the curves obtained at different frequency is almost similar to those obtained in case of nano ZnS/Ag junction. It is already established in chapter III that when synthesized under similar condition the particle size of Cu doped ZnS quantum dot and ZnS quantum dots are same because doping percentage of copper is very small in ZnS:Cu quantum dot. Since particle size determines surface states so we can expect equal amount of charge carriers will take part in current establishment. However more current response in nano ZnS:Cu/Ag junction is believed as lowering of contact potential (difference in work function potential of metal and semi conductor) due to doping of copper in ZnS.

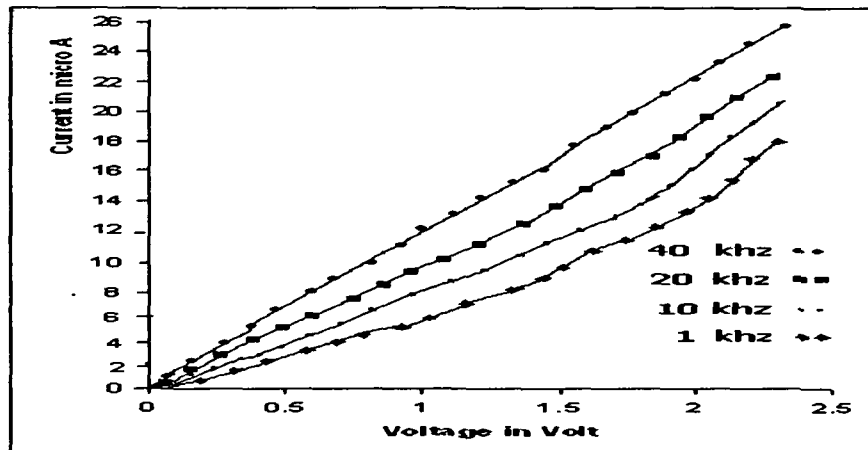


Fig: 5.4 I -V characteristics of nano ZnS:Cu/Ag junction at freq. Range 1KHz-40 KHz

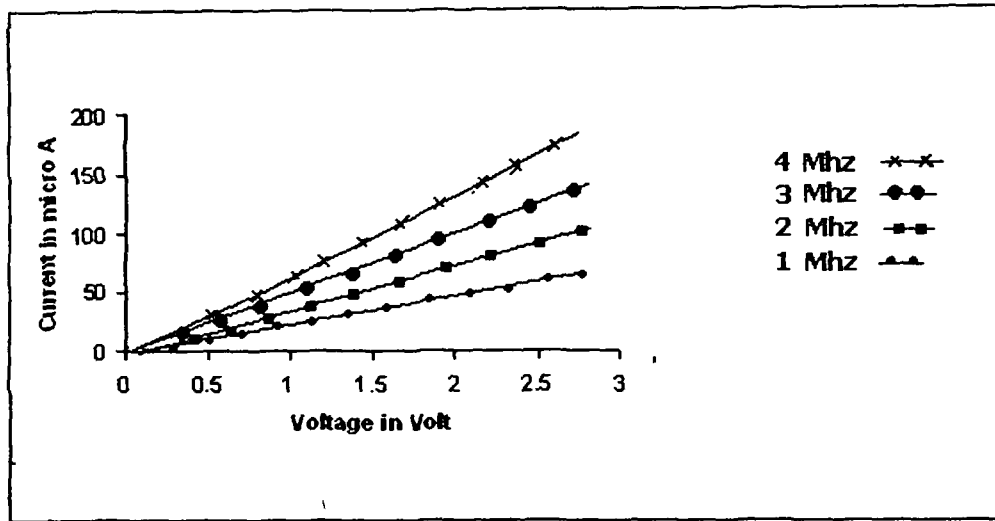


Fig: 5.5 I - V characteristics of nano ZnS:Cu/Ag junction at freq. Range 1MHz-4 MHz

5.1.5 C - V characteristics of nano ZnS/Ag

The C - V characteristics of ZnS qd/Ag were studied for frequency range 1KHz-40 KHz and shown in figure 5.6 .The capacitance increases with voltage and this increment falls as frequency increases. At higher forward bias, the contribution of surface traps present is significant. A high density of surface/interface traps leads to injection of minority carries into the neutral zone. This would give an additional diffusion capacitance besides the normal depletion layer contribution. Hence total junction capacitance is the sum of the diffusion capacitance and the depletion capacitance.

Thus, the junction capacitance can be written as

$$C_j = C_{dc} + C_{diff}. \quad (\text{Eq 5.1})$$

Further, the rearrangement of these injected minority carriers do not take place instantaneously and also become frequency dependent. For

frequencies above the characteristic frequency of the recombination processes, these injected excess minority carriers are able to follow the signal and the C_{diff} contribution to C_j is mainly from the depletion layer. At higher frequencies, C_j attains saturation implying that the domain contribution to C_j is mainly from the depletion layer. The overall feature requires a frequency dispersion relation. Mott-Schottky nano junctions have been reported in case of metal-superconductor-semiconductors ²¹. With experimental frequency variations within 1 KHz-15 KHz, the frequency dispersion discussed through the Mott-Schottky relation for a nano-CdS/ Au junction given by ²²,

$$\frac{1}{C_{dc}^2} = \frac{2}{q\epsilon_0\epsilon_s n_d} (V + V_{bi}) \quad (\text{Eq 5.2})$$

where the quantities ϵ_0 , ϵ_s , n_d , V_{bi} and C_{dc} are permittivity of the free space, the dielectric constant of the semiconductor, the donor concentration, the built in potential and depletion layer capacitance.

In low frequency regime Mott-Schottky response is effective to obtain built in potentials where interfacial effect is dominant. But at higher frequency the trapped carriers can tunnel through the polymer barrier between Ag and nano ZnS. The polymer embedded semiconductor quantum dot collectively behaves as capacitor.

When voltage increases Ag diffuses into ZnS, electrons are loaded and thus increasing the junction capacitance as a result of charging. Maximum charging effect is realized when almost no carriers respond to signal frequency. Conversely, when frequency increases, a fair number of

electrons would try to follow the signal frequency and got no chance to be loaded into nano ZnS .That is why capacitance drops at higher frequency.

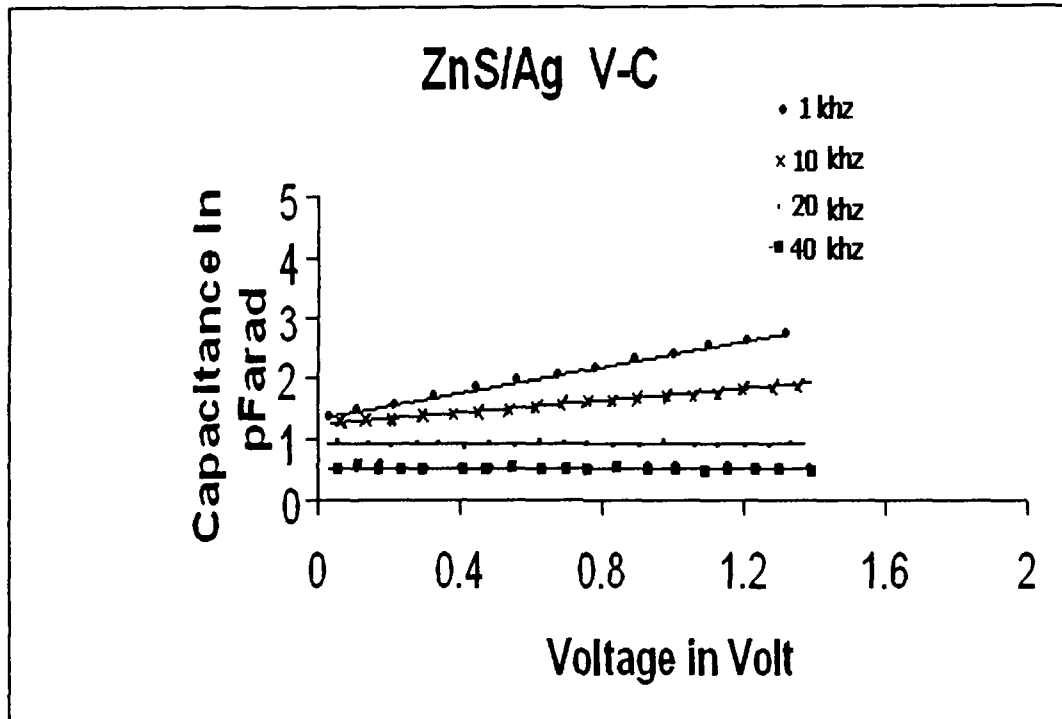


Fig: 5. 6 C -V characteristics of nano ZnS/Ag junction

We can also compare I-V characteristics of nano ZnS/Ag and Cu doped nano ZnS/Ag with ideal diode characteristics and with ideal characteristic of Schottkey diode. When compared the plots in fig 5.2 with the ideal diode characteristic as shown in figure 5.7 it is revealed that the curves in Fig 5.2 shows the phenomena of diode characteristic up to frequency 40 KHz. The reason may be explained in the way that quantum dots are associated with capacitive phenomena and hence have capacitive impedance. At low frequency (up to 40 kHz) capacitive impedance becomes

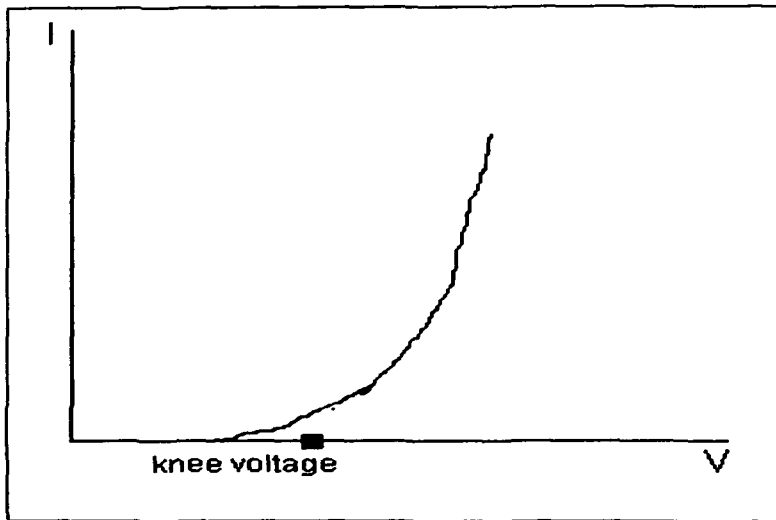


Fig.5.7 Diode Characteristics

significantly high. As the voltage is applied to the device the capacitive impedance opposes the rise in current but after a certain critical voltage current starts rising, because this voltage overcomes opposing impedance and produces current. This impedance can be compared with the barrier voltage of ordinary diodes and the minimum voltage needed for the initial rise of the current is equivalent to knee voltage of diode.

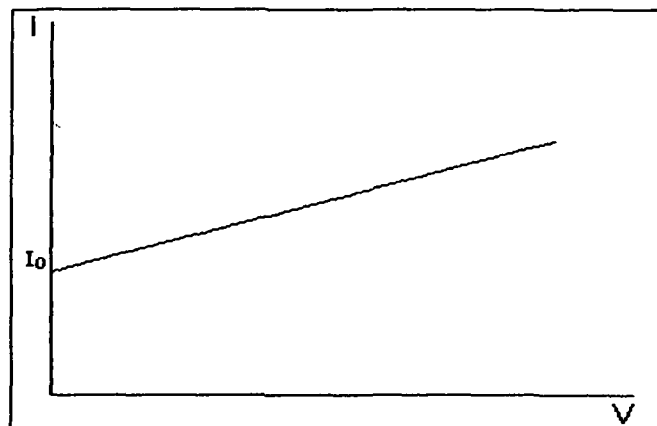


Fig: 5.8 Ideal Schottky behavior

On the other hand, by comparing the plots in fig 5.3 with the ideal characteristic of Schottky diode (Figure 5.8) it is revealed that at higher frequencies the device shows schottky behavior. That is because no knee voltage is required for the rise in initial current. We may explain the phenomena that at higher frequencies (1 MHz to 4 MHz, may be more) capacitive impedance is negligible. In quantum dots basically capacitive reactance plays an important role to oppose the flow of current, but as this impedance is very low at higher frequencies (as capacitive impedance $=1/cw$) there is no effective impedance to oppose the flow of current. Though at higher frequency capacitance becomes small, the over all capacitive reactance comes from frequency, hence current rises sharply and requires no knee voltage.

The only deviation of our device from the ideal characteristic of Schottky is that in our case we do not have I_0 . This is due to presence of impurities at the junction area as we have fabricated the device by crude chemical method.

In the figure 5.4 , the plots show that if ZnS nano sample doped with Cu, the device can act as schottky diode even at low frequency. This is because of the fact that due to doping of copper in the sample, the capacitive impedance (probably) decreases and there is no significant impedance in the device to oppose the flow of current and hence no knee voltage is needed as it is found in the undoped ZnS/ Ag at frequency range 1KHz-40 KHz.

So it can be concluded that Schottky diode with undoped ZnS can act as ordinary diode at low frequency (KHz) while the same behaves as

schottky diode at higher frequency (MHz). But if ZnS quantum dot is doped with Cu the device can act as schottky diode at lower frequency also. Further we can also conclude that schottky behavior in our device is a function of either frequency or doping element.

I-V characteristics of ion beam irradiated Cu doped quantum dot samples were also studied. But we did not find any significant result for these studies. For studying these characteristics we had to pull out the sample from the glass substrate, but smoothly pulling of the sample film was not possible due to its strong adhesion to the glass substrate upon irradiation. On the other hand, the film was not deposited on ITO glass thinking of loss of conductivity of the glass due to the impact of high energetic ion beam. This might be one of the reasons for not getting the significant results.

5.2. Capacitive Structure

Different capacitive structures are fabricated by depositing silver plates on both sides of the quantum dots samples as shown in the figure 5.9. The separation between two silver plates are set for three samples S_1 , S_2 and S_3 as 2 mm, 3 mm and 4mm. The impedance against voltage (*V-Z*) and capacitance against voltage (*V-C*) are studied at different frequencies. From the curves in figures 5.10, 5.11 and 5.12 it is observed that the impedance does not change with voltage change but decreases as frequency increases. Since we have not found any significant contribution of inductive part of the samples, so the impedance is believed to be contribution from resistive and capacitive parts of the samples. From the curves in fig. 5.10 frequency against impedance is plotted at fixed voltage 1 volt for sample S_1 and compared with other same

two curves plotted for sample S_2 (from the curves in figure 5.11) and sample S_3 (curves in figure 5.12) in figure 5.13. From this comparison it is found that there is equal decrement in impedance when the separation between the two plates is reduced by equal amount. This observation suggests that the nano particles are uniformly distributed in the sample. Our TEM and AFM studies have also confirmed this uniform distribution of the particles.

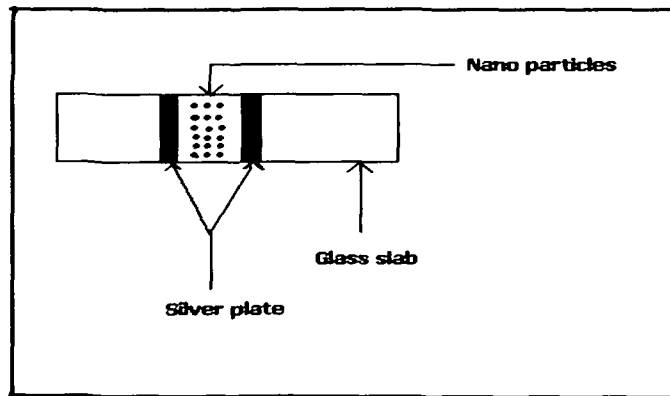


Fig.5.9 Schematic diagram of capacitive structure of qd samples

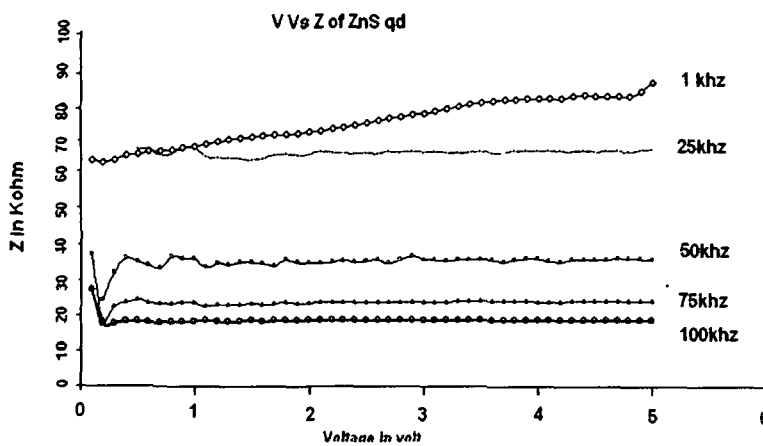


Fig: 5.10 Voltage-Impedance characteristics for ZnS qd (sample S_1)

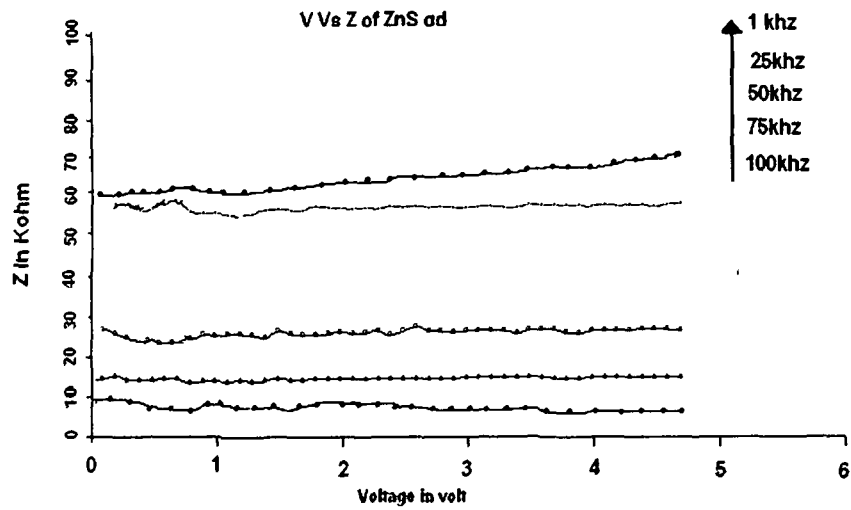


Fig 5.11 Voltage-Impedance characteristics of ZnS qd (sample S₂)

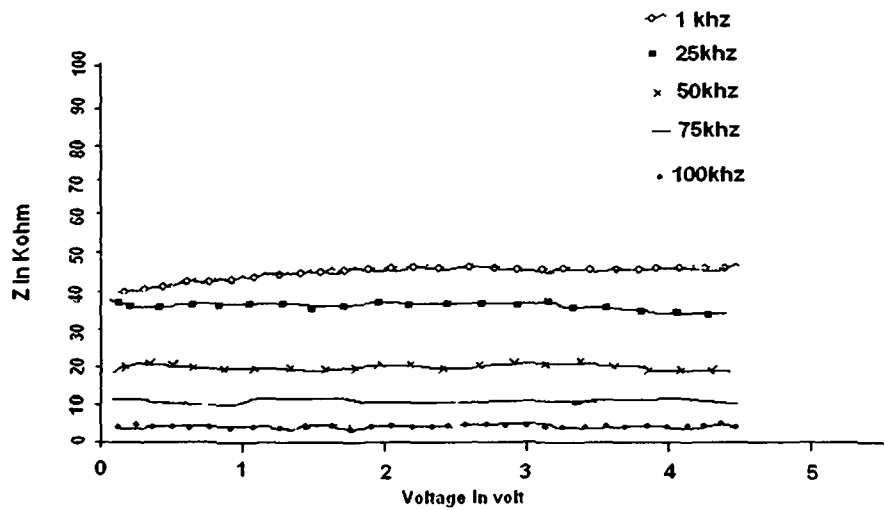


Fig.5.12 Voltage-impedance characteristics of ZnS qd (Sample S₃)

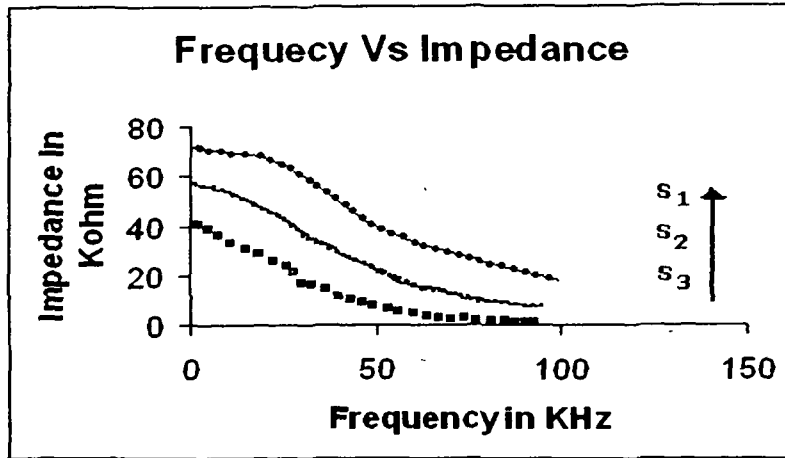


Fig.5.13 Comparison of Frequency Vs Impedance curves for different capacitive structures of ZnS qd

The V-Z curves at fixed frequency for CdS qd and ZnS qd show that CdS qd has higher impedance than that of ZnS qd (Fig. not shown). This suggests that there are more number of quantum dots in CdS assembly than that in ZnS assembly.

The capacitance against voltage at different frequencies was plotted for the capacitive structure of ZnS quantum dots assembly and CdS quantum dots assembly are shown in figure 5.14 and figure 5.15 respectively. The capacitance increases with applied voltage reaches highest value at certain voltage then drops and retains saturation value. However the rate of increment drops when frequency increases. In C-V characteristics of ZnS sample, the capacitance becomes maximum at 0.3V for signal frequency 1 KHz and the maximum capacitance for other higher signal frequencies is obtained at 0.2V. The capacitance remains same beyond the voltage 0.3V for frequency 1 KHz and beyond 0.2V for other frequencies.

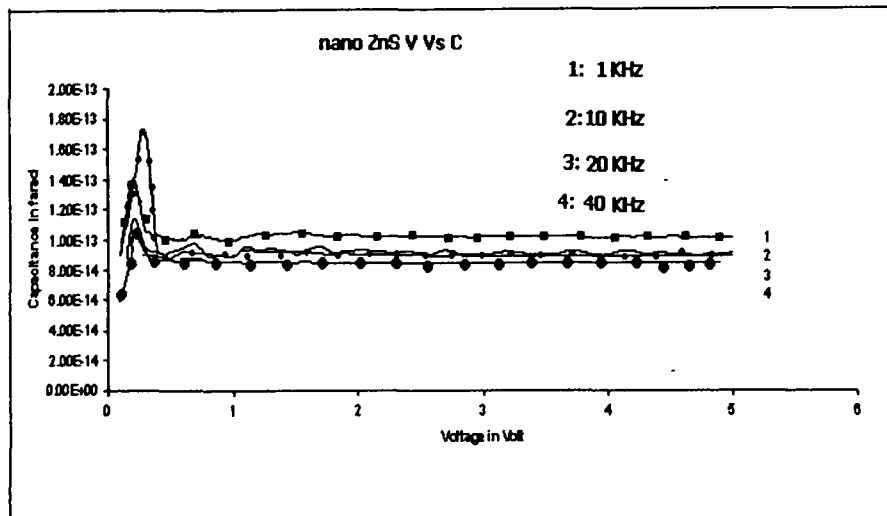


Fig. 5.14 C-V of nano ZnS (capacitive structure) at diff. Frequencies.

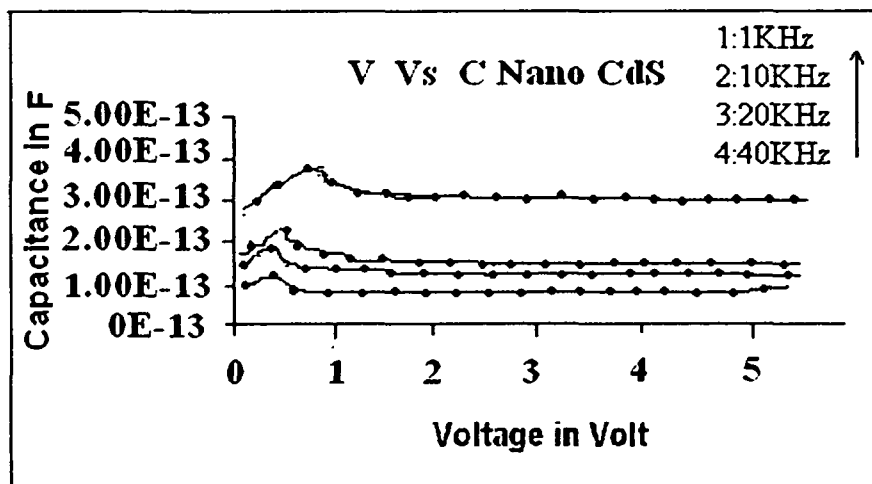


Fig: 5.15 C-V curves of CdS qd (capacitive structure) at different frequencies

The maximum of capacitance for CdS sample is obtained at 0.8 V for signal frequency 1 KHz, at 0.6 V for signal frequency 10 KHz and the same for other frequencies are located at 0.3V. It is also observed that for maximum capacitance, CdS sample draws higher voltage than that of ZnS

sample. It suggests that the CdS quantum dots have large number of deep surface traps of for which comparatively higher voltage is required to set free the charges.

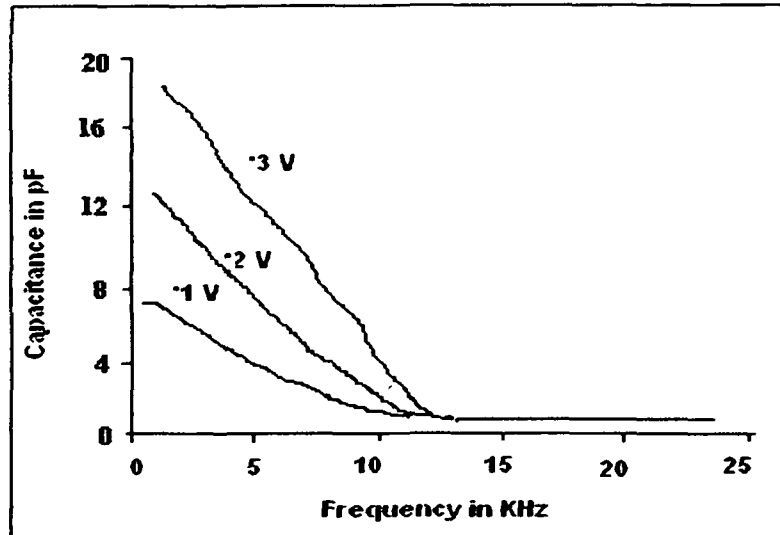


Fig. 5.16 Capacitance-frequency curves for ZnS qd (capacitive structure) at different voltage

The variation of capacitance against frequency of ZnS quantum dots for voltage 0.1V, 0.2V and 0.3 V are plotted and depicted in figure (5.16) It is found that the capacitance response of the structure are compatible with charge injection into the nano particle assembly. As the voltage between the two plates is increased charge is injected into the structure, the capacitance is found to increase. However the capacitance sharply drops at 12 kHz. At this frequency the device is no longer responding to charge injection.

5.3 Photo induced current

A very small nano crystal is essentially a large molecule, the so called grain boundaries existing between large particles and polymers, which can act as carrier traps, are therefore absent. If we have a conducting polymer then only a small amount of nano crystal is needed since polymer matrix is capable of transporting carriers.

The nano crystals in conducting polymer, isolated from each other are responsible for the charge generation and the polymer is responsible for subsequent charge transport.

In summary, we can say that by mixing semiconductor nanocrystals with carrier transporting polymers, one can create an interesting class of photoconductive or field dependence charge generating nano composites.

For measuring photo induced current, conducting polymer was used. The ZnS qd was prepared through quenching method and mixed with polyaniline in the ratio 1:10 and then a paste was prepared. The film was deposited on conducting ITO glass and Silver (Ag) was coated above the sample. The schematic diagram of the sample is depicted in figure (5.17). The sample was irradiated with laser and current response against electric field was studied.

The figure (5.18) shows the variation of current for nanoZnS/Polyaniline and Polyaniline against applied electric field. The higher rate of current growth is observed in nano ZnS/Polyaniline composite when irradiated with laser (curve a). At field strength 5000

volt/cm the device draws 350 μA of current when irradiated with laser, but the same draws 180 μA of current in the absence of laser. Since a nano crystal is very small, so the grain boundaries existing between large particles and polymer are absent. The conducting polymer is now capable of transporting carriers. The absorption of a photon creates a bound electron - hole pair. These pairs separate into free electrons and free holes and free electrons transport through the conducting polymer towards other side and contribute in current growth. At one stage current tends to saturate because at this stage all the carriers generated take part to current growth.

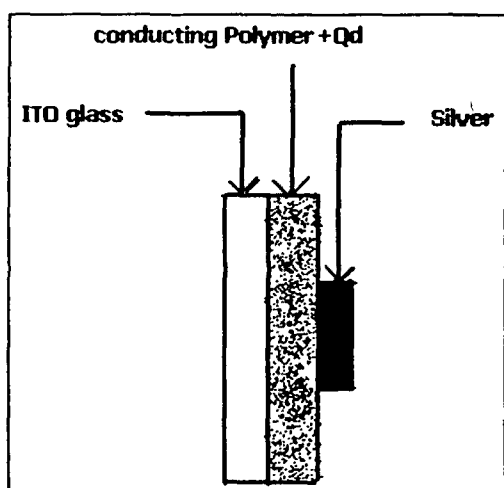


Fig.5.17 Schematic diagram of the sample for measuring photo induced current

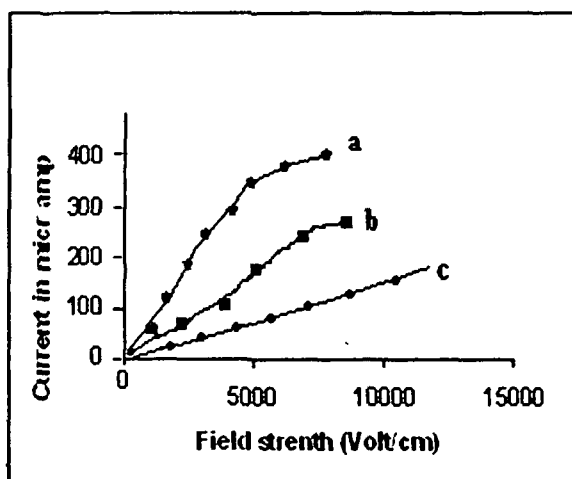


Fig. 5.18 Charge generation in nano (a) nano ZnS/polyaniline (with laser) (b) nano ZnS/polyaniline (without laser) (c) polyaniline

The nonlinear nature corresponding to charging and discharging within a given range of forward bias for highly ordered quantum dots has been reported to have application in single electron device, nano junction diode etc. This property has been observed in our I-V studies for different frequency range. Further we have observed fast photo induced current

which is very important criteria for electro photographic application. On the other hand the sharp rise in current in high frequency range and in Cu doped nano ZnS/Ag junction is a strong candidate for fast switching.

5.4 Summary

In this chapter electrical properties of quantum dots are studied in the form of *I-V* and *C-V* characteristics at different frequency range by fabricating Schottky junction of metal and semiconductor nano particles. The devices are nano ZnS/Ag and Cu doped nano ZnS/Ag junctions.

In *I-V* characteristics of nano ZnS/Ag junction at frequency range 1 KHz-40 KHz we observe that a minimum voltage (built up voltage) is required to produce current. Off course this built up voltage declines when frequency increases. However this voltage is always less than that required for bulk ZnS/Ag junction at any frequency. On the other hand such voltage is absent in *I-V* characteristics at 1MHz-4MHz frequency range. Also the device in this regime draws current at higher rate. The injection of large number of carriers from surface states helps in fast current growing.

In *I-V* characteristics of Cu doped nano ZnS/Ag junction we notice that no built up voltage is necessary for current growth even at frequency range 1 KHz-40 KHz. We also find high current establishment in this device. This high current response is attributed to lowering of contact potential due to doping of Cu in ZnS quantum system.

If we look into the *I-V* characteristics of nano ZnS/Ag and Cu doped nano ZnS/Ag junctions it is established that the device (nano ZnS/Ag) at

lower frequency (1KHz-40 KHz) range shows ordinary diode characteristics and Schottky behavior at higher frequency (1MHz-4 MHz) range. On the other hand when doped with Cu the device plays Schottky behavior even at lower frequency. So Schottky behavior of our device is dependent either on frequency or doping element.

The devices (nano ZnS/Ag nano ZnS;Cu/Ag), we have fabricated are completely new and not reported earlier. The current-voltage characteristics ($I-V$) of Cu doped nano ZnS/Ag junction show unique feature for current drawing.

In the frequency range 1 KHz-40 KHz capacitance-Voltage ($C-V$) characteristics of nano ZnS/Ag Schottky junction were studied and found that at higher frequency capacitance drops. The capacitance rises with voltage at frequency 1 KHz and 10 KHz but remains same even at increase in voltage for frequency 20 KHz and 40 KHz At higher frequencies greater amount of electron follow the signal and hence the chance of loading into nano ZnS is zero. Therefore capacitance drops and remains same.

Capacitive structures were fabricated by depositing Ag plates on two sides of ZnS quantum dots sample and Impedance-Voltage ($V-Z$) characteristics were studied. The uniform distribution of nanoparticles in ZnS quantum dots sample is established from this observation. The variation of capacitance against voltage at different frequencies of such capacitive structure of ZnS and CdS quantum dots samples were also studied and found that capacitance increases with voltage and becomes maximum at certain voltage. However CdS sample needs a higher value of

voltage for maximum capacitance than that in case of ZnS sample, which suggests presence of deep traps of surface states in CdS sample.

Photo induced current generation was studied using conducting polymer. For this ZnS quantum dot was prepared through quenching method, mixed with polyaniline and then the prepared paste was deposited on ITO glass. Irradiating with laser, variation of current against electric field was studied. The bound electron-hole pair created due to absorption of photon separates into free electron and hole which in turn contribute to higher current growth. Though photo induced discharge in CdS/PVK is reported earlier, our device is new and simple where we measured photo induced current. On the other hand use of polyaniline in such device is so far not reported.

All the current - voltage measurement were done with Hioki 3532-50 LCR Hi Tester with basic accuracy of $\pm 0.08\%$ of reading and with measurement time at normal speed 21 ms.

References

1. U. Woggon, *Optical Properties of Semiconductor Nanostructures*, volume 136 of *Springer Tracts in Modern Physics*, Springer, Berlin (1997).
2. D. Bimberg, M. Grundmann, and N. N. Ledentsov, *Quantum Dot Heterostructures*, John Wiley & Sons, Chichester (1998).
3. L. Jacak, P. Hawrylak, and A. Wojs, *Quantum Dots*, Springer, Berlin (1998).
4. A. D. Yoffe, *Semiconductor quantum dots and related systems: electronic, optical, luminescence and related properties of low dimensional systems*, *Adv. in Phys.* **50** (1), 1 (2001).
5. Y. Wang. US Patent 5,250,378 (1993)
6. Y. Wang. *Nature* **356**, 585 (1992)
7. Y. Wang, R. West, C. H. Yuan, *J. Am. Chem. Soc.* **115**, 3844 (1993)
8. Y. Wang, N. Herron *Chem. Phys. Lett.* **200**, 71 (1992)
9. N. Herron, Y. Wang US Patent 5, 238, 607 (1993)
10. B. O. Dabbousi, M. G. Bawendi, O. Onitsuku and M. F. Rubner. *Appl. Phys. Lett.* **66**, 1316 (1995)
11. E. H. Rhoderick and R. H. Williams, *Metal-Semiconductor Contacts* - Oxford University Press, London, (1988)
12. R. T. Tung, *Phys. Rev. Lett.* **84**, 6078 (2000)
13. H.-J. Im, Y. Ding, J. P. Pelz, and W. J. Choyke, *Phys. Rev. B* **64**, 07 5310 (2001)
14. S. M. Sze, *Physics of Semiconductor Devices*, John Wiley & Sons, New York, 2nd edition (1981).

15. S. M. Sze, *Semiconductor Devices - Physics and Technology*, John Wiley & Sons, New York (1985).
16. P. Blood and J. W. Orton, *The Electrical Characterization of Semiconductors: Majority Carriers and Electron States*, Academic Press, London (1992).
17. A.K.Bordoloi, D.Mahanta, S.K.Dolui and A.Choudhury.*Indian journal of Physics,accepted* (2006)
18. D. Mohantaa and A. Choudhury. *Eur. Phys. J. B* **45**, 63–68 (2005)
19. M.C. Schlamp, P. Xiaogang, A.P. Alivisatos, *J. App. Phys.***82**, 5837 (1997)
20. D. Braun, A.J. Heeger, *Appl. Phys. Lett.* **58**, 1981 (1982)
21. D.D. Shivagan, P.M. Shirage, S.H. Pawar, *Pramana*, **58** (5, 6), 1183 (2002)
22. S.N. Sahu, B. Patel, S.N. Behera, K.K. Nanda, *Indian J.Phys.* **74A** (2), 93 (2000)

Chapter 6

APPLICATIONS

The quantum dots have got many applications. The unique optical and electronic features of quantum dots' films are being exploited to develop photocromic display/switches, optical switches, ultra fast switches¹⁻⁸, chemical sensors, dielectric/super capacitors and photovoltaic cell.

The perhaps most evident quantum dot application, is to use these "artificial atoms" as active medium in a laser. Since the requirements are the same as for the conventional quantum well based laser diodes, the conversion to quantum dots is in principle straight forward. Laser diodes based on quantum dots have a variety of advantages over QW based lasers. These include higher efficiency and reduced temperature effects. In order to take full advantage of quantum dots, the growth has to be well controlled to create a dot distribution that is as homogeneous as possible. In research environments, QD lasers have been available for some time. As an example, among many others, the coworkers of Bimberg in Berlin have constructed an 11.7 W laser diode based on InGaAs/GaAs emitting at 1135 nm ⁹. Commercially, lasers based on quantum dots have recently appeared on the market (Zia Quantum Dot Solutions). More exciting are the new kind of devices that not only are improved by the use of quantum dots but actually rely on the physics of quantum dots. Recently, single photon emission from quantum dots was demonstrated by several groups. There is a demand for controlled single photon sources for applications in quantum cryptography and quantum computation. Although quantum dots are promising

candidates (the group of Shields' has demonstrated both a single photon LED¹⁰ and a single photon detector based on quantum dots¹¹ the usefulness is limited to the low light extraction efficiency. However, by resonantly coupling the quantum dots to a single mode of an optical micro cavity this can be drastically improved^{12,13}.

According to the present state of knowledge, chemically tailored nanoparticles in the sub-10 nm range are suitable building blocks for SE devices. Their minute size combined with the well-defined insulation barrier (matrix) opens access to ultra small electrical capacitances in the range of 10^{-19} F, a value that can not be reached by classical techniques because of their physical limit. The most remarkable opportunities for SE will occur in the field of digital circuits. According to Averin and Likharev it will provide the first available realistic physical basis for devices that perform digital information processing on the molecular scale.

The applications of quantum dots will be discussed in this chapter mainly on (I) optical switching and (II) fast switching element.

The applications in optical switching will be discussed utilizing photoluminescence properties of the dots and that in fast switching will be discussed from the *I-V* characteristics of nano semiconductor/metal Schottky junction.

6.1 Electronic Switching

Semiconductor diodes possess switching characteristics. The time required for the removal of the excess charge is referred as the storage time. The

speed of operation of a semiconductor diode is reduced due storage of minority carriers. But this storage time can be reduced significantly in metal-semiconductor Schottky diode. Hence Schottky diode has faster switching property than that of an ordinary semiconductor diode. On the other hand metal nano semiconductor Schottky diode is a faster switching device. It has been seen that nano ZnS/Ag Schottky junction draws current at lower potential than that in case of bulk ZnS/Ag Schottky junction due to presence of surface states. It has also been observed that current response in nano ZnS/Ag Schottky junction is frequency dependent. The built-up voltage at which current grows decreases as frequency increases and at higher frequency range (1 MHz – 4 MHz) this voltage is zero. The built-up voltage observed at different frequencies are shown table 6.1. On the other hand this built-up voltage is completely absent for Cu doped nano ZnS/Ag junction even at lower frequency range (1 KHz-40 KHz). So it might be concluded that if the semiconductor quantum dot is arranged to combine with metal then the device can act as a very fast switching device and as more importantly faster than general Schottky diode. The reason is the existence of intermediate energy states between valance band and conduction band (traps e.g. surface states, oxygen vacancies etc). However the device can be made more fast if metal is doped in semiconductor quantum dots. Such fast current response has also been observed in Cu doped nano ZnS/Ag junction. So this fast response of current can be used suitably for fast switching.

Table: 6.1. Built-up voltage at different frequencies

Frequency	Built-up voltage in Volt
1 KHz	0.46
10 KHz	0.41
20 KHz	0.35
40 KHz	0.28
≥ 1 MHz	0

6.2 Photo detector

Semiconductor quantum dots with conducting matrix are of great importance. This device can act as efficient photo detector. As light is illuminated on the device charge carrier generation takes place and due to the presence of conducting matrix (poly aniline) these carries can easily be transported from one quantum dot to the other. Also conducting matrix offers low impedance to the charge carries and hence energy loss is minimum. Thus quantum dots with conducting matrix may act as fast, efficient photo detector with minimum energy loss.

The nonlinear nature corresponding to charging and discharging within a given range of forward bias for highly ordered quantum dots has been reported to have application in single electron device, nano junction diode etc. This property has been observed in our I-V studies for different frequency range. Further we have observed fast photo induced current which is very important criteria for electro photographic application. Fig 5.18 in chapter 5 shows the current flow through quantum dots assembly. It

is observed that little current flow takes place through Polymer (curve c, fig. 5.18) and a distinct increased in current is observed for quantum dots when embedded in the polymer. But it is very interesting to observe the increase in current intensity (curve a, fig. 5.18) when illuminated with laser. This behavior infers that the prepared quantum dot assembly can act as photo detector where the current in curve b in figure 5.18 can be treated as dark current of conventional photo detector. The advantage of quantum dots photo detector is its small dimensions and faster response.

6.3 Application as variable capacitor

We have performed the experiments for to show the capacitive behaviour of quantum dots and photo induced current generation.

The variation of capacitance against frequency of ZnS quantum dots for different bias voltage were studied and explained in chapter 5. The plots were drawn between frequency and capacitance for voltage 0.1V, 0.2V and 0.3 V and depicted in figure (5.16) in chapter 5. It is found that the capacitance responses of the structure are compatible with charge injection into the nano particle assembly. As the voltage between the two plates is increased charge is injected into the structure, the capacitance is found to increase. The capacitance sharply drops at 12 kHz. At this frequency the device is no longer responding to charge injection.

In the fig 5.16 (chapter 5) it is observed that the capacitance of quantum dot assembly varies with (1) applied voltage and its (2) frequency. This is novel characteristics of our prepared quantum dot assembly (quantum dots + polymer). This property has distinct advantage over conventional capacitor, as the conventional capacitors are of fixed capacitance. Our prepared quantum dots can be compared with varactor,

which is basically a voltage dependent capacitor. But the most important advantage of our quantum dots over varactor is that the capacitance of quantum dots varies with frequency of the applied voltage also. With calibration it may be possible to measure the unknown voltage/ frequency by monitoring the changes in the capacitances of quantum dots assembly.

6.4 Optical switching

As we know, a current of electrons may or may not flow through the device depending on whether it is the ON or OFF state. Of course an ordinary transistor, and even a vacuum tube, perform a similar function. So it can be concluded that there are no alternatives to electrons for switch. All the switching elements that considered require an electrical signal as input and produce an electrical output. In order to transmit optical signals between devices of electronic processing elements, a conversion between optical and electrical signal is needed. But one needs a switch of which switching speed is very fast. If the electron is replaced by photon in switching elements, the problem can be solved. Concentrating on semiconductor based optical switches one can explore the possibilities of optical computing for using to create logic gates. It is seen that the delay of electrical signal in propagating through the interconnects is due to resistive and capacitive effects. These delays remain the same as the circuit is scaled down in size. So it concludes that the operating speed of an electronic computer will ultimately be determined by the time required to communicate signals between the devices. However, optical signals do not suffer from capacitive or resistive effects. So use of optical signals suggests that the communication time is scaled down in proportion with the device size. Further it is significant that

the speed of light is approximately hundred times greater than the speed at which an electrical signal travels through interconnects.

The electronic transistor acts as a switch because it has two possible states. These are characterized by the ability of the device to conduct or not to conduct electricity depending on the magnitude of another electrical signal. A similar function could perhaps be obtained in an optical context by devising a device which either absorbs or does not absorb light depending on frequency or intensity. For this, such materials are needed that exhibit a non linear optical response. The quantum dots serve this purpose. Because of quantum size effect there is increase in band gap of semiconductor quantum dots. As a result, number of electronic states called surface states are produced within the band gap. These surface states influence photoluminescence. Utilizing this luminescence property one can use semiconductor quantum dots as frequency converter. In other words, one wavelength can be converted to another wavelength. Photoluminescence studies of the quantum dots show that these can act as very efficient frequency/ wavelength converter with very high conversion speed of the order of 10^{-9} sec to 10^{-14} sec or less than that. Therefore, these wavelength /frequency converters can be called as optical switch. The mechanism behind the frequency/ wavelength conversion is the existence of intermediate energy states in the forbidden gap of the host quantum dot. These are surface states, imperfections like vacancies, and the impurity levels, explained in photoluminescence study. The different quantum dots are now being discussed as optical switch.

Many II-VI semiconductor quantum dots samples were synthesized including some metal doped samples. But discussion will be focused on two

samples; Cu doped ZnS quantum dots (ZnS:Cu) and Fe doped ZnS quantum dots (ZnS:Fe). Both the samples were irradiated with 150 MeV Ti⁺ ion. The photoluminescence peaks of the virgin and irradiated samples of ZnS:Cu quantum dots and ZnS:Fe quantum dots are being discussed in context of frequency converter.

Sample: ZnS:Cu

Notation: S1

The Virgin and ion irradiated ZnS:Cu samples are excited with wave length from 200 nm to 600 nm. The emission peak is obtained at 480 nm corresponding to frequency 6.25×10^{14} Hz. The key reason behind the wavelength conversion due to transition from conduction band of ZnS to the t_2 level of excited $Cu^{2+}(d^9)$ in ZnS band gap. The intensity, hence the quantum efficiency of the device increases with higher ion fluences. The reasons for that have been already been explained in chapter IV. The switching time is ranging from 10^{-13} to 10^{-14} sec. Table 6.2 shows the different notations corresponding to un irradiated and irradiated ZnS:Cu samples with different ion fluences. The wavelength detection range along with output photoluminescence peak for the samples is depicted in table 6.3.

Table:6.2 Ion fluence and corresponding sample code for ZnS:Cu

Fluence notations	Irradiated sample notation
ϕ_1	S1d ₁
ϕ_2	S1d ₂
ϕ_3	S1d ₃
ϕ_4	S1d ₄
Un irradiated	S1

Table:6.3 Wave length detection range with output luminescence of different ZnS:Cu samples

Sample	Wave length detection range (nm)	Corresponding frequency detection range (Hz)	Luminescence at wavelength (nm)	Luminescence at frequency (Hz)	Intensity
S1	220 to 600	1.36×10^{15} to 5×10^{14}	480	6.25×10^{14}	5
S1d1	220 to 600	1.36×10^{15} to 5×10^{14}	480	6.25×10^{14}	6
S1d2	220 to 600	1.36×10^{15} to 5×10^{14}	480	6.25×10^{14}	10
S1d3	220 to 600	1.36×10^{15} to 5×10^{14}	480	6.25×10^{14}	24

Sample: ZnS:Fe

Notation: S2

The different notations corresponding to un irradiated and irradiated ZnS:Fe samples with different ion fluences are shown in table 6.4. When excited with signal wavelength ranging from 220 nm to 600 nm, the corresponding output luminescence peaks are obtained at wavelength 546 nm corresponding to frequency 5.46×10^{14} Hz. for both virgin and irradiated samples table 6.5.

Table 6.4. Ion fluence and corresponding sample code for ZnS:Fe

Fluence notations	Irradiated sample notation
ϕ_1	S2d ₁
ϕ_2	S2d ₂
ϕ_3	S2d ₃
ϕ_4	S2d ₄
Un irradiated	S2

Table:6.5 Wave length detection range with output luminescence of different ZnS:Fe samples

Sample	Wave length detection range (nm)	Corresponding frequency detection range (Hz)	Luminescence at wavelength (nm)	Luminescence at frequency (Hz)	Intensity
S2	220 to 600	1.36×10^{15} to 5×10^{14}	546	5.49×10^{14}	6
S2d1	220 to 600	1.36×10^{15} to 5×10^{14}	546	5.49×10^{14}	8
S2d2	220 to 600	1.36×10^{15} to 5×10^{14}	546	5.49×10^{14}	11
S2d3	220 to 600	1.36×10^{15} to 5×10^{14}	546	5.49×10^{14}	24

It is seen that doped ZnS quantum dots exhibit efficient luminescence property. Both Cu doped ZnS and Fe doped ZnS quantum dots samples efficiently convert optical signal ranging from wavelength 220 nm to 600 nm to another wavelength. The output of ZnS:Cu samples are obtained at 480 nm and that for ZnS:Fe samples at 546 nm. In ZnS:Cu samples the Cu induced level is responsible for output luminescence and hence for mechanism of switching.

6.5 Summary

One of the main features of quantum dots for using in electronic devices is its ultra small size. Moreover power consumption is very low and they have high switching speed. We have mentioned about the advantages of our quantum dots capacitive structure over varactor diode. The device is therefore quite useful for tunable band-pass filter. It can also be used as automatic frequency control device, FM modulator and in tuned circuits.

The device explained for photo induced current generation can be used as photo detector. Therefore, the remarkable opportunities for the device will occur in the field of optical communication, optical counter, detection and switching.

The special optical properties observed in our chemically grown quantum dots samples, such as a particle size dependent wavelength of fluorescence is a strong candidate for fabrication of optical probes for biological and medical imaging.

Further our studies of electrical and optical properties of quantum dots reveal that prepared quantum dots samples can be used as fast

switching, optical switching, photo detector and variable capacitors which are some of the real life applications of our chemically grown quantum dots samples.

References

1. A Sengupta, B Jhang, K C Moandal and J Z Zhang; *J. Phys. Chem.B*, **103** (1999)
2. E Lifshiz, M Yassan, L Bykovo, I Dag , R Chem.; *J. Phys. Chem.* **92** (1995)
3. A D Dinsmore, D S Hsu, S B Qauadri, J O Cross; *J Of Applied Physics*, **88**, 9 (2000)
4. R L Singhal, *Semiconductor Physics*, Keder Nath Ram Nath, Meerut, (U.P), India, (1999)
5. M Boroditsky, I Gontijo, M Jackson, R Vrijen and E Yablonovitch; *Journal Of Applied Physics*, **87**, 7 (2000)
6. S Benejee, R Pal, A B Mity, S Chowdhury, and A K Pal; *Nanostructure Material*, **8** , 3 (1997)
7. L E Bruss, IEEE, *Quantum Electronics*, **72**, 416 (1994).
8. W Hoeisel, V L Colvin, C S Johnson and A P Alivisatos; *J. Chem. Phys.* **101** (1994)
9. R. L. Sellin, C. Ribbat, D. Bimberg, F. Rinner, H. Konstanzer, M. T. Kelemen, M. Mikulla, *High-reliability MOCVD-grown quantum dot laser*, *ElectronHigh-Electron.Lett.* **38**, 883 (2002)
10. Zhiliang Yuan, Beata E. Kardynal, R. Mark Stevenson, Andrew J. Shields, Charlene J. Lobo, Ken Cooper, Neil S. Beattie, David A. Ritchie, and Michael Pepper, *Electrically driven single photon source*, *Science* **295**, 102 (2001)
11. A. J. Shields, M. P. O'Sullivan, I. Farrer, D. A. Ritchie, R. A. Hogg, M. L. Leadbeater, C. E. Norman, and M. Pepper. *Detection of single photons using a fi eld-effect transistor gated by a layer of quantum dots*, *Appl. Phys. Lett.* **76**, 3673 (2000)

12. G. S. Solomon, M. Pelton, and Y. Yamamoto, Single-mode spontaneous emission from a single quantum dot in a three-dimensional microcavity, *Phys. Rev. Lett.* **86**, 3903 (2001)
13. C. Santori, D. Fattal, J. Vuckovic, G. S. Solomon, and Y. Yamamoto, Indistinguishable photons from single-photon device, *Nature* **419**, 594 (2002)

Chapter 7

CONCLUSIONS AND FUTURE

PROJECTION

We have successfully fabricated II-VI semiconductor quantum dots namely CdS, ZnS and ZnO in polymer matrices. The formation of extremely small particle range down to the size ~ 5 nm in case of CdS quantum dots on polyvinyl alcohol has been observed. From XRD studies the average sizes of quantum dots have been estimated. Optical absorption study has given the information about blue shift of the nano particles (quantum dots). Next the sizes of the particles have been confirmed from TEM studies. The decrease of particles' sizes at higher pH value of the solution has also been observed. The presence of surface states within the band gap has been confirmed from thermo luminescence and photoluminescence studies.

Among many semiconductors, ZnS plays an important role as phosphors for luminescence. doped with metals like Mn, Cu and Fe, ZnS quantum dots can yield both high luminescent efficiencies and lifetime shortening at the same time. Therefore, extensive studies have been carried out on ZnS doped ZnS quantum dots. We have synthesized two doped ZnS quantum dots samples namely ZnS:Cu (Cu doped ZnS quantum dots) and ZnS:Fe (Fe doped ZnS quantum dots).The efficient luminescence peaks have been observed for both the samples.

Swift heavy ions are the means to form ion tracks in materials (polymer, semiconductor, superconductor etc.). To explore the effect of ion irradiation ZnS:Cu and ZnS:Fe quantum dot samples have been irradiated with 150 MeV Ti ion beam with different fluences. The formation of bigger particle at higher ion fluences has been confirmed by XRD and TEM studies. However photoluminescence of Cu doped ZnS and Fe doped ZnS quantum dots have shown significant enhancement of fundamental emission as ion fluence increases. The enhanced luminescence peak for ZnS:Cu quantum dots samples has been found at wavelength 480 nm and that for ZnS:Fe has been observed at wavelength 546 nm. Both Cu doped ZnS and Fe doped ZnS quantum dots samples efficiently convert optical signal ranging from wavelength 220 nm to 600 nm to another wavelength. Based on this characteristics doped ZnS quantum dots can be used as frequency converter.

The virgin and irradiated samples have been characterized with Atomic Force microscopy (AFM). The atomic force microscopy has provided the information about surface roughness and uniform distribution of the particles.

Magnetic force microscopic studies on Fe doped ZnS quantum dots system have been done to search some magnetic properties. We have not found any appreciable result on the magnetic domains on the phase image of un irradiated and irradiated (1st fluence) ZnS:Fe because of matrix encapsulation. But almost elliptical shaped single domains are obtained in case of the sample irradiated at fluence 2×10^{11} ions/cm². These domains become elongated at fluence 8×10^{11} ions/cm². These aligned domains are extended up to 80-100 nm and can be applied in magnetic tapes, magnetic recording devices and other spin based devices.

To explore electronic properties the interface comprising nano ZnS/Ag and nano ZnS:Cu/Ag junctions have been fabricated and characterized by I-V and C-V studies. Both the studies suggest the presence of surface traps at the junction. These surface trap carriers controlled by signal frequencies can suitably be applied in nano electronics of desired working frequency. Further, from these studies we can also conclude that schottky behavior in our device is a function of either frequency or doping element. The fast current response in Cu doped nano ZnS/Ag junction is a criterion for fast switching.

In comparison with other compound semiconductors, II-VI semiconductors possess high value exciton binding energies (and that is why excitonic absorption can be visible at room temperature) and therefore, further research is essential in the areas of single electron devices, fast optical switching. The research on electrical properties of ion irradiated samples will also open the door in this respect. Recently synthesis of water soluble conducting polymer is reported. So use of water soluble conducting polymer with nanoparticle will also pave the way for future research.

Besides these, the most interesting applications may involve devices in which several artificial atoms (quantum dots) are coupled together to form artificial molecules then to form artificial solids. Because the coupling between the artificial atoms can be controlled, new physics as well as new application may emerge. However the understanding and design, based on quantum mechanics are needed. Further progress on material as well as fabrication technologies is also essential to achieve perfect control over the size and purity of these nano structures. The building of quantum confinement devices in quantities is also an important challenge for future researchers.

Chemically grown quantum dots samples have many advantages for its simplicity of fabrication and possibility in large scale production. It is also a low cost device, but it has short durability which is its prime disadvantage. We have seen that on conducting polymer quantum dots exhibit photo induced current generation. As water soluble conducting polymer is not easily available, therefore it is difficult to prepare quantum dots samples with conducting polymer as done with other insulating polymers (PVOH), through chemical process. We feel availability of water soluble conducting polymer would have more useful while fabricating such devices. Such difficulties like short durability of samples and lack of water soluble conducting polymers may arise in further research on these areas and therefore will be more challenging.

LIST OF PUBLICATIONS

1. Optical and electrical properties of chemically grown quantum dots. A K Bordoloi, D Mahanta, S K Dolui and A Choudhury, *Indian J.Phys.* 81(1) 89-93 (2007)
2. Optical absorption study of 100-MeV chlorine ion-irradiated hydroxyl free ZnO semi conductor quantum dots. D Mahanta, S S Nath, A Bordoloi, S K Dolui, N C Mishra and A Choudhury *Journal of Applied Physics* 92,12 (2002)
3. Preparation of Mn doped ZnS quantum dot on pol matrix and study of its thermo stimulated behavior. S S Nath, D Mahanta ,A K Bordoloi, S Choudhury, S K Dolui and A Choudhury. *Proc. Of Nsl.Conf. on Laser and its application* Dibrugarh University ,(2001)
4. Electrical properties of nano ZnS/Ag and nano ZnS:Cu/Ag junctions (Communicated).